A Comparative Assessment on the Applicability of UAV and TLS for Estimating Aboveground Biomass of Mangrove Forest in Mahakam Delta, East Kalimantan, Indonesia

MD. MAHMUD HOSSAIN
February, 2019

SUPERVISORS:
Ir. L.M. Van Leeuwen-de Leeuw
Dr. Y. A. Hussin

ADVISOR:
Dr. Y. Budi Sulistioadi, University of Mulawarman, Indonesia

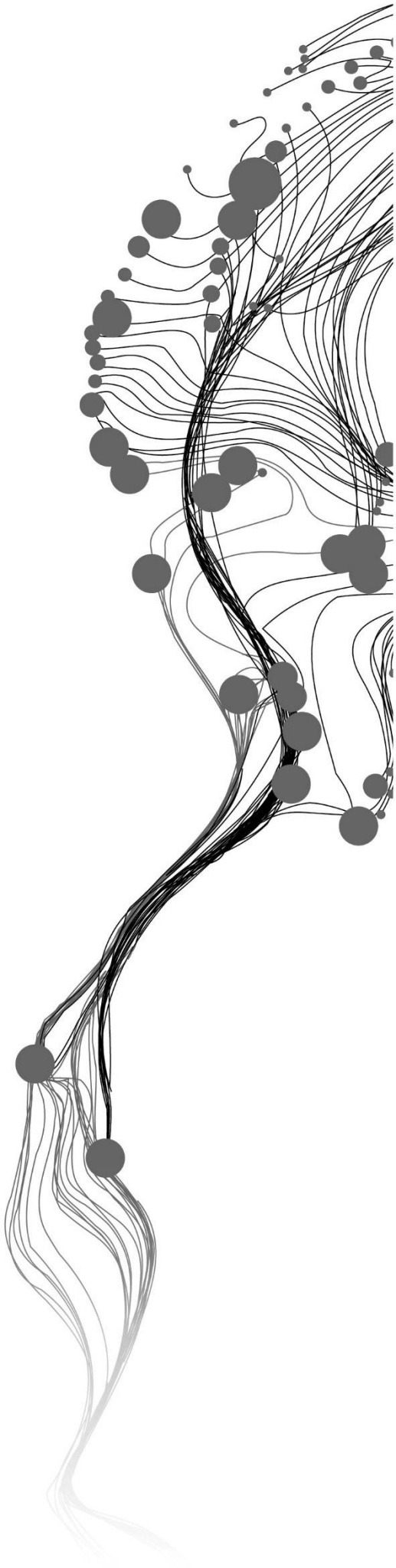

A Comparative Assessment on the Applicability of UAV and TLS for Estimating Aboveground Biomass of Mangrove Forest in Mahakam Delta, East Kalimantan, Indonesia

MD. MAHMUD HOSSAIN

Enschede, The Netherlands, February, 2019

Thesis submitted to the Faculty of Geo-Information Science and Earth Observation of the University of Twente in partial fulfilment of the requirements for the degree of Master of Science in Geo-Information Science and Earth Observation.

Specialization: Natural Resources Management

SUPERVISORS:
Ir. L.M. Van Leeuwen-de Leeuw
Dr. Y.A. Hussin

Advisor:
Dr. Y. Budi Sulistioadi, University of Mulawarman, Indonesia

THESIS ASSESSMENT BOARD:
Prof. Dr. A.D. Nelson (Chair)
Dr. T.L.U. Kauranne (External Examiner)
Lappeenranta University of Technology, Finland

ABSTRACT

Mangrove forests are playing a vital role by storing and sequestering a large amount of global carbon that helps to reduce the GHG emission. Unfortunately, the global mangrove forests are decreasing rapidly due to agricultural expansion, illegal logging, mining, and palm oil production. The UNFCCC initiates REDD+ initiatives for reducing the GHG emission from deforestation and forest degradation. The aboveground biomass and carbon stock estimation is a prerequisite for an MRV system for complying such initiative.

The use of UAV and TLS are considered as a popular remote sensing technique for estimating aboveground biomass and carbon stock appropriately. This study is aimed at a comparative assessment on the applicability of UAV and TLS for estimating aboveground biomass and carbon stock in the mangrove forest. The tree height extracted from CHM of UAV images can provide comparatively accurate tree height. The DBH and tree height measured from TLS 3D point clouds can also give a correct measurement of DBH and tree height. The aboveground biomass was estimated using a specific allometric equation developed for mangrove forests. A total of 30 sample plots containing 893 trees were considered for conducting statistical analysis. The accuracy of DBH, tree height and aboveground biomass estimated from UAV and TLS were assessed for identifying if any significant difference between them or not. In this study, two segmentation algorithm including multi-resolution and SLIC were also evaluated for determining a better algorithm for tree crown segmentation on UAV imagery in mangrove forests.

The result shows that tree height extracted from CHM of UAV imagery compared to tree height measured from TLS point clouds are attained at R^2=0.82 (RMSE=1.44m). The multi-resolution and SLIC segmentation was conducted to evaluate these two segmentation algorithms. The accuracy of multi-resolution segmentation was found 77.99% in 25cm resolution UAV-RGB image while SLIC provides 51.18% accuracy in 20cm UAV-RGB resampled image. A quadratic regression model is found best fitted for developing CPA-DBH relationship with R^2=0.89 where RMSE=3.50cm. The model validation was found as R^2=0.90 and RMSE=3.33cm. The accuracy of DBH predicted from CPA segmentation of UAV imagery compared to field-measured biometric DBH is attained at R^2=0.87 (RMSE=3.21cm) while the accuracy of DBH measured from TLS point clouds is achieved at R^2=0.99 (RMSE=0.30cm). On the other hand, the accuracy of AGB estimated form UAV compared to TLS is achieved at R^2=0.93 while RMSE=3.78 ton/ha. Therefore, there is no significant difference found by t-test for DBH, tree height, and AGB estimated from field-measured biometric, TLS and UAV data.

The study reveals that the measurement of UAV and TLS for estimating aboveground biomass and carbon stock is very close in the mangrove forest. The application of TLS is comparatively difficult in mangrove forests due to its challenging environment. Therefore, as a low-cost technology, UAV can be used to estimate aboveground biomass and carbon stock accurately especially in the mangrove forest. Consequently, as a remote sensing technique, UAV can be used broadly in any inaccessible area of mangrove forest for estimating aboveground biomass and carbon stock towards the implementation of MRV under REDD+ initiatives.

Keywords: Mangrove forest, Aboveground biomass, Carbon stock, Segmentation, UAV, TLS

ACKNOWLEDGEMENTS

I want to express my thankfulness to the Netherlands Fellowship Program (NFP) for providing an opportunity for me to pursue an MSc study in the Netherlands. I am also grateful to the Faculty of Geo-Information Science and Earth Observation (ITC), the University of Twente for enriching my scientific and technical knowledge on GIS and Remote Sensing that will have an immense influence on my career.

I express my heartfelt appreciation to my first supervisor Ir. L.M. Van Leeuwen-de Leeuw, for her intensive supervision, inspiration, prompt and constructive feedback. Her outstanding guidance helped me to complete my research within time. I am also very grateful to my second supervisor Dr. Y. A. Hussin, for his tireless support, valuable advice, and intensive care during the research period. I also express my gratitude to my advisor Dr. Y. Budi Sulistioadi for providing all kind of support especially for UAV data collection. Without his technical support, my research would not have been accomplished.

My heartiest appreciation to Prof. Dr. A.D. Nelson for his constructive comments and suggestions during the period of the research proposal and mid-term defense. I am also very grateful to Drs. R.G. Nijmeijer, course director, NRS for his valuable advice and moral support during my study in ITC.

I am very thankful to the Department of Environment, Ministry of Environment, Forest and Climate Change (MoEFCC), Government of the People's Republic of Bangladesh for permitting me to study in the Netherlands for eighteen months study leave.

I greatly acknowledge and appreciate to the Ministry of Science and Technology and Higher Education, Indonesia for providing me a research permit to execute my research fieldwork in Indonesia. I am profoundly thankful to the Faculty of Forestry, University of Mulawarman, Samarinda, Indonesia for all kind of support related to fieldwork.

I want to thank M.L. Hamdani and M. Priskawanti, Bachelor Student, University of Mulawarman, Indonesia who immensely provided their support during the fieldwork in a very challenging and risky environment. I am also thankful to my fieldwork mates M.A. Hashem, W.B. Tesfay, M.K. Nesha, G.K. Beyene and E. Kustiyanto for their participation and cordial cooperation during the fieldwork.

My heartiest appreciation and regards go to my family especially to my respected mother, beloved wife and lovely daughter for their sacrifice as living without me and providing moral support during my study period. I am also obliged to my relatives, friends, and well-wishers who support me in different ways during my study abroad.

Md. Mahmud Hossain
Enschede, The Netherlands
February 2019

TABLE OF CONTENTS

LIST OF FIGURES

LIST OF TABLES

LIST OF EQUATIONS

LIST OF APPENDICES

LIST OF ACRONYMS

3D	Three-Dimensional
AGB	Aboveground Biomass
BA	Basal Area
CF	Carbon Fraction
CHM	Canopy Height Model
CO^2	Carbon Dioxide
CPA	Crown Projection Area
DEM	Digital Elevation Model
DBH	Diameter at Breast Height
DGPS	Differential Global Positioning System
DEM	Digital Elevation Model
DSM	Digital Surface Model
DTM	Digital Terrain Model
ESP	Estimation of Scale Parameter
GCP	Ground Control Point
GHG	Greenhouse Gas
GPS	Global Positioning System
IPCC	Intergovernmental Panel on Climate Change
LiDAR	Light Detection and Ranging
MRV	Measurement, Reporting, and Verification
OBIA	Object-Based Image Analysis
R^2	Coefficient of Determination
RADAR	Radio Detection and Ranging
REDD+	Reducing Emissions from Deforestation and Forest Degradation
RMSE	Root Mean Square Error
SfM	Structure from Motion
SLIC	Simple Linear Iterative Clustering
TLS	Terrestrial Laser Scanning
UAV	Unmanned Aerial Vehicle
UAV-CHM	Canopy Height Model developed from UAV Imagery
UAV-CPA	Crown Projection Area delineated from UAV Imagery
UNFCCC	The United Nations Framework Convention on Climate Change

1. INTRODUCTION

1.1. Background Information

Forests are considered as one of the most significant carbon sinks in the tropics because they are highly productive ecosystems (Donato et al., 2011). They are playing a vital role by storing and sequestering atmospheric carbon dioxide as well as reducing the greenhouse gas (GHG) emission. Also, forests have an important role in biodiversity conservation and GHG reduction from the atmosphere. But, forests have been decreasing rapidly due to deforestation and forest degradation (IUCN, 2017). It is estimated that 18.7 million acres of global forest land is declining in each year (WWF, 2019). The main reasons for forests degradation are the agricultural expansion, illegal logging, mining, shrimp farming, and palm oil plantation.

Many restoration and regeneration programmes and activities have been undertaken to reduce deforestation and forests degradation (Irving et al., 2011). The United Nations Framework Convention on Climate Change (UNFCCC) adopted the Kyoto Protocol in 1997 and the Doha Amendment in 2012 to reduce global GHG emission. The protocol aimed to reduce GHG emission level to at least 18 percent less than the 1990 level (Kaku, 2011). The UNFCCC is conducting REDD+ initiatives through some mitigation programmes to reduce GHG emission from forest degradation and deforestation towards sustainable forest management, especially in developing countries (USAID, 2013). These initiatives play a key role in protecting forest biomass and reducing GHG emissions from the atmosphere. The REDD+ initiative is committed to providing financial incentives, i.e., funds, credits to the developing countries for reducing CO_2 emission from forest degradation and deforestation (Aikawa et al., 2012). A Measurement, Reporting, and Verification (MRV) system is an essential part of monitoring such initiatives. The biomass and carbon stock estimation is a prerequisite for MRV of the REDD+ initiative.

Aboveground biomass (AGB) is considered one of the major carbon pools and acts as a significant parameter for monitoring the changes in carbon dioxide in the atmosphere (Lucas et al., 2015). Biomass is defined as plant organic materials such as leaves, roots, stalks, and seeds which are treated as the significant indices for both functional and structural variables of the forest ecosystem (Brown, 1997). Also, forest biomass has a significant role in regulating carbon emission generated from deforestation and forest degradation through carbon sequestration and storage (Lu, 2006). Forest biomass can be used for assessing forest condition, productivity, and carbon fluxes (Brandeis et al., 2006). Forest aboveground biomass is estimated in different ways using various methods and techniques. It can be measured either by field-based measurement (Salunkhe et al., 2016) or using remote sensing data (Lu, 2006). Unfortunately, sometimes the field-based biomass estimation is not feasible for its elongated process (Ghosh & Behera, 2018) while remote sensing based aboveground biomass estimation (both optical and active sensors) is considered as a most efficacious and cost-effective technique for sustainable forest management (Ali et al., 2015). At this point, Lu (2006) focused on the integration of field measured data with remote sensing data for estimating aboveground biomass.

Remote sensing techniques are treated as a revolutionary technology for monitoring and sustainable management of forest. Remote sensing instruments are broadly categorized into active and passive sensors where active sensors have their own energy to illuminate the detected object, while passive sensors detect natural radiation reflected by the object (NASA, 2018). The active sensors including Radio Detection and Ranging (RADAR) and Light Detection and Ranging (LiDAR) can assess comparatively accurate forest

biophysical parameters including tree height, Diameter at Breast Height (DBH), forest volume data (Gibbs et al., 2007). The passive sensors like satellite images are also used to measure forest parameters, e.g., tree height and DBH for estimating aboveground biomass and carbon stock. The spatio-temporal information on biophysical and biochemical properties of forest can be accumulated from remote sensing data (Asner et al., 2015). The Unmanned Aerial Vehicle (UAV) imagery is a popular remote sensing technique since last decade. The 3D point clouds can be derived from UAV images which are used to estimate forest biophysical parameters (e.g., trees height and crown projection area) for assessing aboveground biomass and carbon stock.

1.2. Problem Statement and Justification

Mangrove forest is considered as a significant carbon sink of the terrestrial ecosystem as it can sequester and store an enormous volume of carbon compared to other forests (Donato et al., 2011; Twilley et al., 1992). Mangrove forests can store three times higher carbon (including aboveground and belowground) as compared to terrestrial forests (Alongi, 2012). Besides, mangrove forests play an essential role in providing ecosystem services and functions including shelters for the birds and other animals, habitats for the plants, fish, invertebrates and amphibians and foods, woods and livelihoods for the local communities (Duarte et al., 2013). This forest plays a crucial function for stabilizing alluvial sediments and protecting the coastline from erosion and natural hazards (Boone & Bhomia, 2017). Unfortunately, global mangrove forests are degrading rapidly where half of the forest has been lost in the last four decades (Giri et al., 2011).

Mangrove forest has salt-tolerant trees that make it unique as compared to other forests. Also, mangrove forest is an ecosystem with rich biodiversity including various species of flora and fauna. In mangrove, some tree species have an intricate root system which is also the habitation of different aquatic species of flora and fauna (see Figure 1). The flat and even canopy and intermingle crowns make it challenging to identify individual tree crowns in the mangrove. However, the advantage is that it has a single canopy, unlike the tropical forest which is multi-layered. The aboveground biomass estimation in mangrove forest is challenging due to accessibility interrupted by tides and congested roots for field data collection (Gunawardena et al., 2016).

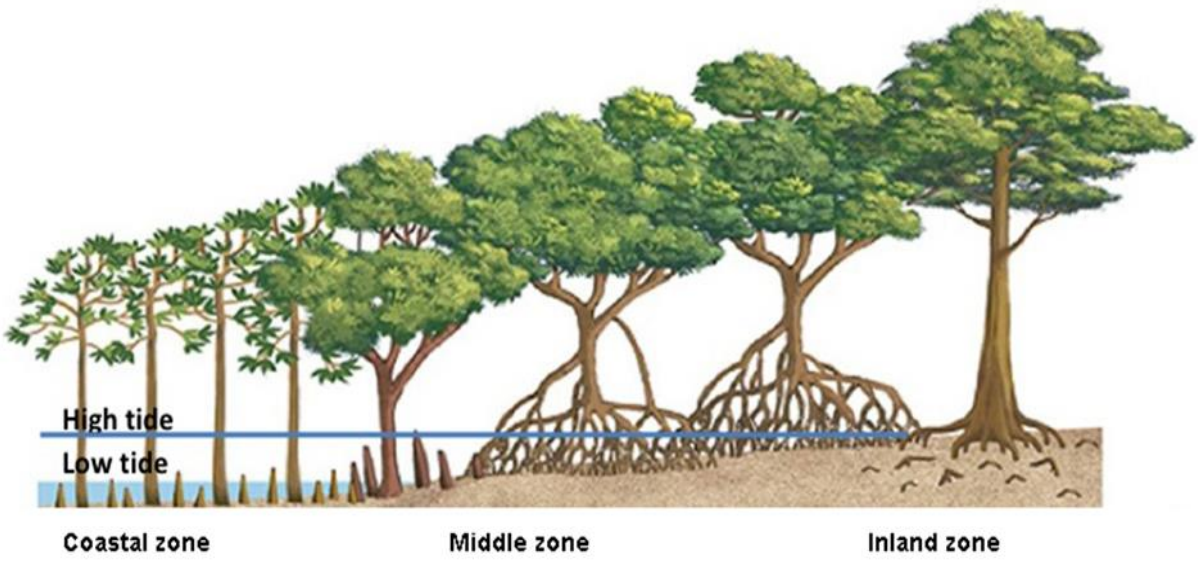

Figure 1: Typical structure of vegetation in mangrove forest

Adapted from: https://www.civilsdaily.com

Nowadays, UAV is a popular technology for monitoring forest management as well as estimating aboveground biomass and carbon stock. The application of UAV technology especially in the forest sector is increasing dramatically over the last decades (Anderson & Gaston, 2013). The UAV technique can take imagery of a relatively large area within a short duration while the cost is lower compared to other remote sensing techniques (Messinger et al., 2016; Dandois & Ellis, 2013). The UAV imagery has a very high spatial resolution which can be used to identify the small-scale objects in details (Dandois & Ellis, 2013). The 3D point clouds can be generated from the multiple partially overlapping images while applying the Structure from Motion (SfM) technique. The SfM technique is the process incomparable with stereographic analysis of aerial photographs to estimate the 3D structure of the object using a set of overlapping 2D images. The UAV can collect multiple images for certain objects, and the specific software can calculate camera position as well as the position of 3D points for overlapping, viewing rays of corresponding points (Westoby et al., 2012). Finally, it can generate 3D point clouds of the surface area. Digital Surface Model (DSM) and Digital Terrain Model (DTM) can be produced (see Figure 2) using 3D point clouds. Hence, Canopy Height Model (CHM) can also be generated by deducting DTM from DSM.

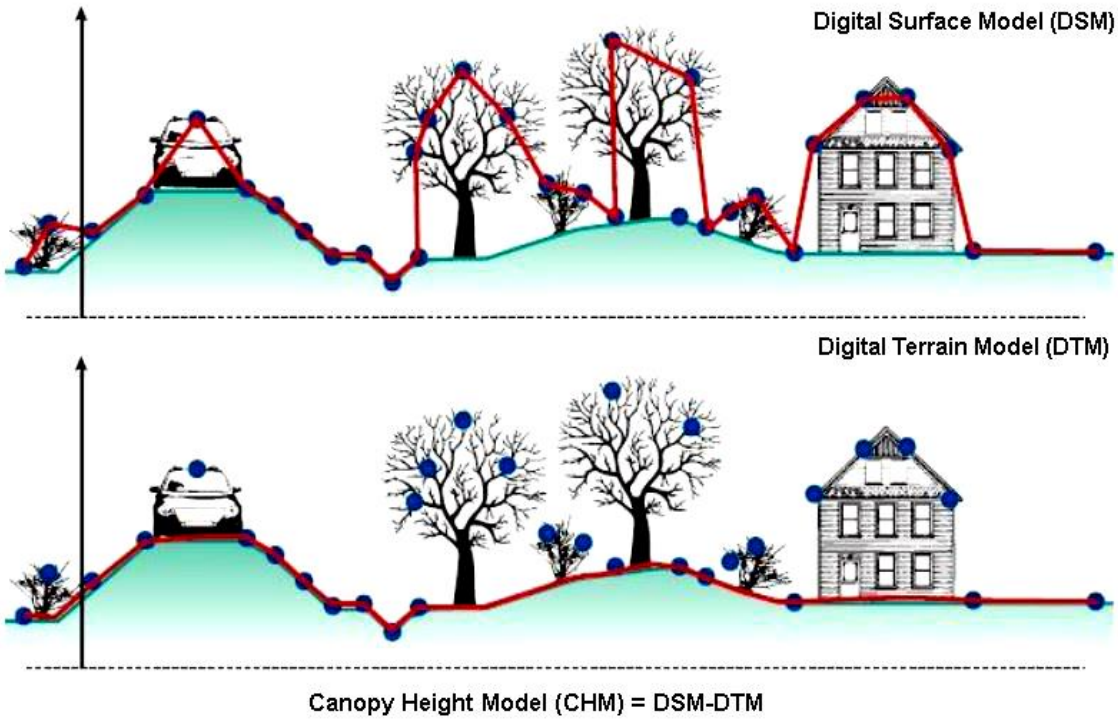

Figure 2: Digital Surface Model, Digital Terrain Model, and Canopy Height Model

Adapted from: Tolpekin (2012)

Another remote sensing instrument is the Terrestrial Laser Scanning (TLS), which is considered as one of the most useful and comparatively accurate techniques for measuring tree attributes in the forest. It is a ground-based active LiDAR instrument which uses laser beams to detect and measure surrounding objects and can generate 3D point clouds of the objects (Bu & Zhang, 2008). TLS can provide an enormous amount of high-resolution 3D information on vegetation biophysical parameters (Kociuba et al., 2014). It can be applied for measuring crown structure, leaf area index, leaf area distribution, canopy radiation, and gap fraction. TLS can use simple allometric and isometric equations for assessing biomass, growth monitoring and disturbance of vegetation structure (Newnham et al., 2015). It can measure high-resolution 3D spatial data of forest structures as a ground-based active remote sensor. TLS can measure lower canopy more precisely compared to other techniques including manual measurement and satellite images. However, the use of TLS in the mangrove forest for measuring biophysical parameters of trees is a big challenge. Because

the weight of TLS instrument is almost 25 kilograms which is difficult to move from one scan position to another on the wet and muddy ground. Moreover, TLS is applicable only plot-based which is considered as a drawback for this technique (Griebel et al., 2015).

Object-Based Image Analysis (OBIA) is an image segmentation and classification method which considers spatial features as objects instead of pixels (Kavzoglu & Tonbul, 2017). It is regarded as an ideal method for high-resolution imagery such as UAV images to delineate tree crowns and isolate species of the forest vegetation (Zhang et al., 2010). However, Yuheng and Hao (2017) claimed that a segmentation technique is challenging for identifying the image objects accurately through a segmentation process. Accurate tree crown segmentation is a prerequisite for accurate estimation of aboveground biomass and carbon stock (Mohan et al., 2017). The OBIA is considered as an effective method because of its ability to integrate spatial information along with higher accuracy for the processing of very high-resolution images (Zhang et al., 2010). Several studies have been conducted on the applicability of OBIA process. Among them, Blaschke (2010) preferred OBIA method for spatial planning as well as sustainable forest management. Chubey et al. (2006) found a robust relationship between high-resolution satellite images and OBIA on species classification, crown closure, and land cover types. Pham and Brabyn (2017) found a good result by applying OBIA techniques to monitor mangrove forest biomass changes in Vietnam. Karlson et al. (2014) stated that OBIA technique could provide higher accuracy for tree crown mapping in managed woodland.

In mangrove forests, several studies have been conducted for estimating aboveground biomass and carbon stock. Among them, satellite imagery or Airborne LiDAR data were mostly used. Some studies used UAV images for aboveground biomass and carbon stock estimation (Husson et al., 2014; Zahawi et al., 2015; Wahyuni et al., 2016; Messinger et al., 2016). However, no studies were found on the applicability of UAV and TLS for assessing aboveground biomass and carbon stock in the mangrove forest. In other studies, for example in tropical forest, UAV images were used to calculate height from CHM while UAV-DBH can be predicted from Crown Projection Area (CPA) based on a model developed from the relationship between CPA and field-measured DBH. On the other hand, TLS can estimate tree height and DBH of trees accurately from its 3D point clouds (Newnham et al., 2015). However, the use of TLS is difficult in the inaccessible area while UAV images can be collected easily from that area. Despite these drawbacks, both UAV and TLS are treated as a comparatively accurate technique for estimating aboveground biomass in the forest. This study will make a comparative assessment on the applicability of UAV and TLS for aboveground biomass and carbon stock estimation in a mangrove forest. The accuracy of UAV derived aboveground biomass depends to a large extent on the accuracy of image segmentation. Therefore, the study will also intend to evaluate two segmentation algorithms including multi-resolution and Simple Linear Iterative Clustering (SLIC) for accurate segmentation of tree crown on UAV imagery.

1.3. Research Objectives, Questions, and Hypothesis

1.3.1. Research Objectives

Overall Objectives

The overall objective of the study is to make a comparative assessment on the applicability of UAV and TLS for estimating aboveground biomass and carbon stock of mangrove forest in Mahakam Delta, East Kalimantan, Indonesia.

Specific Objectives

1. To evaluate the accuracy of tree height derived from CHM of UAV imagery compared to tree height resultant from TLS.

2. To evaluate two segmentation algorithms, more specifically multi-resolution and SLIC for accurate segmentation of tree crowns on UAV imagery.
3. To compare the accuracy of DBH estimated from CPA segmentation of UAV imagery and DBH derived from TLS with the field-measured DBH.
4. To assess the accuracy of aboveground biomass estimated from UAV images compared to aboveground biomass estimated from TLS point clouds.

1.3.2. Research Questions

1. How accurate is the tree height derived from CHM of UAV imagery compared to the tree height resultant from TLS?
2. Which algorithm provides higher segmentation accuracy of tree crowns on UAV imagery?
3. How accurate is the DBH derived from CPA segmentation of UAV imagery with the field-measured DBH?
4. How accurate is the DBH derived from TLS with the field-measured DBH?
5. How accurate is the estimated amount of aboveground biomass from UAV imagery compared to aboveground biomass estimated from TLS?

1.3.3. Research Hypothesis

1. H_0: There is no significant difference between tree height estimated from CHM of UAV imagery and tree height resultant from TLS.
   H_a: There is a significant difference between tree height estimated from CHM of UAV imagery and tree height resultant from TLS.
2. H_0: There is no significant difference between DBH derived from CPA segmentation of UAV imagery and field-measured DBH.
   H_a: There is a significant difference between DBH derived from CPA segmentation of UAV imagery and field-measured DBH.
3. H_0: There is no significant difference between TLS derived DBH and field-measured DBH.
   H_a: There is a significant difference between TLS derived DBH and field-measured DBH.
4. H_0: There is no significant difference between aboveground biomass estimated from UAV imagery and TLS data.
   H_a: There is a significant difference between aboveground biomass estimated from UAV imagery and TLS data.

1.4. Concepts of the Study

The conceptual diagram of the study is illustrated in Figure 3:

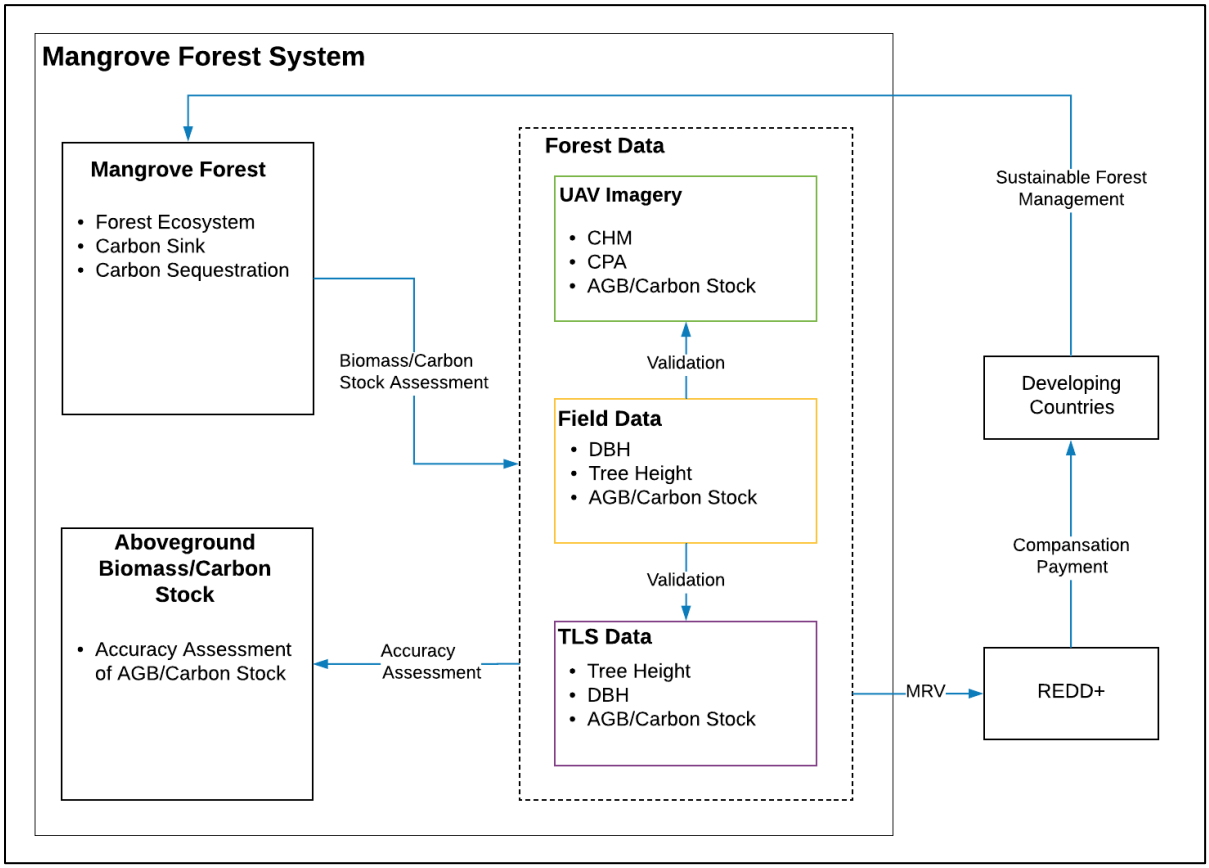

Figure 3: The conceptual diagram of the study

2. STUDY AREA, MATERIALS, AND METHODS

2.1. Study Area

2.1.1. Geographic Location

Indonesia is a Southeast Asian country located in between the Pacific, and the Indian Ocean which has almost 23 percent of the world's mangrove ecosystems (Giri et al., 2011). East Kalimantan is one out of 34 provinces in East Kalimantan. It has a total area of 129,066 square kilometers (49,832 sq. mi) and is the fourth largest province in Indonesia. The study is conducted in the mangrove forest of Mahakam Delta in East Kalimantan. The study area is situated between 0°32'18.20" S and 117°34'3.87" E. The size of the study area is approximately 47 hectares. In East Kalimantan, there are various mangrove swamp forests located far inland up to the Mahakam River (Choong et al., 1990). A simplified map of the study area is shown in Figure 4:

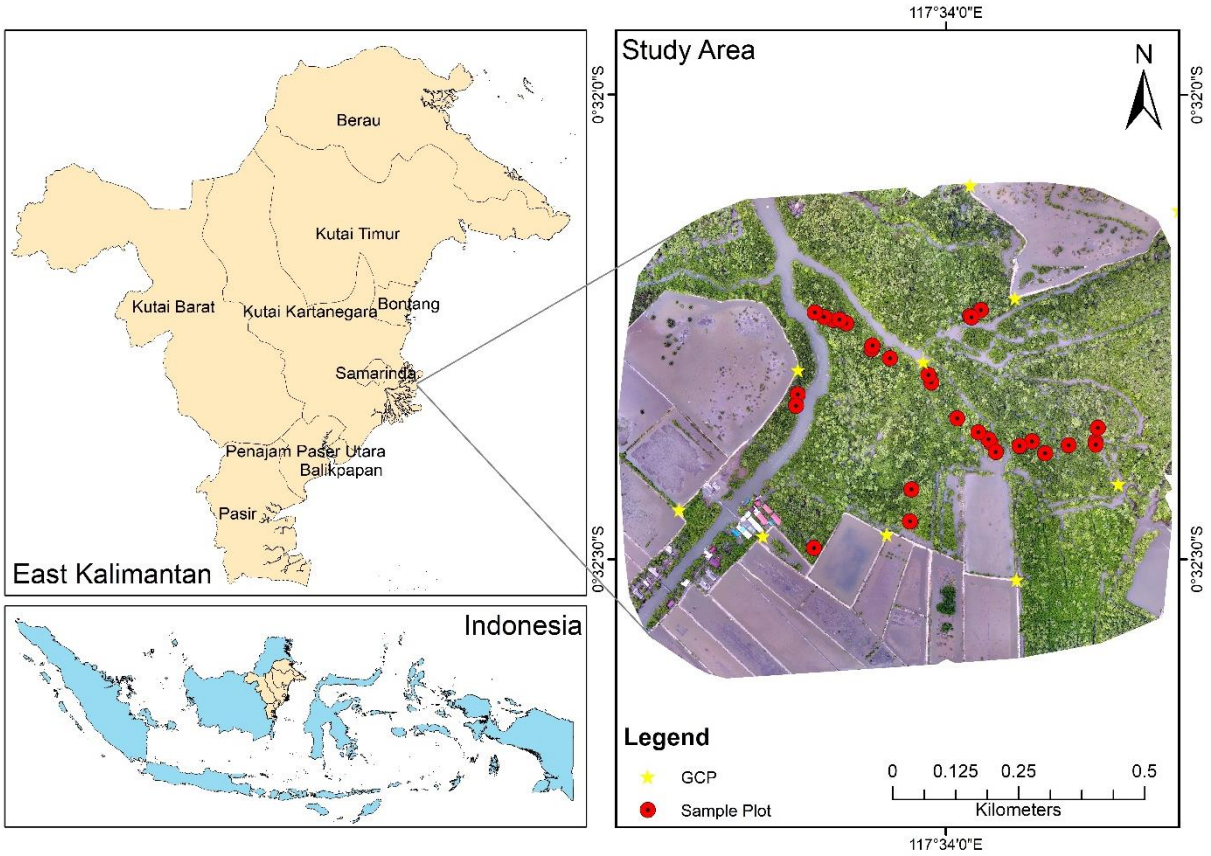

Figure 4: Map shown the study area located in East Kalimantan province in Indonesia

2.1.2. Climate

The climate condition of East Kalimantan is broadly classified into two seasons, i.e., wet season and dry season. The wet season duration is started from November to April while dry season begins from May to October. However, the climate is also influenced by monsoon due to located on the equator line. Nowadays the erratic situation is seen in East Kalimantan with sometimes heavy rain or sometimes no rain. The mean annual temperature in this area is 26.8°C while the average yearly rainfall is 1783 mm/year (BMKG, 2019).

2.1.3. Vegetation

The mangrove forest in Mahakam delta has diversified tree species. Among them, several tree species are considered as dominating species including *avicennia*, *rhizophora*, *bruguiera*, *xylocarpus*, and *sonneratia*, (FAO, 2018). Among those, *avicennia* is the most common genus in Mahakam Delta which is known as 'api api' means 'fires' in the Malay language. It is a flowering plant with aerial roots which is included under the family Acanthaceae. Generally, it is available in the intertidal area of estuarine. *Rhizophora* and *bruguiera* are another genus included in Rhizophoraceae family which are common in the mangrove forest. Like to *avicennia*, it is also found in the intertidal zone of estuarine. It has intricate roots with up to 2.5-meter-high from the ground. X*ylocarpus* is another dominating species under the Meliaceae family. *Sonneratia* is also found in mangrove which is included as a genus under Lythraceae family. It has spread aerial roots similar to *avicennia*. Among these species, three species including *avicennia*, *rhizophora* and *xylocarpus* were identified in the field.

The vegetation of the study area is mostly planted. The age of the trees is in between 12-15 years. The rooting system of these species has superficial anchorage for absorbing groundwater and oxygen (Priya et al., 2017). A diagram of the rooting and aeration system of the dominating species are illustrated in Figure 5. These dominant species have relative occurrence with ecological factors, e.g., salinity, soils, and tidal flows. However, the mixed association is found in some forest areas that indicate succession or zonation of tree species.

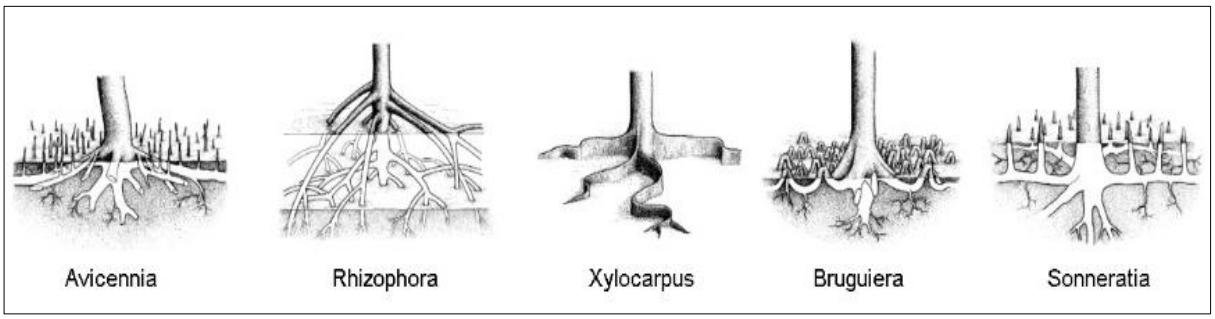

Figure 5: Rooting and aeration system of dominating species in mangrove forest

Adapted from: Göltenboth and Schoppe (2006)

2.1.4. Datasets

The study is based on three types of dataset including field-measured data, UAV and TLS data. Both field-measured and TLS data was collected from the same sample plots while UAV images were taken for the overall area. Later, these sample plots (same as biometric and TLS plot) were identified and extracted from the UAV images. The field-measured data and TLS data was collected between 14 to 22 October 2018, and UAV images were acquired on 21 December 2018. The list of datasets, source, and their characteristics are illustrated in Table 1:

Table 1: List of the dataset, their characteristics, and sources

SN	Data type	Characteristics	Data source
1.	Field-measured data	Biometric data of tree species, tree height, and DBH	Fieldwork (October 2018)
2.	TLS data	3D point clouds	Fieldwork (October 2018)
3.	UAV data	UAV-RGB images	Fieldwork (December 2018)

2.2. Materials

2.2.1. Field Equipment's and Instruments

There are different field equipment's were used during the field work to measure forest attributes including tree height, DBH, navigation, positioning, and setting sample plots. The list of field equipment required for the study is illustrated in Table 2:

Table 2: List of equipment's/instrument's used in the fieldwork and their application

SN	Equipment's/instruments	Application
1.	RIEGL VZ-400-TLS	Tree scanning within sample plots
2.	Phantom 4 DJI Drone	Acquisition of UAV-RGB Images
3.	Differential GPS	GCP Positioning
4.	Garmin eTrex GPS	Navigation and positioning
5.	Leica Disto D510	Tree height measurement
6.	Measuring Tape (30m)	Setting plot area
7.	Diameter Tape (5 m)	DBH measurement
8.	Data Recording Sheet	Data recording

2.2.2. Software and Tools

Different type of software and tools were used for processing and analyzing of UAV imagery, TLS, and field-measured data. The list of required software and tools are illustrated in Table 3.

Table 3: List of required software and tools

SN	Software and tools	Purpose/use
1.	Pix4D Mapper 4.2.27	Photogrammetric processing of UAV imagery
2.	RiSCAN Pro 2.5.2	TLS data processing and extraction of tree height and DBH
3.	eCognition Developer 9.4.0	Tree crown segmentation
4.	Cloud Compare 2.10	View point clouds
5.	ArcGIS 10.6	Data processing and visualization
6.	MS Office (Word, Excel) 2016	Thesis writing and statistical analysis

2.3. Research Methods

The research method is an essential step to response the research objectives and questions of the study. It comprises fieldwork design, sampling method, data collection, processing, data analysis, and findings. The methods used in this study are categorized into 05 (five) steps:

1. The first step was related to fieldwork for collecting the required data and information from the study area. The biometric, TLS and UAV data were collected from the fieldwork. A total of 30 sample plots were identified as purposively for collecting field data.

2. The second step was based on TLS data processing for co-registration and point clouds generation and extraction of all individual trees for measuring tree height and DBH. Aboveground biomass and carbon stock is estimated from TLS data using an allometric equation based on mangrove forest.

3. The third step was involved in the preparation and analysis of field-measured biometric data for estimating aboveground biomass and carbon stock. Biometric data is considered as ground truth for comparing the accuracy of tree height, DBH and aboveground biomass/carbon stock for UAV and TLS data.

4. The fourth step was related to processing and analyzing of UAV data for accurate CPA segmentation for estimating DBH and exploring different segmentation algorithms. The CHM was generated for estimating tree height of the sample plots. Aboveground biomass and carbon stock were calculated from the processed data using the specific allometric equation for mangrove forest.

5. The fifth and final step was based on assessing the accuracy of tree height, DBH and estimated aboveground biomass/carbon stock measured from TLS and UAV using field-measured data and allometric equation as the reference.

The key process of the methods followed in the study is illustrated in Figure 6:

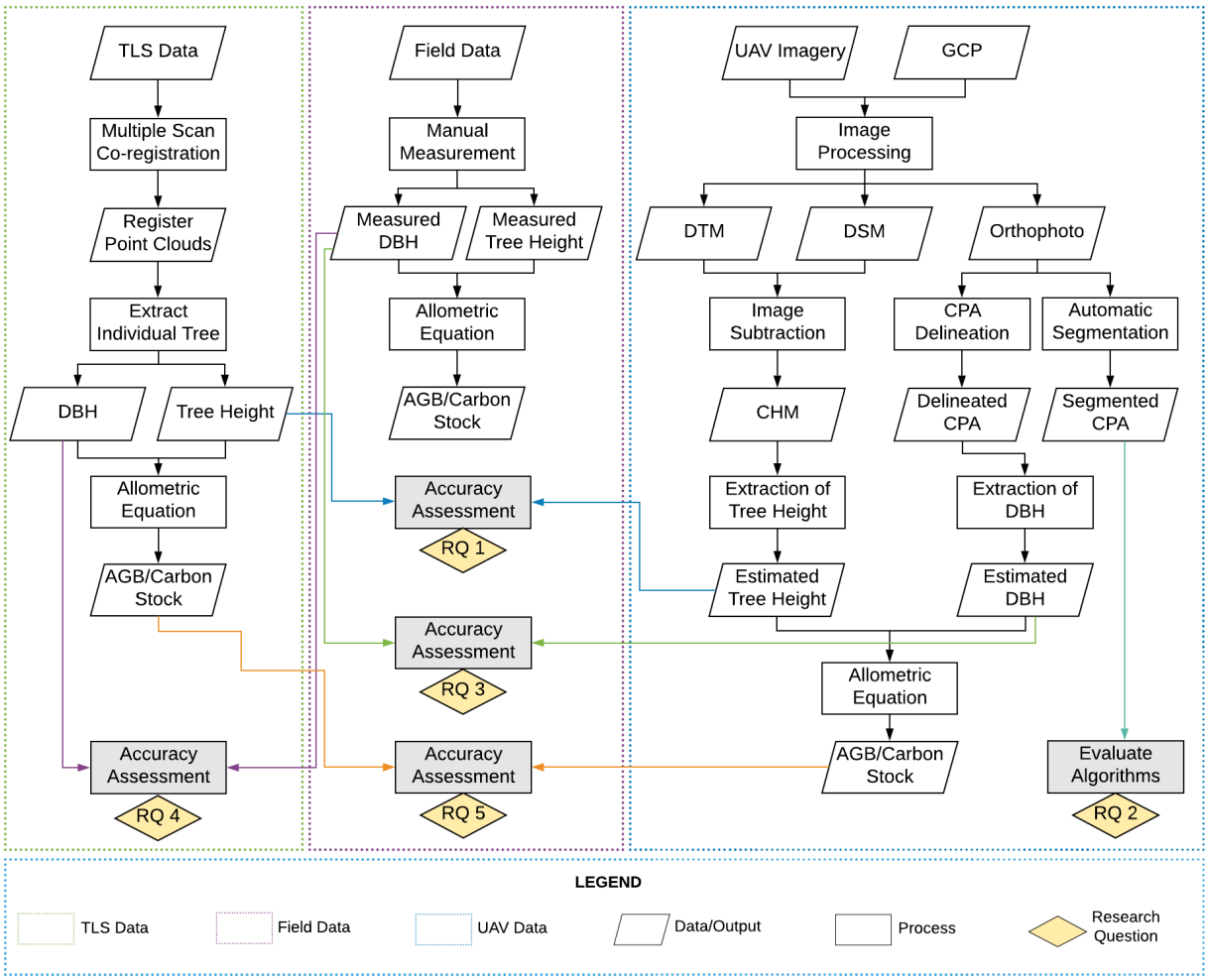

Figure 6: Workflow diagram

2.4. Field Work

2.4.1. Pre-Field Work

The pre-fieldwork activities include preliminary identification of sample plots, designing field data recording sheet, testing and practicing required equipment and instruments for fieldworks were carried out.

2.4.2. Sampling Design

The Sampling design is an essential part of a research study. A purposive sampling method was followed in this study. Mangrove forest is difficult for data collection due to wet ground and complex root system. Carrying a TLS in mangrove forest is very difficult for its weight (almost 25 kg). Therefore, the purposive sampling method was applied to ensure full utilization of the limited time and minimize the risks to collect data from inaccessible places.

2.4.3. Biometric Data Collection

Biometric data (tree species, height, and DBH) was measured by following the purposive sampling method. A Circular plot with 12.62 m radius (500 m^2) was used for both biometric and TLS data collections. A circular plot is convenient to identify in the field and can provide comparatively few errors (Newnham et al., 2015). Moreover, the circular plot is convenient and easy for Terrestrial Laser Scanning. The forest type and species distribution of the study area were almost homogeneous. So a circular plot with 12.62 m radius was used for minimizing the required time as well as labour.

DBH of all individual trees inside the plot was measured with a diameter tape at a 1.3m height from the ground. But some cases, the DBH was measured above the highest prop root for the species *rhizophora* which had longer roots above than 1.3m. During the field measurement, trees that have equal or more than 10cm DBH were considered for measurement. Because, trees with less than 10cm DBH have less contribution to aboveground forest biomass (Brown, 2002). Leica Disto D510 was used to estimate tree height in the field. The coordinates of each plot center and location of four individual trees were also measured using Garmin eTrex GPS. The specific coordinate system (WGS_1984_UTM_Zone_50S) was followed in this study. The species of trees inside the sample plots were collected from the fieldwork. The collected field-measured data (tree height, DBH and tree species) were recorded in data collection sheets. A photograph of biometric data collection is shown in Figure 7:

Figure 7: Biometric data collection during fieldwork

2.4.4. TLS Data Collection

The TLS (see Figure 8a) was used to scan the same 30 sample plots which were used for biometric data collection at the same time. It is generally mounted on a tripod on the ground. It emits a laser beam to the objects around the scanning positions and receives the reflected beams with 3D points of those objects. A

multiple scan approach was followed with 4 (four) different scan positions for each plot. Because four scan position (1 center and three outers) is easy to identify in the field as well as can reduce the scan duration compared to more scan position in each plot. The center position of each plot was used as the first scan position. The three other scan positions were set outside of the perimeter of the circular plot which is 15 m away from the center scan position with an angle of 120 degrees (see Figure 8b). Because scanning from center position with three other positions can scan the objects from a 360-degree angle and can generate comparatively accurate 3D point clouds of those objects. A multiple scan position can minimize the occlusion problem and can produce a sufficiently dense 3D point cloud that can be used as an accurate measurement of tree height and DBH (Liu et al., 2017).

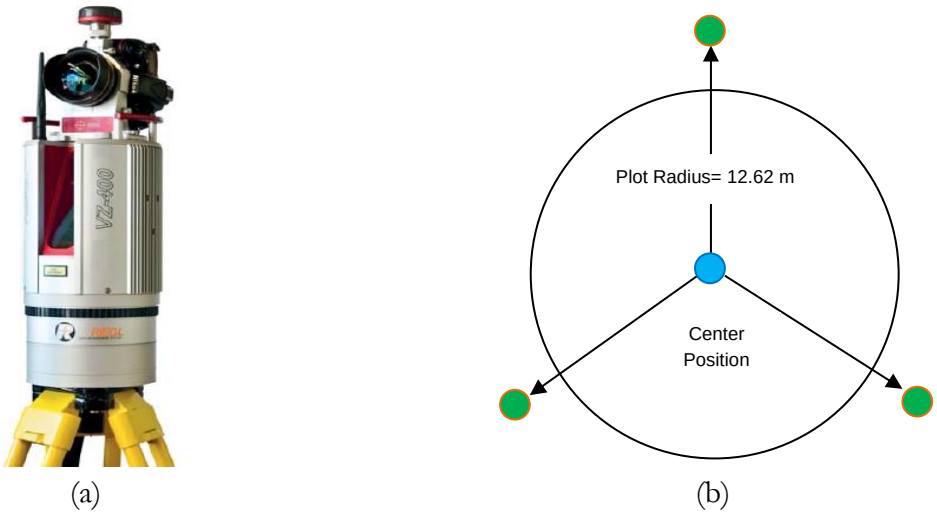

Figure 8: (a) RIEGL VZ-400 TLS ; (b) Diagram of TLS multiple scan position

Plot Preparation

Plot preparation is an integral part of TLS data collection. After selecting the center plot, a 12.62m radius was used to identify the plot area. The center plot should be located a minimum of one meter away from the nearest tree. All the trees inside the plot area should be visible from the center plot. The long and congested roots and branches which made an obstacle to clear view of the tree crown and the tree stem from scan position were cleared after setting the plot area. After that, trees inside the plot were identified and marked with tree tags for finding them in 3D point clouds. The trees which have at least 10 cm DBH were considered for measurement.

Setting the Reflectors

The retro-reflectors were used as tie points among the multiple scan positions. It improves the accuracy of the scanning as well as regulate the alignment of each scan. The reflectors are required for accurate co-registration of all scans for generating 3D point clouds. Both circular and cylindrical reflectors were used for scanning of each plot in the fieldwork. A total of 10-12 cylindrical reflectors were placed on the top of sticks for their visibility from all scan positions. Moreover, 8-10 circular reflectors were tagged (see Figure 9a) on the tree trunk facing to the center position with a clear view.

Figure 9: (a) Plot preparation before TLS Scanning and setting the reflectors; (b) TLS scanning

TLS Setup and Scanning

After plot preparation and setting the retro-reflectors, TLS was fitted on the tripod and leveling it manually by adjusting the tripod legs until getting an accurate level. After adjusting the level, TLS was started to scan for data collection (see Figure 9b).

2.4.5. Acquisition of UAV Imagery

A Phantom 4 DJI Drone with an RGB camera was used for UAV image acquisition in the study area. A UAV flight was operated for covering 0.47 ha area located in Tani Baru village in Mahakam Delta.

Flight Mission Planning

A total of two UAV flight plan fulfilling the research requirements were prepared to acquire UAV imagery covering 30 sample plots in the study area. The Pix4D capture android application was used to prepare these flight plan (see Appendix 1). The duration of the UAV flight mission was considered according to UAV battery capacity. The UAV flight parameters used for image acquisition is illustrated in Table 4:

Table 4: UAV flight parameters used for image acquisition

Parameter		Value
Flight Mission	:	Grid
Flight Speed	:	Moderate (10 m/sec)
Angle	:	90^0
Flight Height	:	164.58 – 172.63 meter
Front Overlap	:	85%
Side Overlap	:	75%
Image Size	:	4000x3000

Allocation of GCP Markers

A total of 8 (eight) GCP markers were allocated in the study area for identifying accurate spatial reference of 3D maps generated from the UAV images. Differential GPS was used to measure the accurate position of all GCPs in the study area. The GCP marker allocation and model of the Phantom 4 DJI drone are illustrated in Figure 10:

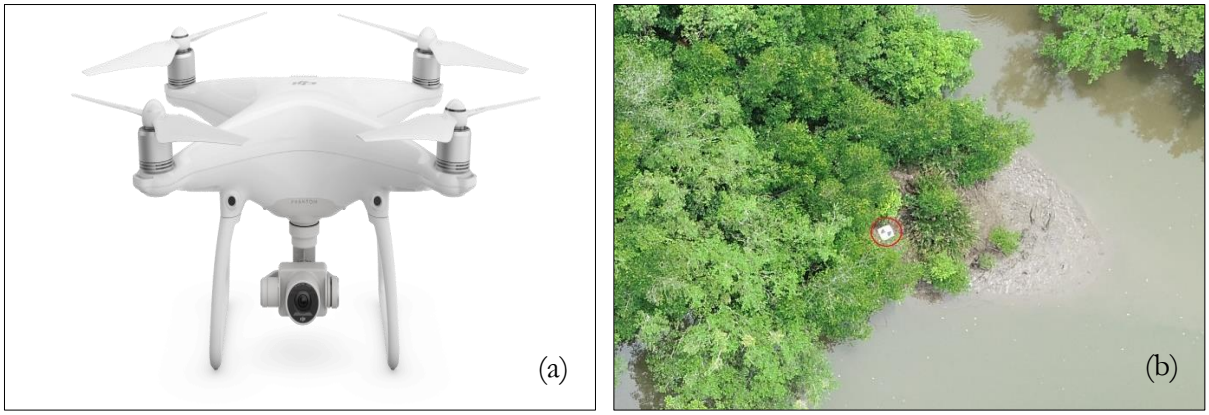

Figure 10: (a) A Phantom 4 DJI Drone; (b) A GCP marker placed in the study area

Source: www.dji.com

Data Acquisition

After allocating the GCP markers, Phantom 4 DJI UAV was flown for capturing images according to the defined parameters (speed, altitude, angle, and overlap) and stored the images in the memory card installed in the UAV.

2.5. Data Processing

2.5.1. Biometric Data Processing

The field-measured biometric data collected from the field was manually entered into a MS Excel sheet for data analysis. The biometric data that were collected from the fieldwork includes sample plot number, tree ID, tree species, tree height, DBH, the coordinate of 4 (four) individual trees and the plot center. The coordinates of all trees were not measured due to lack of time. However, measured four trees in each plot was well enough for identifying the location of all other trees in each plot in UAV orthophoto. A total of 30 sample plots data were collected during the fieldwork.

2.5.2. TLS Data Processing

RiScan Pro software was used to process field acquired TLS data. A process flow diagram for UAV image processing is illustrated in Figure 11.

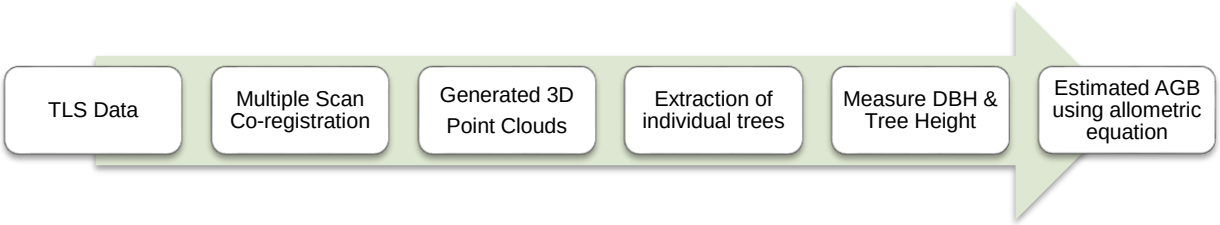

Figure 11: Process flow diagram for TLS data processing

Co-registration

Multiple scan co-registration is the first step of TLS data processing to merge several scans to generate 3D point clouds. The 3D point clouds were generated based on the tie points (retro-reflectors) that were visible from all the scan position in a plot (Lu et al., 2008). RiSCAN Pro software was used for co-registering the outer three scans to the center scan position in each plot. The 3D point clouds (black and white) of a sample plot are illustrated in Figure 12.

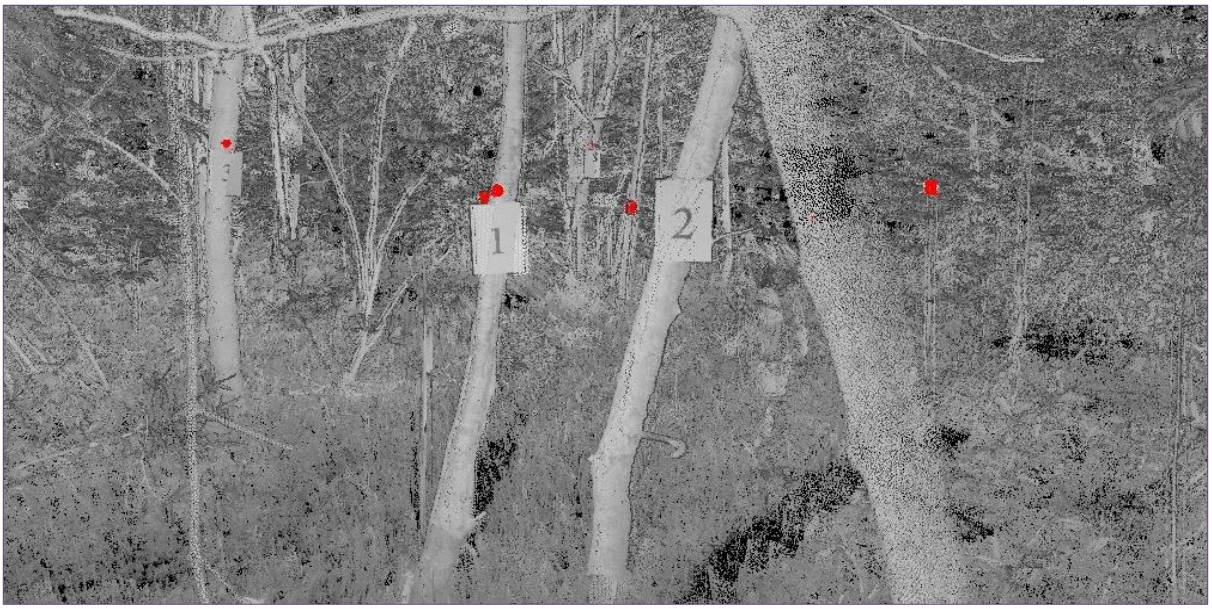

Figure 12: 3D point clouds after co-registration

Plot Extraction

Generally, 3D point clouds of the registered multiple scans covered a greater area than the plot area. After completing the co-registration, sample plots were extracted to exclude the point cloud outside the plot area. For extracting plots, the point cloud inside the plot area was filtered with 12.62 m radius using the range tool of RiSCAN Pro software. After that, all point clouds inside the plot radius was extracted and stored for measuring individual tree height and DBH.

Individual Tree Extraction

RiSCAN Pro software was used for extracting individual trees from the 3D point clouds generated from multiple co-registration. For the identification and separation of a particular tree, the extracted plot was displayed in true color mode for enhancing the visualization of the tree label. The individual trees were identified based on their color and shape with selection tools. After that, the trees were extracted and saved as new point clouds. An extracted individual tree in different angles is shown in Figure 13.

Figure 13: A tree extracted from TLS 3D point clouds seen from three different angles

DBH Measurement

The DBH can be measured using different methods including distance measurement tool and circle fitting. The circle fitting method is based on a circle center that can adjust to projected points of the stem for structuring a radius to measure DBH (Wu et al., 2018) while the distance measure tool calculates the distance between two points to measure DBH. The distance measure tool in RiSCAN Pro was used to measure DBH in this study. The DBH was computed at the height of 1.3m from the base (see Figure 14a and Figure 14b). The measured DBH of all individual trees were manually entered into MS Excel for analysis.

Tree Height Measurement

Similar to DBH measurement, the tree height was also measured with measure distance tools in RiSCAN Pro software. The highest point and lowest point of individual trees were identified and calculate the distance between two points. The resultant distance was considered as the tree height. The species *rhizophora* has a long and congested root system. Sometimes its aboveground roots are up to 2.5m high from the ground. The tree height of *rhizophora* was measured including the height of the root (see Figure 14c).

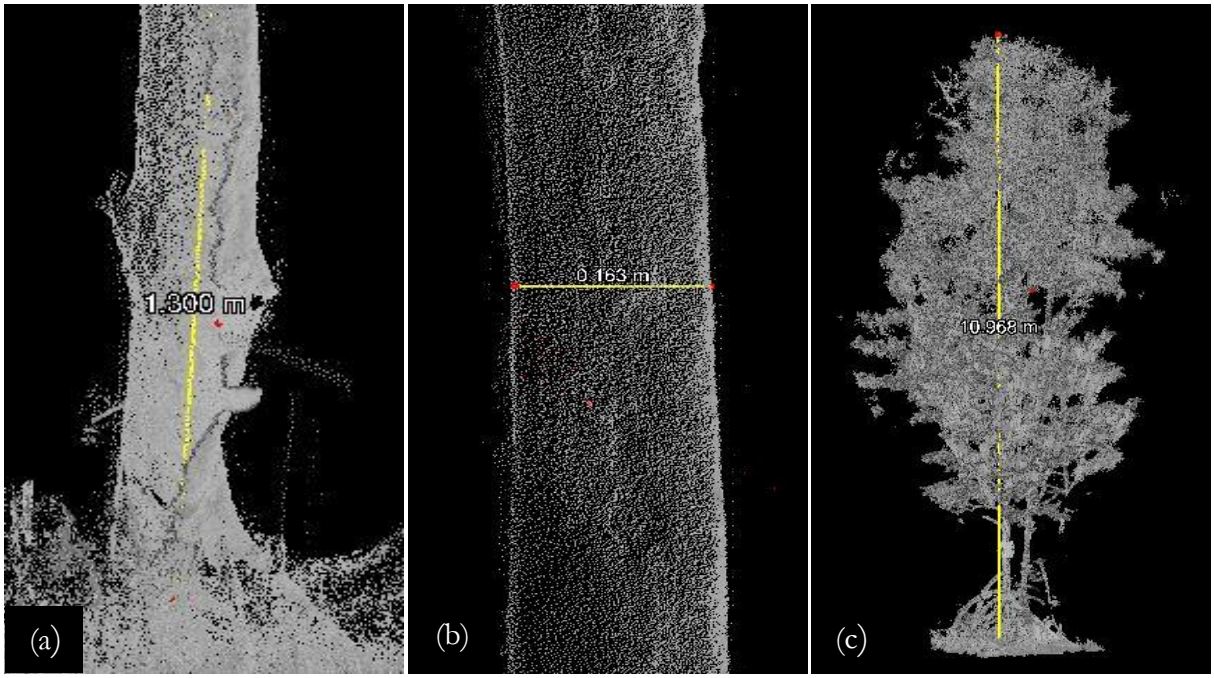

Figure 14: (a) Measurement of 1.3m height from ground; (b) DBH measurement; (c) height measurement

2.5.3. UAV Image Processing

The photogrammetric software Pix4D Mapper Pro was used to process the UAV images for generating DSM, DTM, and orthophoto. A process flow diagram for UAV image processing is illustrated in Figure 15.

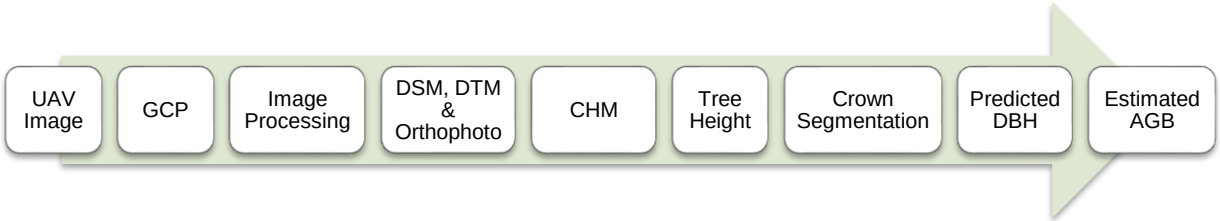

Figure 15: Diagram showing the processing steps of UAV images

The following steps were carried out for preparing and processing of UAV dataset:

Ground Control Points (GCPs)

GCP is a mark point on the ground which has known geographic coordinate. It is a prerequisite element for processing the UAV dataset. Before flying UAV, 8 (eight) GCP markers were placed on the ground for finding those markers from the UAV images (see Figure 16). The coordinates of the location of those markers were measured with Differential GPS before flying UAV in the study area. Because accurate GCPs are essential for geometric correction of the UAV images.

Image Orientation and Alignment

Image orientation is a vital step for processing of UAV dataset. In Pix4D Mapper, images need to be uploaded for setting orientation and alignment of the images. The software can automatically detect the camera position and alignment of each image. After that, recorded GCPs were imported in the software for geo-referencing and spatial accuracy of the UAV images.

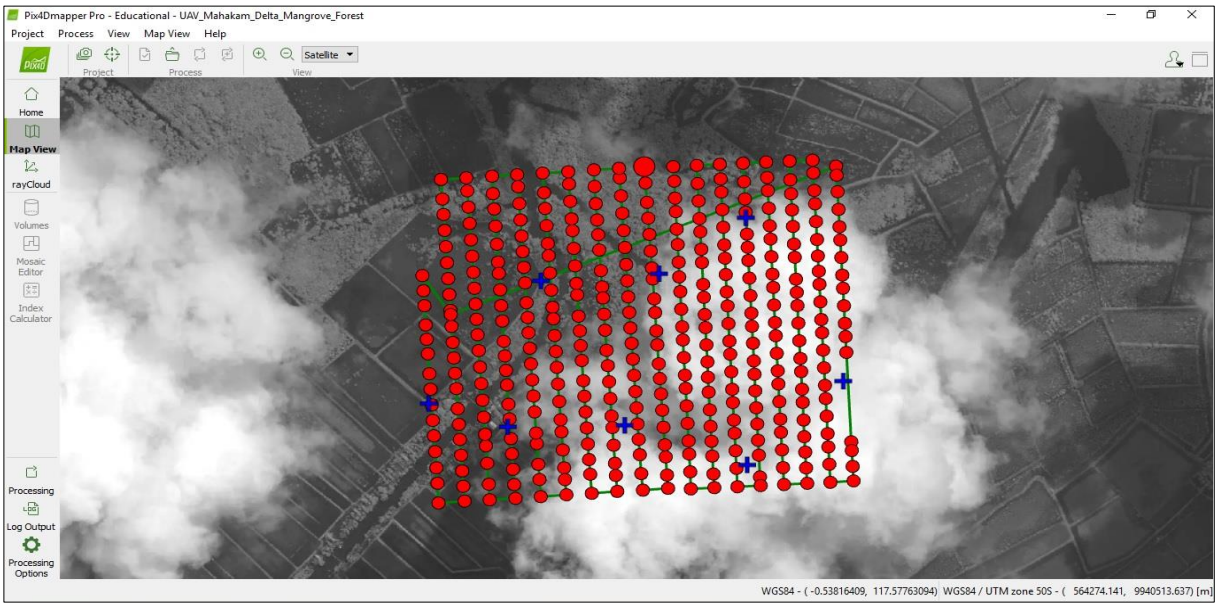

Figure 16: Image orientation and location of GCPs on a google earth basemap

Quality Check

After completing the image processing, a quality report was automatically generated to show the quality and accuracy of image processing. The quality report (see Appendix 2) shows the calibration, camera optimization, matching and geo-referencing accuracy of the processed image. In this study, all the images were calibrated where the mean RMS error is 0.047 meter. However, camera optimization has some error with 15.64% relative difference between initial and optimized internal camera parameters. Nevertheless, the overall quality of the processing is good enough for analyzing.

Generation of 3D Point Clouds

The 3D point clouds were generated using SfM technique where multiple partially overlapped UAV images generated the 3D structure of the objects (Prosdocimi et al., 2015). The point clouds are a 3D imaging of an object comprising millions of points having georeferenced information. Pix4D Mapper can automatically generate dense 3D point clouds (see Figure 17a) after adjusting image orientation and image alignment. The 3D point clouds are essential for generating DSM, DTM, and orthophoto (see Figure 17b) accurately. The average density of point clouds made from image processing was found 30.29 (per m^3) which indicates sufficient point clouds were created for getting good measurement data.

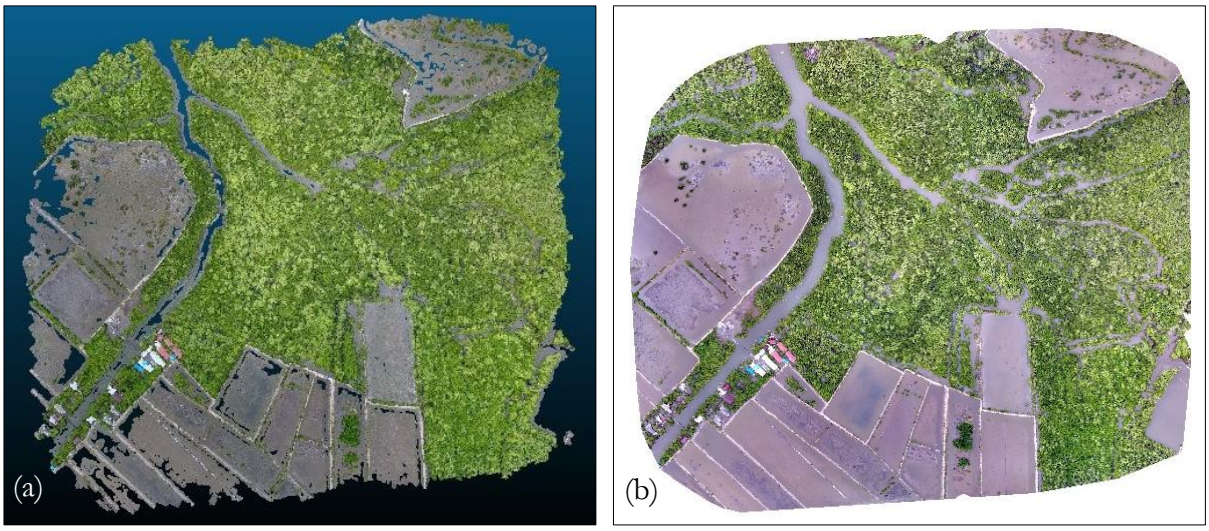

Figure 17: (a) Generated 3D point clouds of the study area; (b) Orthophoto of the study area

Generation of Digital Surface Model, Digital Terrain Model, and Orthophoto

After generating 3D point clouds, Pix4D Mapper can generate orthophoto, DSM and DTM. The orthophoto is a geometrically corrected image, made from multiple raw images using a uniform scale. The orthophoto was used to identify the crown projection area (CPA) for estimating DBH for individual trees. Besides, a DSM is a surface model considering the height value of objects while DTM is a terrain which represents the terrain heights originated on the surface of the earth (Wilson, 2016). The DSM and DTM are illustrated in Figure 18.

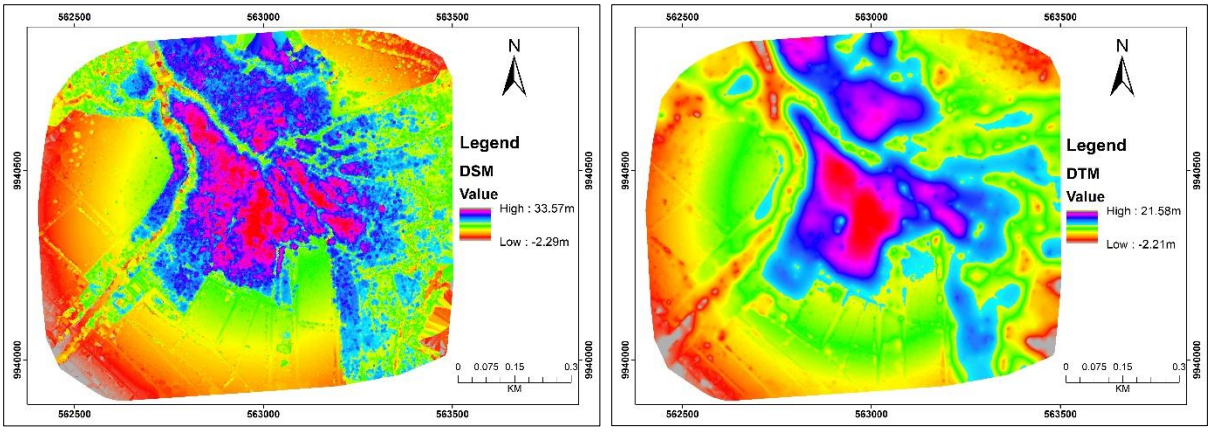

(a) (b)

Figure 18: (a) DSM of the study area; (b) DTM of the study area

The DSM and DTM show negative values here because the edges do not have sufficient image matching. Therefore, the point clouds were not densely generated in that area. As a result, the lowest values of DSM and DTM were calculated as negative. All of the sample plots are located around the centre position of the area (see Figure 4). So, the negative values do not affect the height measurement of the plot area.

Generation of Canopy Height Model and Extraction of Tree Height

The Canopy Height Model (see Figure 19) was generated by subtracting the DTM from the DSM. The Raster Calculator tool in ArcGIS was used to calculate the Canopy Height Model using DTM and DSM. The Canopy Height Model was used to estimate individual tree height from the sample plots. For tree height estimation, field-measured trees were identified and matched with corresponding tree crown in Canopy Height Model.

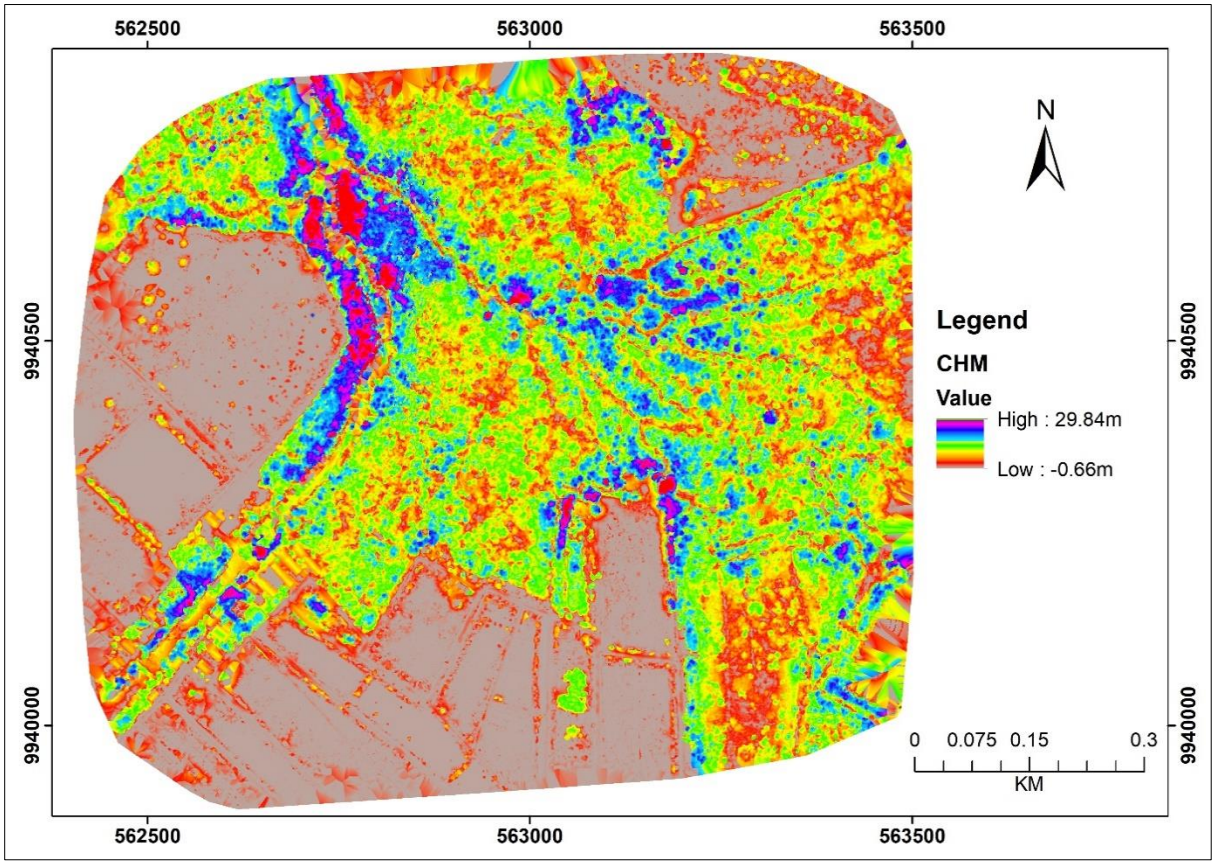

Figure 19: Generated Canopy Height Model (CHM) from DSM and DTM

Estimation of Crown Projection Area

The Crown Projection Area (CPA) is required to estimate DBH from UAV images. The CPA was digitized manually in ArcGIS based on the orthophoto. All the trees inside the plots were identified using field-collected coordinates of the trees and matching them with TLS images for higher accuracy. Moreover, manually digitized CPA was also used as reference data for evaluating the accuracy of multi-resolution and SLIC segmentation.

CPA Model Development and Validation

The manually digitized CPA were used to develop a model based on biometric DBH and CPA from UAV images. In the model, four different regression functions were compared, and the one with the highest accuracy was selected for predicting DBH for UAV data. The validation of the CPA model was conducted using a scatter plot for examining its consistency with biometric DBH as a reference.

2.5.4. Segmentation Algorithms

The image segmentation is the process of splitting the image into different segments based on the image pixels. The segmentation algorithms play a vital role for accurate segmentation of image objects. The segmentation process defines a homogeneous spatial object depending on its color, shape, and size. There are various segmentation algorithms can be used for image segmentation. Among them, multi-resolution, edge-detection, SLIC are widely used for their accuracy and simplicity. The segmentation algorithm is based on trial-and-error for adjusting different parameters to get a good result. In this study, multi-resolution and SLIC segmentation were used to evaluate the accuracy of the tree crown segmentation. Because multi-resolution segmentation is recognized as a perfect image segmentation algorithm especially for geographic objects (Witharana & Civco, 2014) while SLIC is a superpixel based algorithm which requires less

computational power and easy to implement (Achanta et al., 2012). The eCognition developer software was used for both multi-resolution and SLIC for accurate segmentation of individual tree crown from the UAV images.

Multi-Resolution Segmentation

The multi-resolution segmentation is one of the most widely used segmentation algorithms in OBIA. This segmentation is mainly based on three user-oriented parameters including scale, shape, and compactness. It is followed by bottom-up region based technique to segment images into different levels (Kavzoglu & Tonbul, 2018). This process is started by considering an individual pixel to create an image object, and subsequently, a couple of image objects are merged into a bigger one (Saha, 2008). The merging process is based on the local homogeneity to reduce the heterogeneity of the pixels of the same objects. This step ends when the user-defined threshold (scale parameter) is exceeded by the lowest increase of homogeneity (Baatz et al., 2000). The scale parameter is used to regulate the higher limit for an acceptable change of heterogeneity in the process of segmentation. The scale parameter can control the average size of the image objects. Consequently, a higher value of scale parameter can allow greater merging of the polygons. The multi-resolution segmentation also depends on the spatial continuity including texture and topology.

Multi-resolution segmentation was performed in eCognition 9.3.0 version using different resampled images. A high-resolution image could have some noises which are required to resample for aligning the input cells with the converted cell centers of desired resolution. The orthophoto generated from UAV-RGB images were resampled to 20cm, 25cm, and 30cm resolution using nearest neighbor method in ArcMap because tree crown segmentation performs better in 20cm or higher resolution (Ke & Quackenbush, 2011). The UAV derived 6.2cm resolution orthophoto was filtered using low pass (3-by-3) in ArcMap before resampling to lower resolution. Because image filtering can reduce image noises which can increase the accuracy of image segmentation. So, the filtered UAV-RGB resampled images were used as input layers in eCognition for achieving higher accuracy in segmentation of tree crowns.

The Estimation of Scale Parameter (ESP2) tool was used for defining scale in multi-resolution segmentation. This tool is an automated method for estimating scale parameter conforming to homogeneity in eCognition Developer (Csilik & Lang, 2016). It can compute local variances of image objects (mean standard deviation) for three (03) different level. Also, the local variances can be portrayed with the rate of change in a graph to illustrate the optimal scale parameter for multi-resolution segmentation (Drăguț et al., 2010). Figure 20 shows the estimation of scale parameter using ESP2 tool.

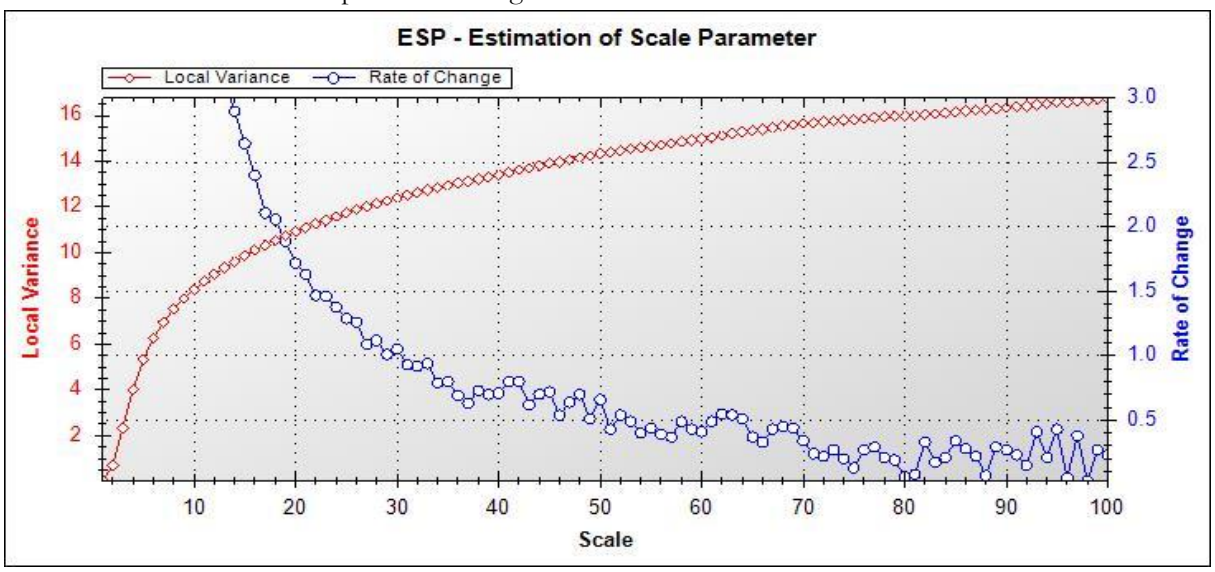

Figure 20: Estimation of scale parameter in ESP2 tool

In Figure 20, the blue line (downward slope) shows the rate of change of image objects while the red line (upward slope) indicates local variance of the image pixel. The graph shows that the local variance moves upward due to the higher resolution image while the rate of change moves downward gradually for the image scene (Drăguţ et al., 2010). The graph also indicates that the scale parameter fitted best with value 20 for multi-resolution segmentation in this study.

The step size level (three levels) parameters were checked with different values for getting higher segmentation accuracy. Also, other parameters including shape, and compactness were used for adjusting better segmentation. The parameters including shape and compactness are required to adjust before performing segmentation. The scale parameter defines the highest acceptable heterogeneity in segmented objects while the shape determines the extent of spectral values of image layer influence the heterogeneity. The compactness defines the concentration of the segmented objects. After adjusting the parameters (scale=20, shape=0.3 and compactness=0.7), shadow masking was performed to separate trees from shadows, open space, and waterbodies based on the brightness value of the pixels. The watershed transformation was executed for splitting the cluster of tree crowns. It considers the image as a topographic surface which consists of local maxima, watershed lines and catchment basins (Chen et al., 2004). The remove objects algorithm was also performed for removing undesired objects from the image (see Appendix 3 for ruleset). Finally, the best segmentation was exported as a shape file as 'polygon smoothed' for evaluating segmentation accuracy in ArcMap. The output of the multi-resolution segmentation is illustrated in Figure 21.

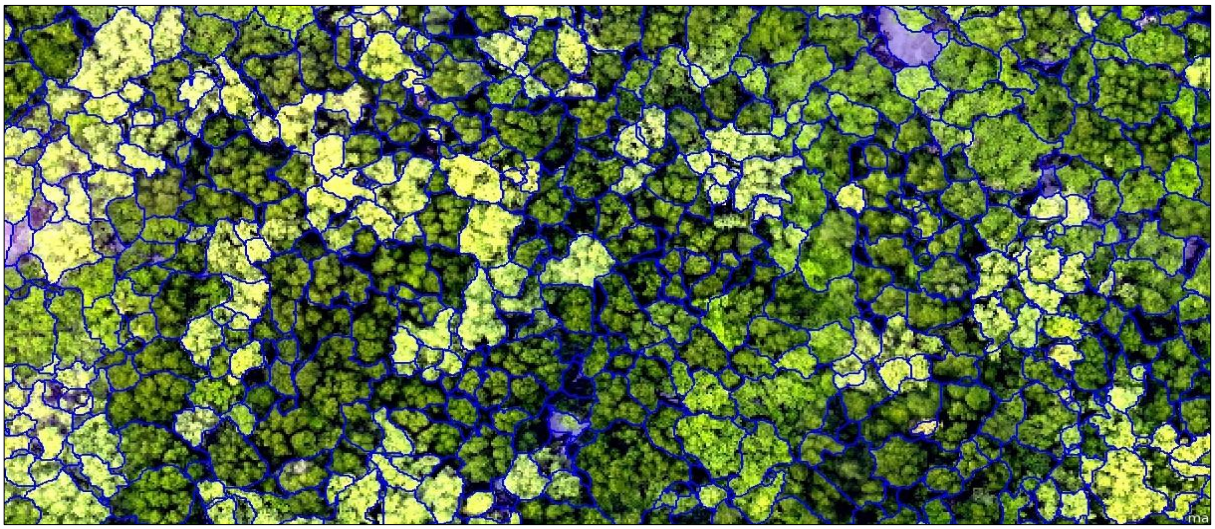

Figure 21: Multi-resolution segmentation in 25cm resolution filtered UAV-RGB image

SLIC Segmentation

The Simple Linear Iterative Clustering (SLIC) is a superpixel based segmentation algorithm which needs less computational power. This algorithm can make superpixels by color similarity and proximity of the image plane. As a gradient centric algorithm, it can adopt k-mean cluster for generating identical superpixels based on object color (Crommelinck et al., 2017) and can segment any part of an image according to the image background layer (Dhanachandra et al., 2015). SLIC segmentation is based on assessing two parameters including 'k-parameter' which upholds the size of superpixels and 'm-parameter' that maintain similarity and edge of superpixels (Yuan & Hu, 2016). The difference between multi-resolution and SLIC segmentation is that multi-resolution segmentation is a bottom-up region based technique where it starts from an individual pixel to form a bigger one and can segment images into several levels. On the contrary, SLIC can generate the desired number of similarly shaped superpixels (Kavzoglu & Tonbul, 2018).

SLIC can also be conducted in other software like eCognition, R, MATLAB, GRASS GIS, and QGIS. The eCognition Developer was used to perform SLIC segmentation in this study. A filtered UAV-RGB image (low pass 3-by-3) with different resampled resolution (20cm, 25cm, and 30cm) images were used. Different parameters, i.e., iterations, region size, minimum element size, and ruler were used for adjusting the accuracy of segmentation. The iteration is the repetition of the process while the minimum element size defines the percentage of superpixels that would be assimilated to a greater one. The region size represents an average superpixel size, and the ruler is used for smoothening of the superpixels. The trial-and-error approach was applied for adjusting the parameters (iterations=50, minimum element size=10, region size=30, and ruler=50), and shadow masking was used to delineate trees from shadows based on pixel brightness value. Like multi-resolution segmentation, an algorithm like watershed transformation and remove objects were also used for removing undesired objects (see Appendix 4 for ruleset). Finally, the best segmentation was exported as a shape file with 'polygon smoothed' for estimating segmentation accuracy in ArcMap. The output of the SLIC segmentation is shown in Figure 22.

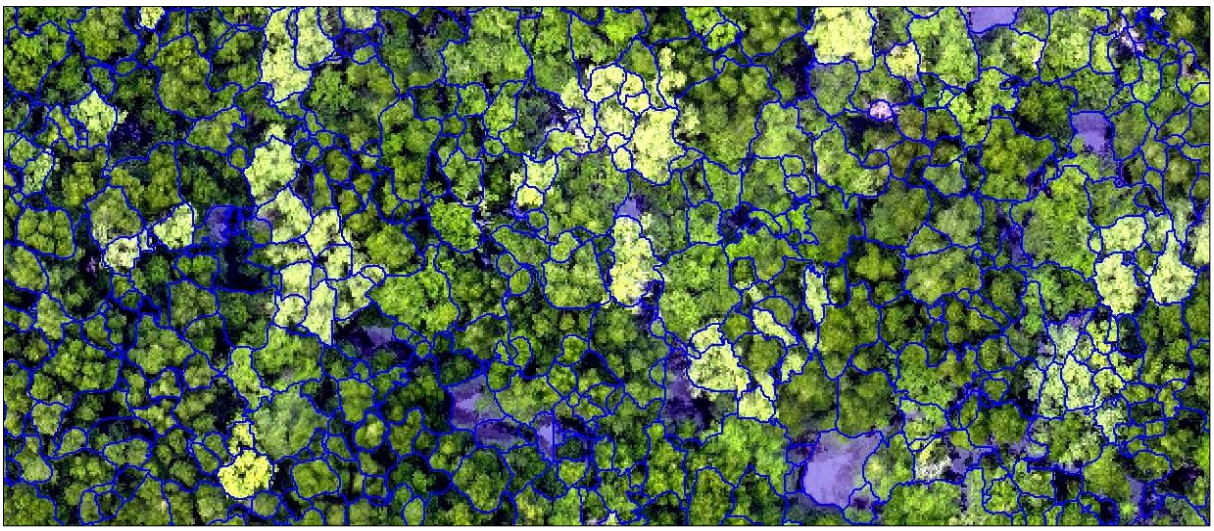

Figure 22: SLIC segmentation in 20cm resolution UAV-RGB image

2.5.5. Accuracy Assessment of Segmentation Algorithms

The accuracy assessment of segmentation was conducted for evaluating multi-resolution and SLIC segmentation. The assessment can be carried out following the empirical statistical approach including discrepancy methods and goodness of fit (Zhang et al., 2008). The discrepancy method is based on the matching of target objects with reference objects (manually digitized tree crown) for identifying mismatches. The goodness of fit method assesses homogeneity of intra-segments, heterogeneity of inner segments and the characteristics of the shapes (Lübker & Schaab, 2009).

The evaluation of segmentation accuracy depends on the variance between two different segmentation of the same feature. The difference is the consequences of error for segmentation. The segmentation error is related to underestimation or overestimation of CPA. In this study, the segmentation accuracy was calculated using area-based measurement. Because the study area was consists of 30 isolated sample plots identifying by purposive sampling. So, it was easier to compare the manually digitized polygons (reference polygons) with segmented polygons using area-based measurement. The following equations formulated by Clinton et al. (2010) were used in this study to assess the accuracy of multi-resolution and SLIC segmentation.

Equation 1: Calculation of under segmentation

$$\text{Under segmentation} = 1 - (\text{area}(ATi \cap ARi)/\text{area}(ARi)) \quad \ldots Equation\ (1)$$

Equation 2: Calculation of over segmentation

$$\text{Over segmentation} = 1 - (\text{area}(ATi \cap ARi)/\text{area}(ATi)) \quad \ldots Equation\ (2)$$

Where, $area(ATi \cap ARi)$ = Correctly segmented area of the reference polygon
ATi = Area of targeted polygons (automatic segmented polygons)
ARi = Area of reference polygons (manual delineated polygons)

Equation 3: Calculation of error

$$\text{Error} = \sqrt{((\text{over segmentation}^2 + \text{under segmentation}^2)/2)} \quad \ldots Equation\ (3)$$

The accuracy assessment of both multi-resolution and SLIC segmentation was conducted in ArcGIS 10.6 with 3 (three) resampled UAV-RGB images including 20cm, 25cm and 30cm resolution. The accuracy was assessed based on manually digitized CPA (reference polygons) with automatically segmented polygons (targeted polygons) from multi-resolution and SLIC segmentation. For doing this, all manual polygons of 30 sample plots were merged into a shapefile. Then a spatial join between manually digitized polygons and segmented polygons were conducted and separated the polygons which have to join count value greater than 0 (>0) by using select by attribute option. This process identified only those polygons which have a spatial connection with manually digitized polygons. These identified polygons were considered as targeted polygons. Hence, an intersection process was carried out to determine the intersection between manually delineated polygons and automatically segmented polygons. Then the area of manually digitized reference polygons (ARi), segmented polygons (ATi) and their intersected area(ATi∩ARi) were calculated. The under segmentation and over segmentation was also estimated for calculating the error. Finally, the percentage of accuracy was calculated for both multi-resolution and SLIC segmentation.

2.6. Data Analysis

2.6.1. Allometric Equation

The allometric equation is a commonly used method to estimate aboveground biomass using forest biophysical parameters including tree height and DBH. Several researchers have developed some equations for simplifying biomass estimation using wood density, tree height and DBH (Nam et al., 2016). However, site-specific allometric equation needs to be applied for accurate estimation of aboveground biomass (Basuki et al., 2009). Among different allometric equations for estimating aboveground biomass, the equation developed by Chave et al. (2005) specified for mangrove forest is comparatively simple and renown to estimate aboveground biomass in a mangrove forest.

Equation 4: Allometric equation for AGB estimation

$$AGB_{est} = \exp(-2.977 + in(\rho D^2 H)) \equiv 0.0509 x \rho D^2 H \quad \ldots Equation\ (4)$$

Where, AGB_{est} = Estimated aboveground biomass in kg;
D = Tree DBH in cm (measured at 1.3m from ground but some cases at above prop root);
H = Tree Height in meter (measured from the ground);
p = Wood Specific Gravity in g/c3.

For estimating carbon stock, a carbon fraction (CF) of 0.47 (IPCC, 2006) was used to calculate carbon stock using aboveground biomass.

Equation 5: Carbon stock calculation from AGB

$$C = AGBxCF \ \ldots\ldots\ldots\ldots\ldots\ldots Equation\ (5)$$

Where, C = Carbon Stock,
AGB = Aboveground Biomass, and
CF = Carbon Fraction

2.6.2. Aboveground Biomass and Carbon Stock Estimation

Aboveground biomass and carbon stock was estimated using three different datasets including field-measured biometric data, TLS and UAV data. The above-mentioned specified allometric equation (see Equation 4) developed for mangrove forest, was applied to calculate AGB in this study. Besides, specific wood density for specific tree species provided by ICRAF (2018) was also used to estimate aboveground biomass accurately. The specific wood density used for *avicennia*, *rhizophora* and *xylocarpus* species are 0.6987 g/cm3, 0.9204 g/cm3 and 0.6721 g/cm3 respectively.

a. Aboveground Biomass and Carbon Stock Estimation using Biometric Data

The field-measured tree height and DBH were used to estimate aboveground biomass and carbon stock from field-measured. The abovementioned allometric equation was applied to calculate the AGB from biometric data. The carbon stock was also estimated from aboveground biomass.

b. Aboveground Biomass and Carbon Stock Estimation using TLS

The tree height and DBH measured from TLS point clouds were used to estimate aboveground biomass and carbon stock for TLS dataset.

c. Aboveground Biomass and Carbon Stock Estimation from UAV

The tree height extracted from UAV-CHM and DBH predicted from UAV-CPA were used for estimating aboveground biomass and carbon stock for UAV dataset.

2.6.3. Statistical Analysis

The regression analysis is a statistical process to determine the relationship between the dependent and independent variables. It helps to identify how dependent variable changes while the value of the independent variable is varied (Domingo et al., 2017). Besides, it is an essential step for modeling the relationship for two different types of data. The regression analysis is used to make a relationship between tree height and DBH measured in TLS and tree height and DBH estimated in CHM of UAV imagery. Furthermore, this analysis is also carried out to make a relationship between aboveground biomass estimated from TLS and UAV data. The RMSE (Root Mean Square Error) and the coefficient of determination (R^2) were also used for signifying the relationship among the variables.

Equation 6: Calculation of RMSE

$$RMSE = \sqrt{\frac{\sum_{i=1}^{n}(X_{obs} - X_{\mathrm{mod}})^2}{n}} \quad \ldots\ldots\ldots\ldots\ldots\ldots Equation\ (6)$$

Where RMSE = Root Mean Square Error
X_{obs} = Observed value of the dependent variable
X_{mod} = Modelled value of the dependent variable
n = Number of sample size

Equation 7: Calculation of %RMSE

$$\%RMSE = RMSE * n * 100 / \sum X_{obs} \ldots\ldots\ldots\ldots\ldots\ldots Equation\ (7)$$

Where %RMSE = Percentage of Root Mean Square Error
n = Number of sample size
X_{obs} = Observed value of the dependent variable

3. RESULTS

3.1. Descriptive Statistics

A descriptive statistics of tree height and DBH extracted from the TLS, UAV and field-measured biometric data were executed to identify the nature and extent of those data. The biometric data was analyzed to identify the distribution of tree species, DBH and tree height. The analytical results are described below:

3.1.1. Species Distribution

A total of 3 (three) tree species were identified in the sample plots area. The dominant species were *avicennia* and *rhizophora*. Among 893 trees, *avicennia* is 467, *rhizophora* is 415 and rest 11 is identified as *xylocarpus*. Figure 23 shows the distribution of the species identified in the field.

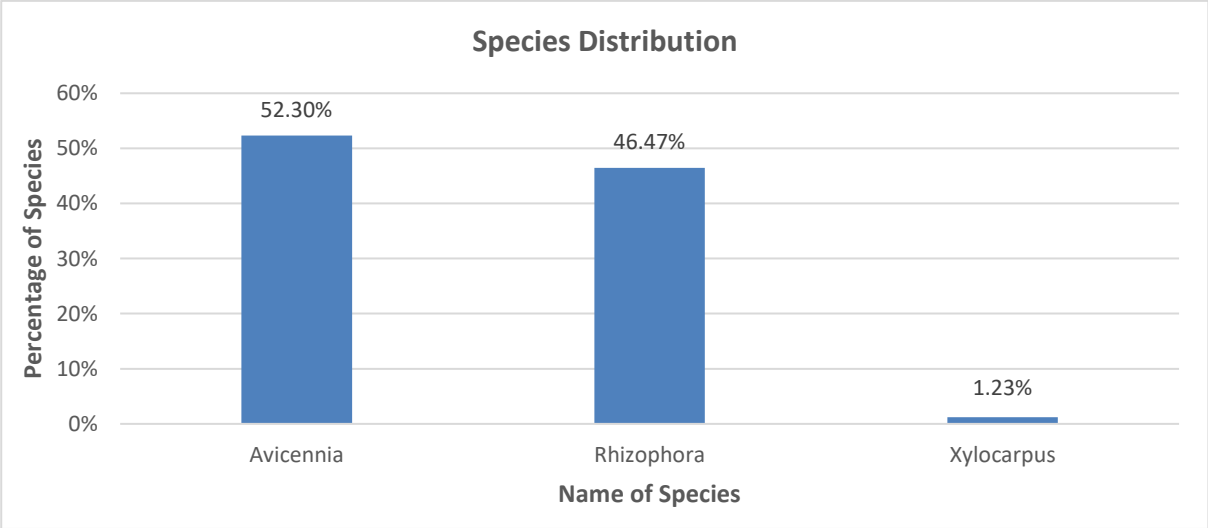

Figure 23: Distribution of different tree species

3.1.2. Tree Height

The tree height of the field-measured biometric, TLS and UAV data were analyzed and summarized. It is estimated that field-measured biometric tree height is comparatively less than TLS and UAV estimated tree height. The average tree height from biometric data is 13.29m while the TLS and the UAV estimated height is 14.75m and 14.03m respectively. The calculated standard deviation of biometric, TLS and UAV are 2.89, 2.81 and 2.93 respectively. The summary statistics of tree height is illustrated in Table 5.

Table 5: Summary statistics of tree height measured from biometric, TLS and UAV data

	Biometric	TLS	UAV
Mean	13.29	14.75	14.03
Standard Error	0.10	0.09	0.10
Median	12.60	14.49	13.71
Mode	12.60	15.95	14.67

	Biometric	TLS	UAV
Standard Deviation	2.89	2.81	2.93
Sample Variance	8.33	7.87	8.58
Kurtosis	-0.11	-0.05	0.55
Skewness	0.63	0.42	0.66
Range	15.72	15.69	16.73
Minimum	6.87	7.23	6.66
Maximum	22.59	22.92	23.40
Sum	11867.15	12891.75	12526.26
Count	893	874	893

3.1.3. Diameter at Breast Height (DBH)

The DBH of the field-measured biometric, TLS and UAV data were analyzed and summarized. In biometric data, all 893 trees were analyzed while 19 trees were missing in TLS data. It is observed that biometric measured DBH was comparatively higher than TLS and UAV estimated DBH. The average DBH of biometric data is 16.05cm while TLS and UAV have 16.02cm and 16.04cm respectively. The standard deviation of biometric, TLS and UAV are 8.84, 8.82 and 8.64 respectively. The summary statistics of tree height is illustrated in Table 6.

Table 6: Summary statistics of DBH measured from biometric, TLS and UAV data

	Biometric	TLS	UAV
Mean	16.05	16.02	16.04
Standard Error	0.30	0.30	0.29
Median	13.30	13.23	13.65
Mode	10.00	10.00	11.48
Standard Deviation	8.84	8.82	8.64
Sample Variance	78.09	77.86	74.56
Kurtosis	28.31	27.13	41.06
Skewness	4.24	4.16	5.37
Range	98.90	97.00	98.36
Minimum	10.00	10.00	9.06
Maximum	108.90	107.00	107.42
Sum	14334.02	13997.69	14319.46
Count	893	874	893

3.2. The Accuracy of Tree Height Extracted from UAV-CHM Compared to Tree Height Measured from TLS 3D Point Clouds

The accuracy of UAV-CHM extracted tree height compared to tree height measured from TLS point clouds (as reference height) was conducted using a scatter plot based on these two tree heights. A total of 874 trees were considered for evaluating the accuracy of tree height extracted from UAV-CHM compared to tree height extracted from TLS point clouds. The result (see Figure 24) shows that there is a strong correlation of 0.90 with R^2 (coefficient of determination) 0.82 (see Table 7). The Root Mean Square Error (RMSE) is 1.44m that is equivalent to 9.75% of total tree height measured from TLS point clouds.

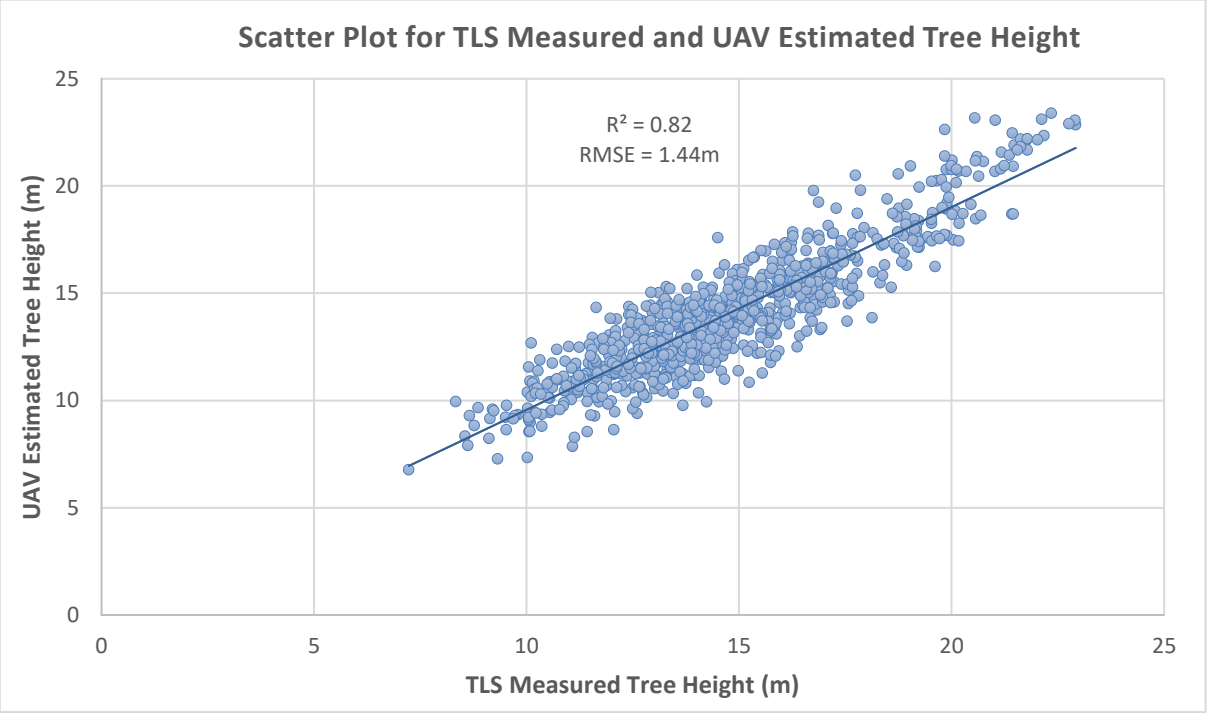

Figure 24: The relationship between tree height extracted from UAV-CHM and TLS point clouds

Table 7: Summary statistics of tree height extracted from UAV-CHM and TLS point clouds

Pearson Correlation	**0.90**
R Square	0.82
Adjusted R Square	0.82
Standard Error	1.25
Observations	874

F-test for Two-Sample Variance

The F-test was checked to find out if there equal or unequal variance of two datasets (UAV-CHM and TLS height) for deciding which t-test need to be used for assessing the difference between two datasets. The F-test (see Table 8) indicates an equal variance (F-Stat<F-Critical (P>0.05) between tree height extracted from UAV-CHM and TLS point clouds. So t-test assuming equal variance was carried out for identifying if any significant difference between two datasets.

Table 8: F-test for two sample variance

	UAV Height	***TLS Height***
Mean	14.05	14.75
Variance	8.59	7.87
Observations	874	874
df	873	873
F-Stat	1.09	
P(F<=f) one-tail	0.09	
F-Critical one-tail	1.12	

Decision: F-Stat<F-Critical (P>0.05): Equal variance

T-Test Assuming Equal Variance

A T-test was conducted to check is there any significant difference between UAV and TLS measured tree height. The test shows (see Table 9) that there is no significant difference (t-Stat<t-Critical at P>0.05) between tree height measured in UAV-CHM and TLS point clouds.

Table 9: T-test assuming equal variance for UAV and TLS measured tree height

	UAV Height	*TLS Height*
Mean	14.05	14.75
Variance	8.59	7.87
Observations	874	874
Pooled Variance	8.23	
Hypothesized Mean Difference	0	
df	1746	
t-Stat	-5.07	
P(T<=t) one-tail	1.95E-08	
t Critical one-tail	1.64	
P(T<=t) two-tail	4.39E-07	
t Critical two-tail	1.96	

Decision: t-Stat<t-Critical (P>0.05): The null hypothesis is accepted. So there is no significant difference between UAV derived tree height, and TLS measured tree height.

3.3. Accuracy Assessment of Image Segmentation

3.3.1. The accuracy of Multi-resolution Segmentation

The accuracy assessment of multi-resolution segmentation was conducted in ArcMap for estimating the level of accuracy. A total of 3 (three) resampled UAV-RGB images, i.e., 20cm, 25cm and 30cm were taken for assessing accuracy. The accuracy was estimated based on the manual digitized CPA of individual trees as the reference area. An overlaid manual digitized CPA on multi-resolution segmentation is illustrated in Figure 25.

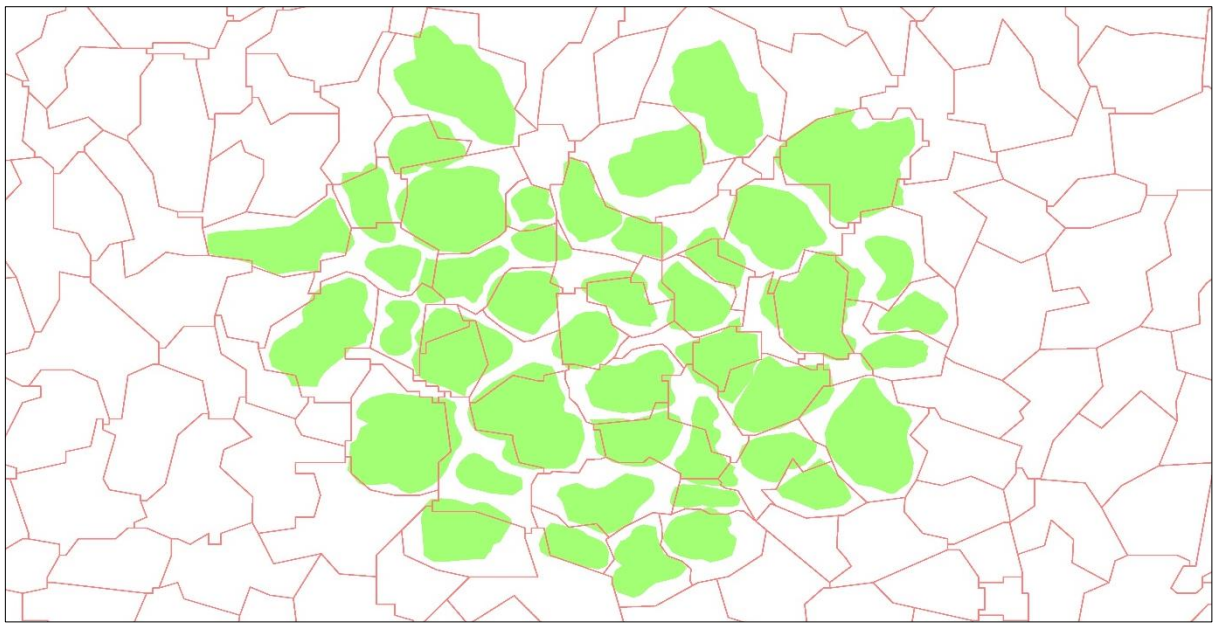

Figure 25: Overlaid of manual digitized CPA on multi-resolution segmented CPA

The accuracy of multi-resolution segmentation results for each resampled images (20cm, 25cm, and 30cm) are illustrated in Table 10:

Table 10: Accuracy of multi-resolution segmentation

	UAV-RGB Resampled Image Resolution		
	20cm	**25cm**	**30cm**
Reference Area (ARi)	6768.33	6768.33	6768.33
Segmented Area (ATi)	13780.71	9811.85	15318.68
Intersection (ATi∩ARi)	6505.14	6758.45	6749.06
Over Segmentation	0.53	0.31	0.56
Under Segmentation	3.9E-02	1.5E-03	2.8E-03
Error	0.37	0.22	0.40
Accuracy	62.57%	77.99%	60.44%

The result shows that the 25cm resolution image has the highest segmentation accuracy with 77.99% while the accuracy of 20cm and 30 resolution images were 62.57, and 60.44% respectively.

3.3.2. The accuracy of SLIC Segmentation

The accuracy assessment of SLIC segmentation was also experimented in ArcMap for assessing its level of accuracy. Like multi-resolution segmentation, a total of 3 (three) resampled UAV-RGB images (20cm, 25cm, and 30cm) were considered for accuracy assessment. The accuracy was assessed based on the manual digitized CPA of 893 trees as the reference area. An overlaid of manual digitized CPA on multi-resolution segmented CPA is illustrated in Figure 26.

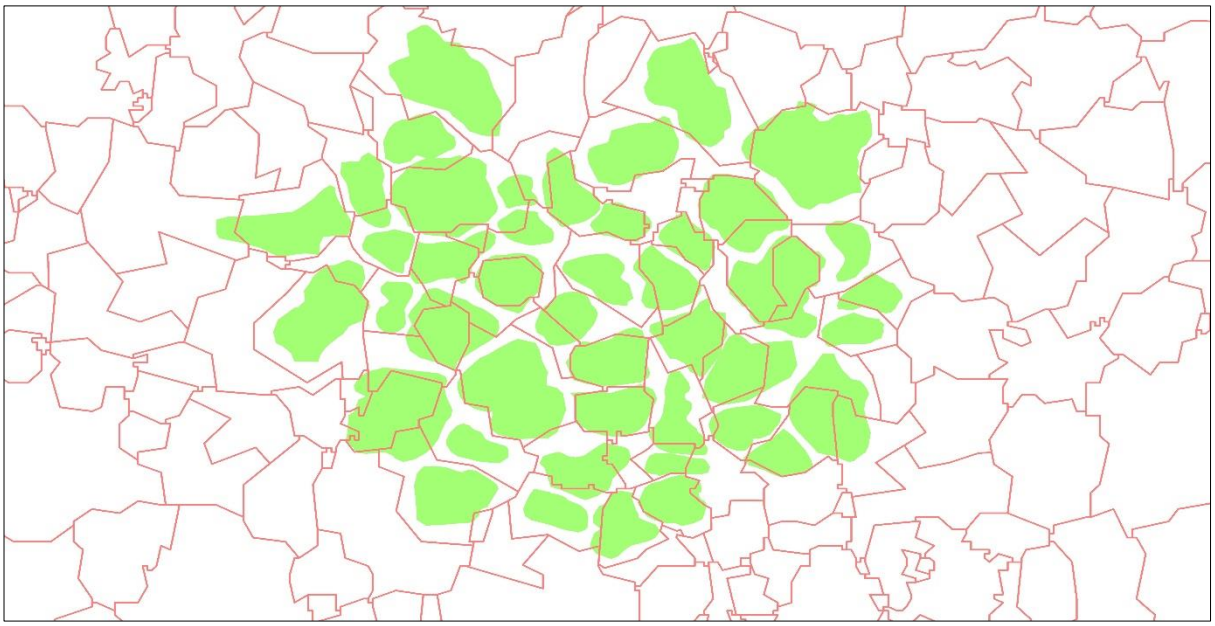

Figure 26: Overlaid of manual digitized CPA on SLIC segmented CPA

The accuracy of SLIC segmentation results for each resampled images (20cm, 25cm, and 30cm) are illustrated in Table 11:

Table 11: Accuracy of SLIC segmentation

	UAV-RGB Resampled Image Resolution		
	20cm	**25cm**	**30cm**
Reference Area (ARi)	6768.33	6768.33	6768.33
Segmented Area (ATi)	21730.48	24379.97	26548.52
Intersection (ATi∩ARi)	6728.46	6746.02	6731.25
Over Segmentation	0.69	0.72	0.75
Under Segmentation	5.9E-03	3.3E-03	5.5E-03
Error	0.49	0.51	0.53
Accuracy	51.18%	48.85%	47.22%

The result shows that the 20cm resolution resampled image has the highest segmentation accuracy with 51.18% while the accuracy of 25cm and 30cm resampled images were 48.85% and 47.22% respectively.

3.3.3. Comparison of Segmentation Accuracy between Multi-resolution and SLIC

The segmentation accuracy of multi-resolution is higher in each resampled UAV-RGB images compared to SLIC segmentation. The highest accuracy of multi-resolution segmentation was found 77.99% in 25cm resolution while the highest accuracy of SLIC was also found in 20cm resolution with 51.18% accuracy. The accuracy of multi-resolution and SLIC segmentation in different resampled images (20cm, 25cm and 30cm) are illustrated in Figure 27.

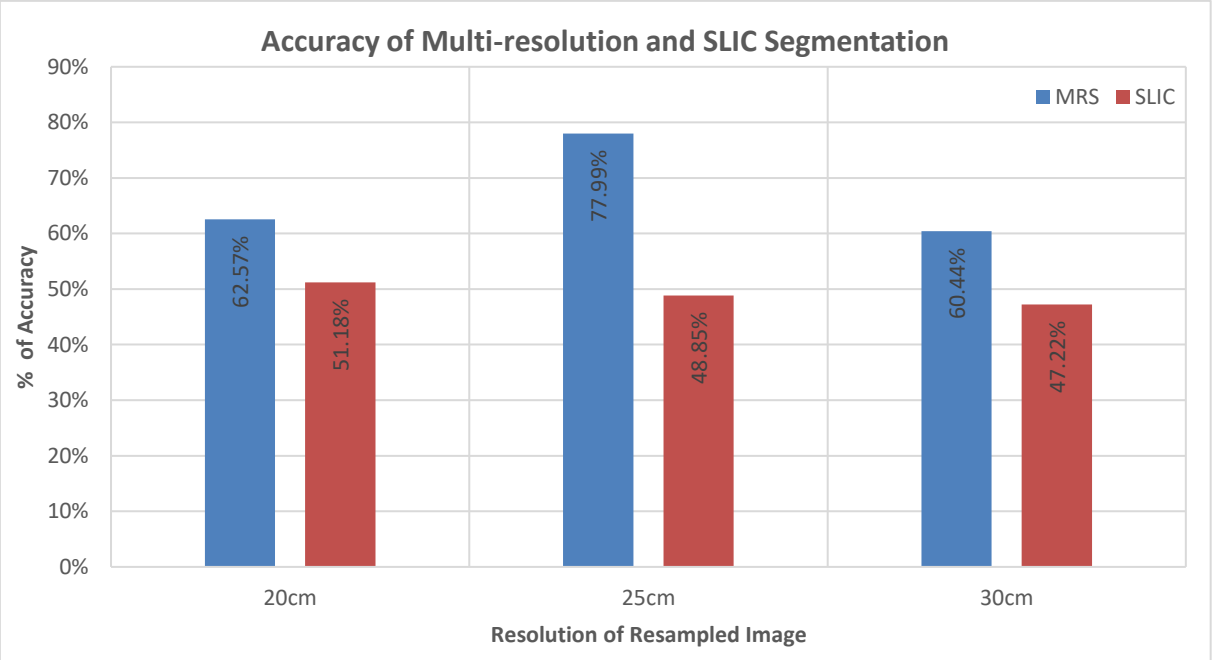

Figure 27: Accuracy of multi-resolution and SLIC segmentation

3.4. Model Development and Validation

Several models were developed and validated for predicting DBH of individual trees using field-measured biometric DBH. A total of 90 trees were selected for model development and validation. Among them, 54 trees (60%) were selected for model development, and 36 trees (40%) were chosen for model validation.

3.4.1. CPA Model Development

A total of 54 trees were randomly selected from 18 sample plots for model development. The trees were selected with biometric DBH (ranging from 10.00cm to 58.80cm) for representing field-measured DBH with a different range. It is found that most of the trees have DBH within 30cm while very few (42 out of 893) have higher DBH. A relationship between the UAV derived CPA, and field-measured biometric DBH was developed in a scatter plot. Four different regression functions, i.e., linear, logarithm, power and quadratic were developed. The results are illustrated in Figure 28.

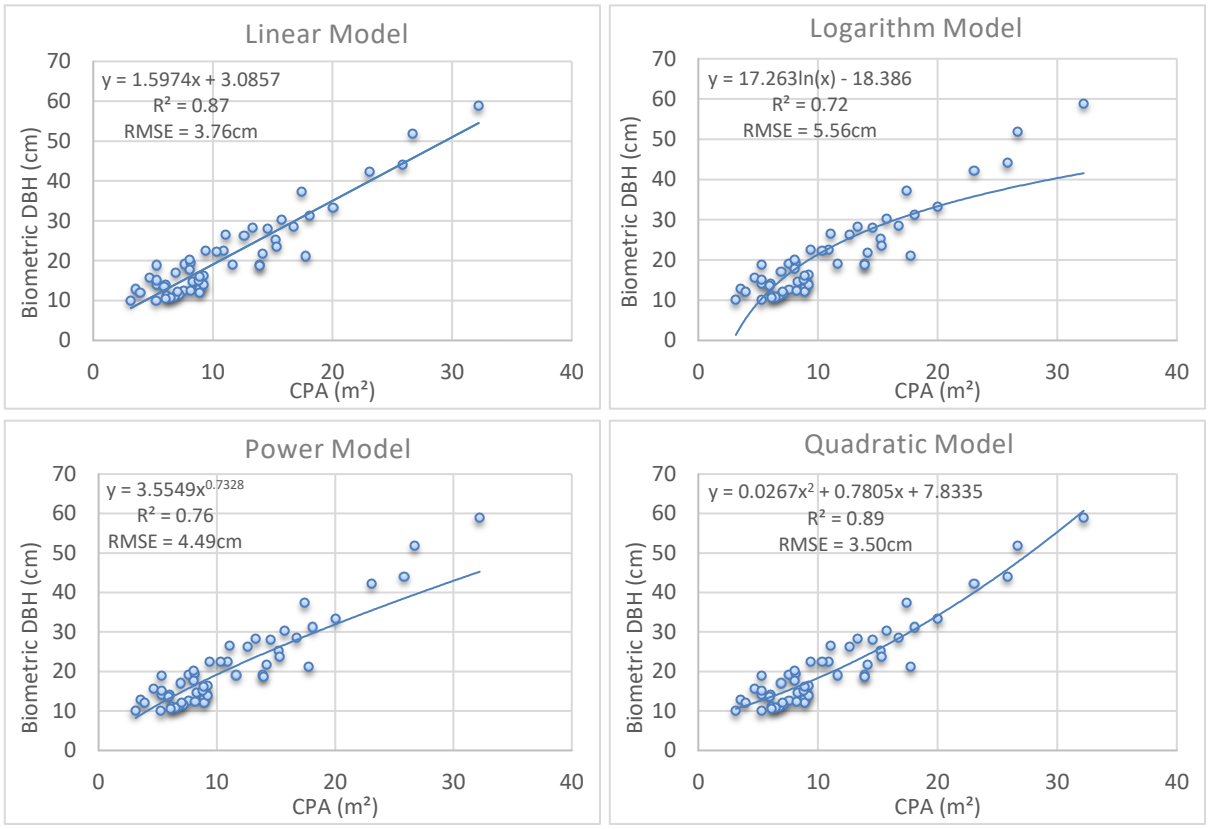

Figure 28: Different regression model for predicting DBH from CPA

Table 12: Summary of the results of different regression functions

Model	Equation	R^2	RMSE
Linear	DBH = 1.5974*CPA + 3.0857	0.87	3.76 cm
Logarithm	DBH = 17.263ln(CPA) – 18.386	0.72	5.56 cm
Power	DBH = 3.5549$(CPA)^{0.7328}$	0.76	4.49 cm
Quadratic	DBH = 0.0267*CPA^2 + 0.7805*CPA + 7.8335	0.89	3.50 cm

It is observed that linear and quadratic functional models have the highest R^2 value. However, the quadratic function has comparatively better RMSE with 3.50cm (see Table 12). Therefore, the quadratic functional model was accepted for predicting DBH from UAV data.

3.4.2. Model Validation

The quadratic functional model was selected for predicting DBH for UAV dataset. The equation (DBH = 0.0267*CPA^2 + 0.7805*CPA + 7.8335) developed by the quadratic model was used for predicting UAV derived DBH. A total of 36 individual trees were randomly selected from the rest 12 sample plots (not used

for model development). The result shows that R^2 is 0.90 which means that 90% of UAV predicted DBH data are fitted with biometric DBH. The goodness of fit was examined by RMSE which is 3.33 cm. Therefore, the result is well fitted with referenced biometric DBH. A scatter plot for model validation is illustrated in Figure 29.

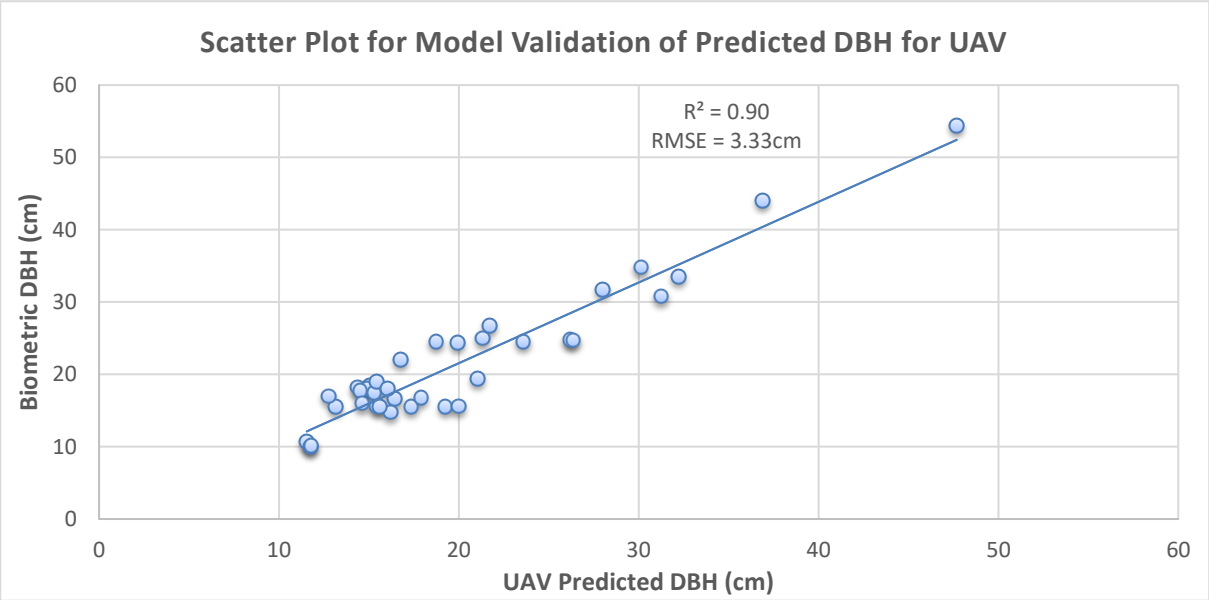

Figure 29: Scatter plot for model validation of predicted DBH for UAV

3.5. The Accuracy of UAV-CPA Estimated DBH Compared to Biometric DBH

The accuracy of DBH predicted from UAV-CPA was evaluated with biometric DBH (referenced DBH) using a scatter plot based on these two measured DBH. The UAV predicted DBH and biometric DBH were placed in a scatter plot. A total of 893 trees were considered for conducting this assessment. The result (Figure 30) shows that there is a strong correlation with 0.93 where the coefficient of determination (R^2) is 0.87 (see Table 13). The Root Mean Square Error (RMSE) is found 3.21 cm which is equivalent to 19.97% of field-measured biometric DBH. Therefore, there is a strong correlation between biometric DBH and TLS measured DBH.

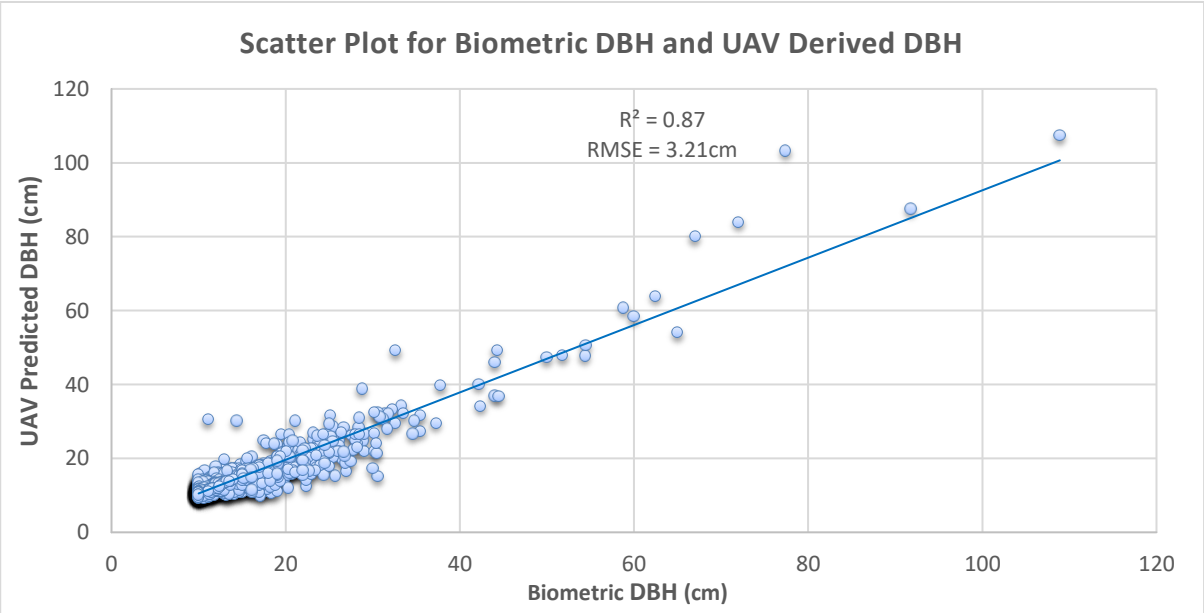

Figure 30: Scatter plot for biometric DBH and UAV predicted DBH

Table 13: Summary statistics of comparison of TLS measured DBH and Biometric DBH

Pearson Correlation	**0.93**
R Square	0.87
Adjusted R Square	0.87
Standard Error	3.11
Observations	893

F-test for Two-Sample Variance

The F-test was conducted to find out datasets (biometric DBH and UAV derived DBH) are an equal or unequal variance for deciding which t-test need to be used for assessing the difference between two datasets. The F-test (Table 14) indicates an equal variance (F-Stat<F-Critical (P>0.05) between biometric DBH and TLS measured DBH. So t-test assuming equal variance was carried out for identifying if any significant difference between these two DBH or not.

Table 14: F-test for two sample variance

	Biometric DBH	***UAV Predicted DBH***
Mean	16.05	16.03
Variance	78.09	74.56
Observations	893	893
df	892	892
F-Stat	1.04	
P(F<=f) one-tail	0.24	
F-Critical one-tail	1.12	

Decision: F-Stat<F-Critical (P>0.05): Equal variance

T-Test Assuming Equal Variance

The T-test assuming equal variance was conducted to check if there any significant difference between biometric DBH and UAV derived DBH. The test shows (see Table 15) that there is no significant difference (t-Stat<t-Critical at P>0.05) between biometric DBH and UAV derived DBH.

Table 15: T-test assuming equal variance for UAV estimated DBH and Biometric DBH

	Biometric DBH	***UAV Predicted DBH***
Mean	16.05	16.03
Variance	78.09	74.56
Observations	893	893
Pooled Variance	76.33	
Hypothesized Mean Difference	0	
df	1784	
t-Stat	0.04	
P(T<=t) one-tail	0.48	
t Critical one-tail	1.64	
P(T<=t) two-tail	0.97	
t Critical two-tail	1.96	

Decision: t-Stat<t-Critical (P>0.05): The null hypothesis is accepted. So there is no significant difference between biometric DBH and UAV derived DBH.

3.6. The Accuracy of TLS Measured DBH Compared to Biometric DBH

The accuracy of DBH derived from TLS 3D point clouds was assessed with biometric DBH (referenced DBH) using a scatter plot based on these two measured DBH. A total of 874 trees were considered for this assessment. The result (see Figure 31) shows that there is a correlation of 0.99 where the coefficient of determination (R^2) is 0.99 (see Table 16). The RMSE is 0.30 cm which is equivalent to 1.87% of biometric DBH. Therefore, there is a strong correlation between biometric DBH and TLS measured DBH.

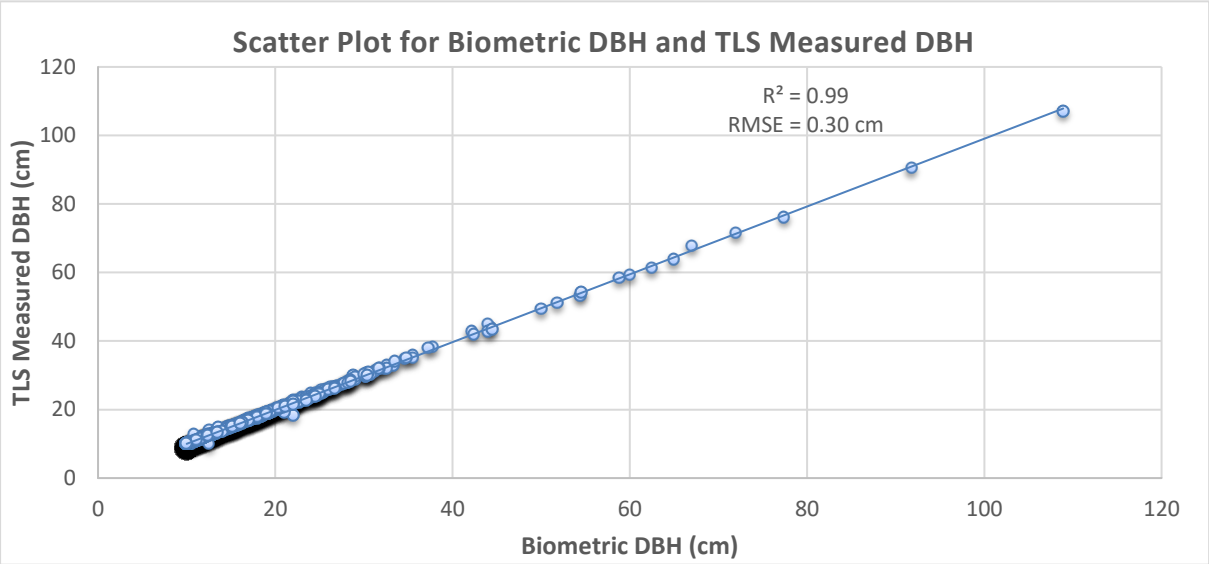

Figure 31: Scatter plot for biometric DBH and TLS measured DBH

Table 16: Summary statistics of comparison of TLS measured DBH and Biometric DBH

Pearson Correlation	**0.99**
R Square	0.99
Adjusted R Square	0.99
Standard Error	0.34
Observations	874

F-test for Two-Sample Variance

The F-test was conducted to find out is there an equal or unequal variance for deciding which t-test need to be used for assessing the difference between two datasets. The F-test (see Table 17) indicates an equal variance (F-Stat<F-Critical (P>0.05) between TLS measured DBH and biometric DBH. So t-test assuming equal variance was carried out for identifying if any significant difference between two datasets or not.

Table 17: F-test for two sample variance

	Biometric DBH	***TLS DBH***
Mean	16.08	16.01
Variance	79.48	77.86
Observations	874	874
df	873	873
F-Stat	1.02	
P(F<=f) one-tail	0.38	
F-Critical one-tail	1.12	

Decision: F-Stat<F-Critical (P>0.05): Equal variance

T-test Assuming Equal Variance

A t-test was conducted to check is there any significant difference between TLS measured DBH and biometric DBH. The test shows (see Table 18) that there is no significant difference (t-Stat<t-Critical at P>0.05) between biometric DBH and TLS measured DBH.

Table 18: T-test assuming equal variance for TLS measured DBH and Biometric DBH

	Biometric DBH	***TLS DBH***
Mean	16.08	16.01
Variance	79.48	77.86
Observations	874	874
Pooled Variance	78.67	
Hypothesized Mean Difference	0	
df	1746	
t-Stat	0.14	
P(T<=t) one-tail	0.44	
t Critical one-tail	1.64	
P(T<=t) two-tail	0.88	
t Critical two-tail	1.96	

Decision: t-Stat<t-Critical (P>0.05): The null hypothesis is accepted. So there is no significant difference between TLS measured DBH and field measured DBH.

3.7. AGB Estimation

Aboveground biomass was estimated from all the datasets including field-measured biometric, TLS and UAV. All trees of 30 sample plots were considered for estimating aboveground biomass.

3.7.1. AGB Estimation using Field-measured Biometric Data

The field-measured 30 sample plots data were processed and analyzed for estimating aboveground biomass of the study area. It is observed that the highest AGB was estimated in plot 5 with 262.25 ton/ha whereas the lowest is calculated in plot 12 with 29.56 ton/ha. The average AGB derived from 30 plots is 109.98 ton/ha. It is observed that the highest AGB estimated plots are mostly dominated by *rhizophora*. Figure 32 shows the plot-wise AGB estimation from field-measured biometric data.

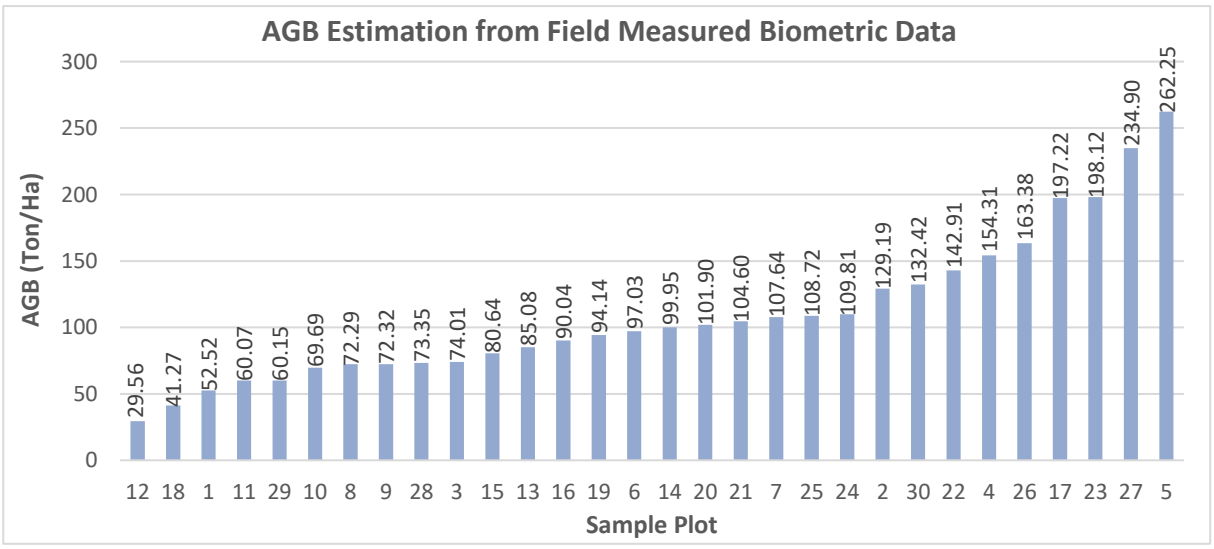

Figure 32: Plot-wise distribution of field measured AGB

3.7.2. AGB Estimation using TLS Data

The TLS measured 30 sample plots data were processed and analyzed for calculating the aboveground biomass. Similar to field-measured biometric data, the highest AGB was estimated in plot 5 with 303.10 ton/ha whereas the lowest was calculated in plot 12 with 33.25 ton/ha. The average AGB from all 30 plots was calculated as 116.33 ton/ha. The plot-wise AGB estimation from TLS is illustrated in Figure 33.

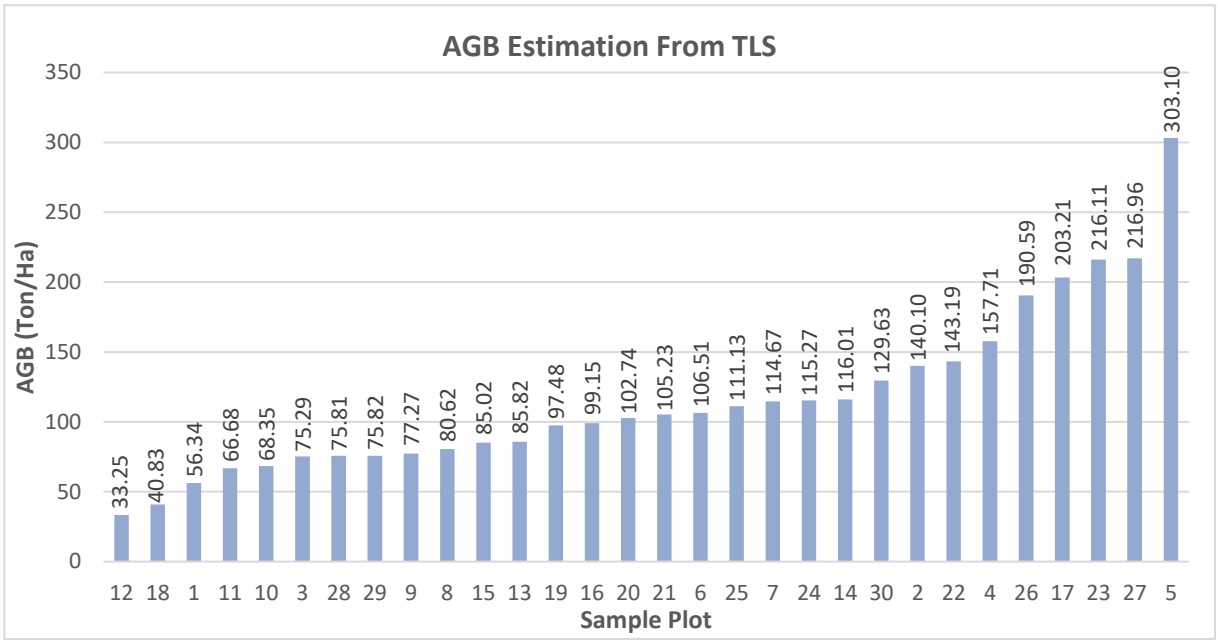

Figure 33: Plot-wise distribution of TLS measured AGB

3.7.3. AGB Estimation from UAV Data

The field-measured 30 sample plots were identified from UAV processed data and analyzed for assessing the aboveground biomass. The highest AGB was estimated in plot 5 with 315.63 ton/ha whereas the lowest was calculated in plot 18 with 39.76 ton/ha. The average AGB from all 30 plots was estimated as 112.38 ton/ha. The plot-wise AGB estimation from UAV is illustrated in Figure 34.

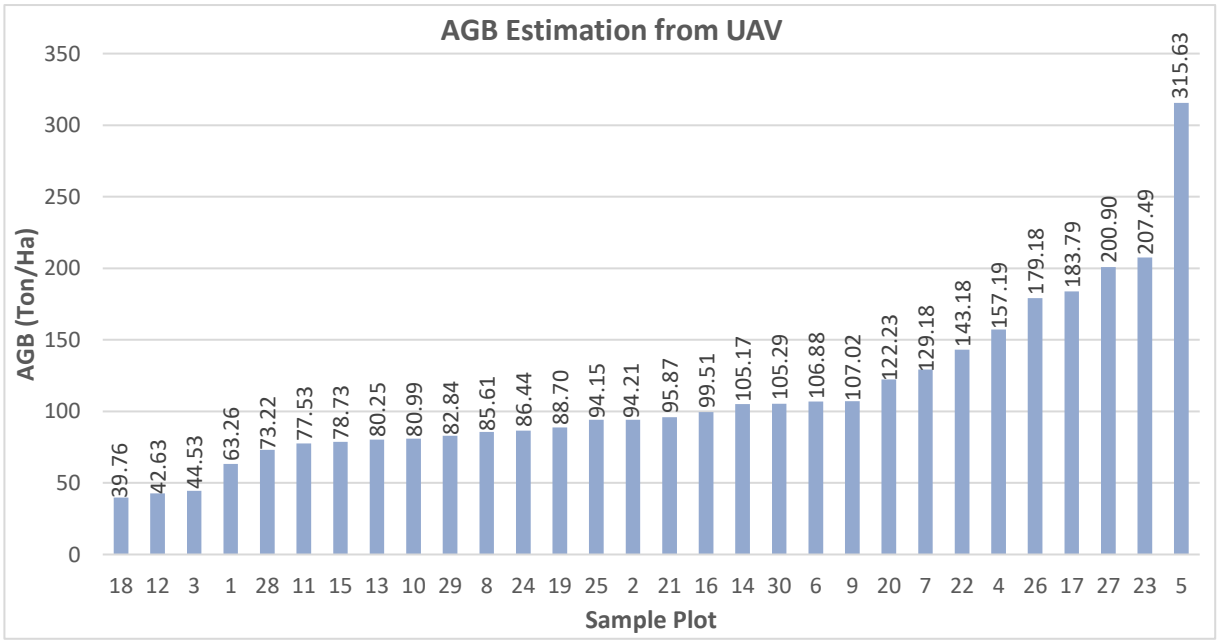

Figure 34: Plot-wise distribution of UAV estimated AGB

3.8. The Accuracy of AGB Estimated from UAV Compared to AGB Estimated from TLS

The UAV and TLS estimated AGB were placed in a scatter plot for evaluating the accuracy of UAV estimated AGB compared to TLS measured AGB. The TLS scanned 30 sample plots data (reference data) were considered for developing this assessment. The result (Figure 35) shows that there is a strong correlation with 0.96 where the coefficient of determination (R^2) is 0.93 (see Table 19). The Root Mean Square Error (RMSE) is found as 3.78 ton/ha which is equivalent to 3.25% of TLS estimated AGB.

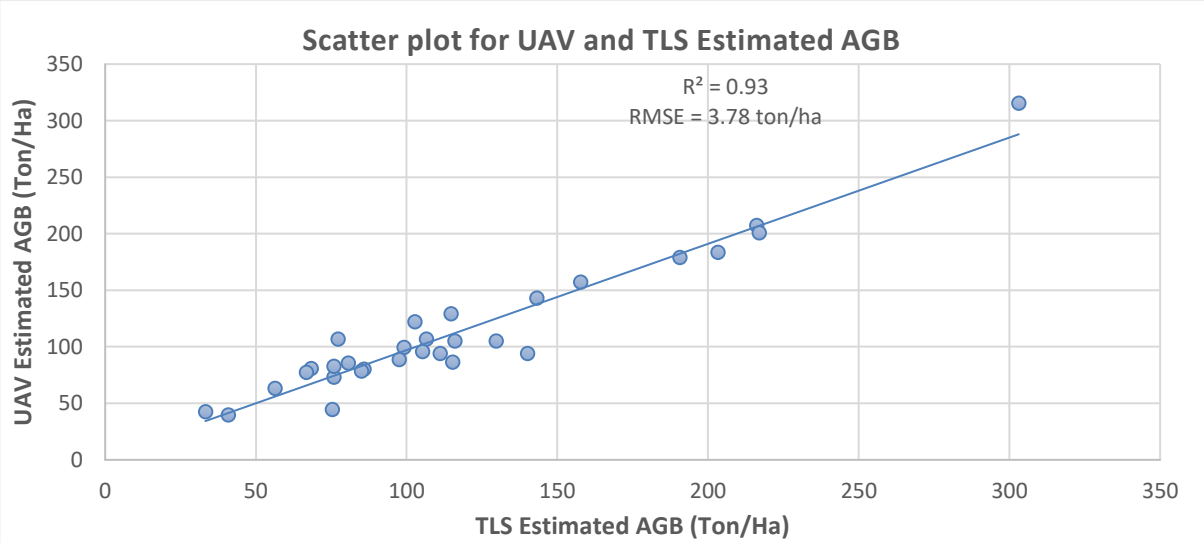

Figure 35: Scatter plot for UAV and TLS estimated AGB

Table 19: Summary statistics of comparison of TLS and UAV estimated AGB

Pearson Correlation	**0.96**
R Square	0.93
Adjusted R Square	0.92
Standard Error	16.09
Observations	30

F-test for Two-Sample Variance

The F-test was conducted to find out the TLS measured AGB and UAV estimated AGB have an equal or unequal variance for deciding which t-test need to be used for assessing the difference between two datasets. The F-test (see Table 20) indicates an equal variance (F-Stat<F-Critical (P>0.05) between UAV and TLS estimated AGB. So t-test assuming equal variance was carried out for identifying if any significant difference between these two AGB or not.

Table 20: F-test for two sample variance

	TLS Measured AGB	***UAV Estimated AGB***
Mean	116.33	112.38
Variance	3549.62	3387.09
Observations	30	30
df	29	29
F-Stat	1.05	
P(F<=f) one-tail	0.45	
F-Critical one-tail	1.86	

Decision: F-Stat<F-Critical (P>0.05): Equal variance

T-Test Assuming Equal Variance

The T-test assuming equal variance was conducted to check if there any significant difference between UAV and TLS estimated AGB. The test shows (see Table 21) that there is no significant difference (t-Stat<t-Critical at P>0.05) between biometric AGB and TLS estimated AGB.

Table 21: T-test assuming equal variance for TLS measured DBH and Biometric DBH

	TLS Measured AGB	***UAV Estimated AGB***
Mean	116.33	112.38
Variance	3549.62	3387.09
Observations	30	30
Pooled Variance	3468.35	
Hypothesized Mean Difference	0	
df	58	
t-Stat	0.26	
P(T<=t) one-tail	0.40	
t Critical one-tail	1.67	
P(T<=t) two-tail	0.79	
t Critical two-tail	2.00	

Decision: t-Stat<t-Critical (P>0.05): The null hypothesis is accepted. So there is no significant difference between UAV and TLS measured AGB.

3.9. AGB Estimation by Tree Species

A comparative analysis was conducted to calculate average DHB, tree height and AGB by different tree species, i.e., *avicennia*, *rhizophora* and *xylocarpus* found in the study area. A total of 874 trees were considered for this statistical analysis. The result shows that the average DBH of *avicennia* was higher than *rhizophora* for biometric, TLS and UAV data. On the contrary, the average tree height of *rhizophora* was comparatively greater than *avicennia*. A comparative statistics of average DBH and tree height of *avicennia* and *rhizophora* are shown in Table 22. The species *xylocarpus* was excluded for this comparison due to its inadequate number (only 11).

Table 22: A comparative statistics of average DBH and tree height of avicennia and rhizophora

Tree Species	No. of Trees	DBH (cm)			Tree Height (m)				
		Biometric	TLS	UAV	Biometric	TLS	UAV	% of Deviation for UAV from Biometric	% of Deviation for UAV from TLS
Avicennia	456	18.40	18.31	17.88	13.14	14.21	13.84	5.31%	-2.59%
Rhizophora	407	13.53	13.48	14.14	13.48	15.38	14.30	6.09%	-7.03%

The AGB was also calculated according to different species for making a comparative analysis of tree species. The result shows that the average AGB (tree/kg) is highest in *avicennia* while lowest in *xylocarpus*. The difference between *avicennia* and *rhizophora* was found almost 100 kg/tree. The AGB estimation scenario of two species is illustrated in Figure 36.

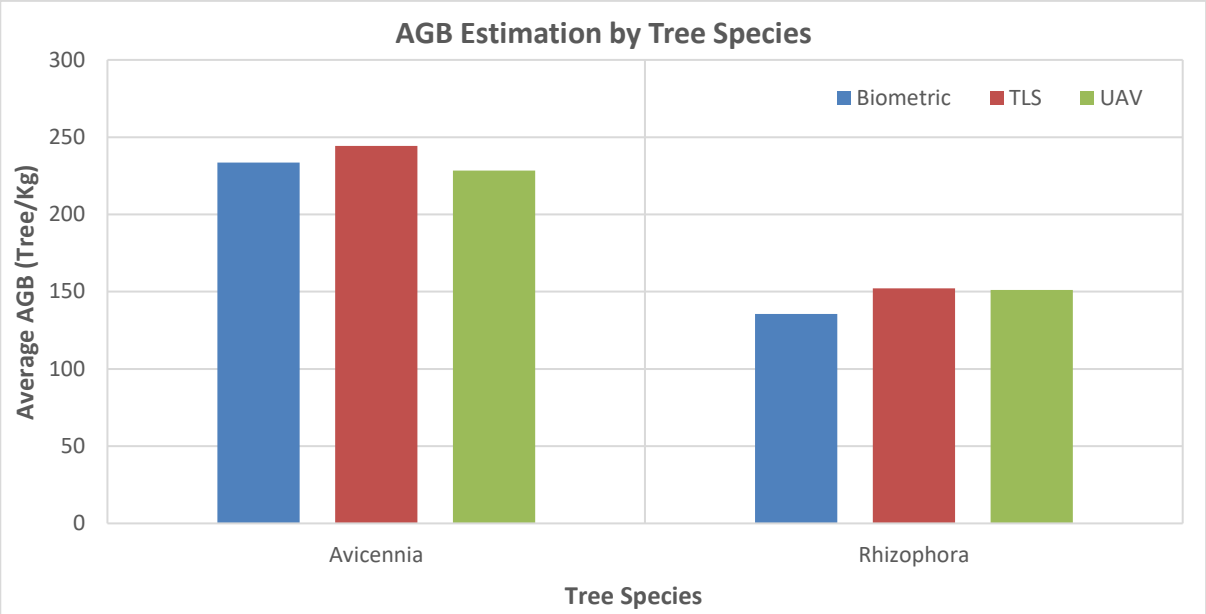

Figure 36: AGB estimation by tree species

3.10. Carbon Stock Estimation

The carbon stock estimation was conducted to identify the amount of carbon in the study area. The carbon stock was estimated using the equation (see Equation 5) provided by IPCC (2006). The carbon stock was calculated from stand-alone biometric, UAV and TLS dataset. The plot-wise estimated carbon stock for field-measured biometric, TLS and UAV are illustrated in Figure 37.

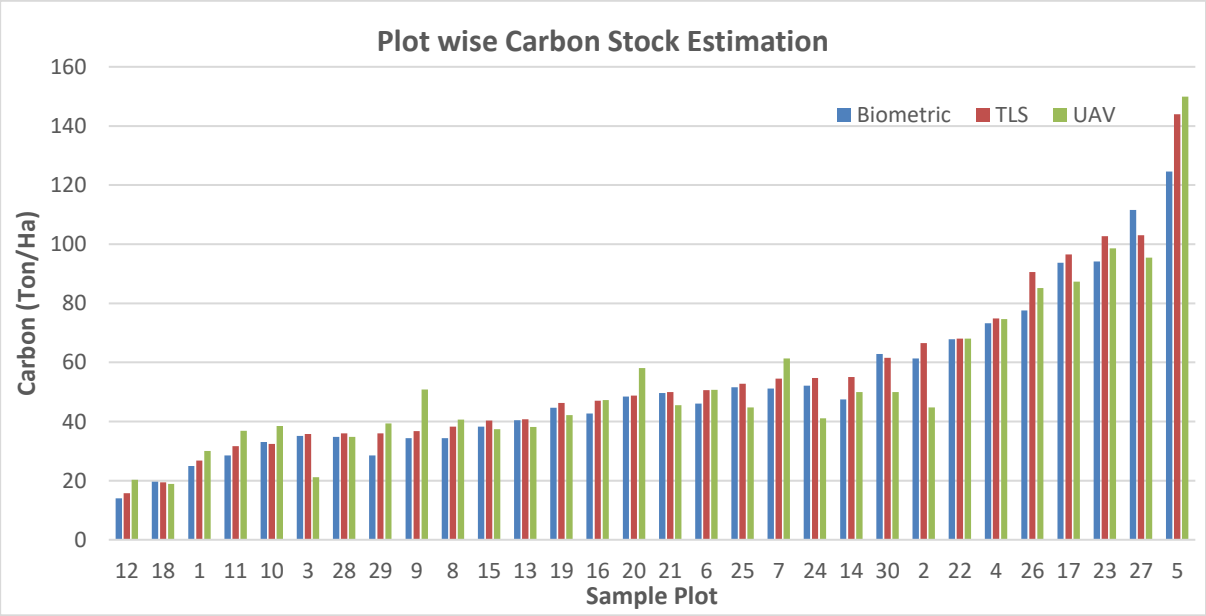

Figure 37: Plot-wise carbon stock of biometric, TLS and UAV

The result shows that most of the plots have carbon stock below 60 tons/ha while only five plots have more than 80 ton/ha carbon. But two plots (plot 12 and 18) have carbon stock below 20 tons/ha. The average carbon stock (ton/ha) for biometric, TLS and UAV are 52.24, 55.26 and 53.38 respectively.

4. DISCUSSION

4.1. Descriptive Analysis of DHB and Tree Height

The skewness determines the extent of distribution (see Figure 38) while the value 0 indicates normal distribution (Hastie et al., 2009). The descriptive statistics of DBH measured from the field, TLS and UAV shows a positive skewness in an asymmetrical distribution. This is because trees having minimum 10cm DBH were only considered in this study. The minimum and maximum value for DBH varied over a comparatively broad range (≈ 97.00cm). The median and mode are smaller than the mean. Like DBH, the tree height measured from biometric, TLS and UAV also shows a positive skewness. The skewness in tree height is relatively minimal where the range lies between 6.66 and 23.40. Because the mean, median and mode are close. Also, the skewness for DBH and tree height measured from the field, TLS and UAV have fewer differences (see Appendix 5 & Appendix 6). Because the standard deviation of this measurement was close to each other.

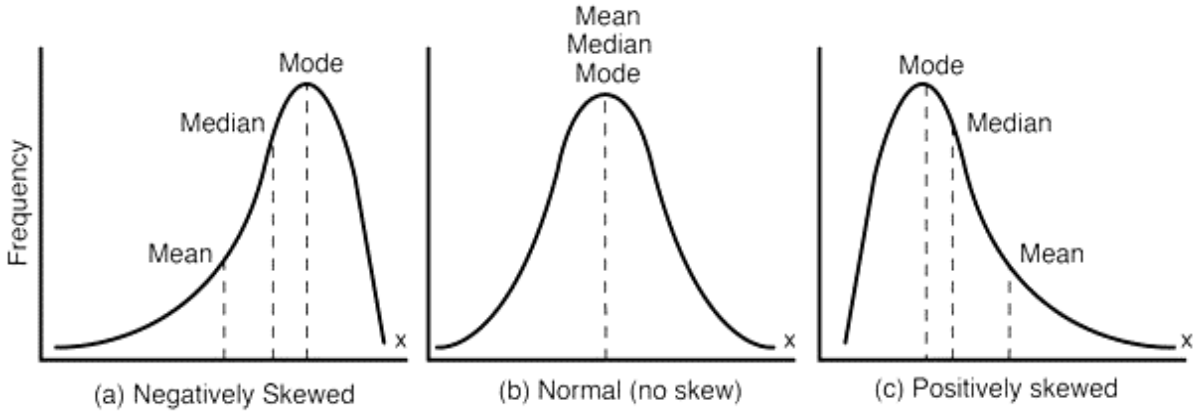

Figure 38: Normal distribution and skewness

Source: https://www.fromthegenesis.com/skewness

4.2. Tree Height Extracted from UAV-CHM and TLS Point Clouds

The mean tree height of UAV-CHM was underestimated compared to tree height extracted from TLS point clouds. Only four plots were overestimated, and 26 plots were underestimated. There were some errors in 3D point clouds generated from UAV images. This is because not enough point hit on the ground of some areas due to dense canopies (Ni et al., 2014). The UAV images could have some errors including systematic and accidental due to the processing of the images (Jiménez et al., 2017). The systematic error was occurred because of the inaccuracy of GPS for measuring GCP coordinates (Candón et al., 2014). The image altitude of UAV images was varied between 164m to 172m because of wind during UAV image acquisition in the field. Also, regular overlap and equal altitude were not possible due to the existence of wind (Nex & Remondino, 2014). As a result, the UAV-CHM has some inaccuracy which affects to the height measurement. But the images were taken using fixed-wing UAV while multi-rotor UAV has comparatively less systematic error compared to fixed-wing UAV (Jiménez et al., 2017). On the contrary, the accidental errors could occur due to insufficient calibration of internal parameters of the camera. In this study, 15.64% relative difference between initial and optimized internal camera parameters were detected (see Appendix 2) because parameters of internal camera varied with a different altitude between two flights. Therefore, this

relative difference made some inaccuracies in 3D point clouds that affect tree height generated from UAV-CHM. Also, the UAV image acquisition was conducted during high tide while most of the ground area was flooded. Therefore, this flooded ground has some influences on the height measurement from UAV images.

The tidal flow and the hydrodynamic process are acted as an influential factor in mangrove forests ecosystem. The water level increases up to 1.5 meters during the high tide of Mahakam Delta. The sediment from the river Mahakam is deposited along the river bank. The sediments and muds are carried towards the intertidal zone in mangrove and accreting its mudbanks. However, most of the sediments return to the river during the period of low tides but some sediments accumulated with grounds. The rate of surface accretion in mangrove has a range from 2.9 to 20.8 mm/year (Krauss et al., 2010). As a result, surface elevation is changing both in short and long term basis in a mangrove forest. Figure 39 shows the sedimentation process where marine sediments are accreted on the surface.

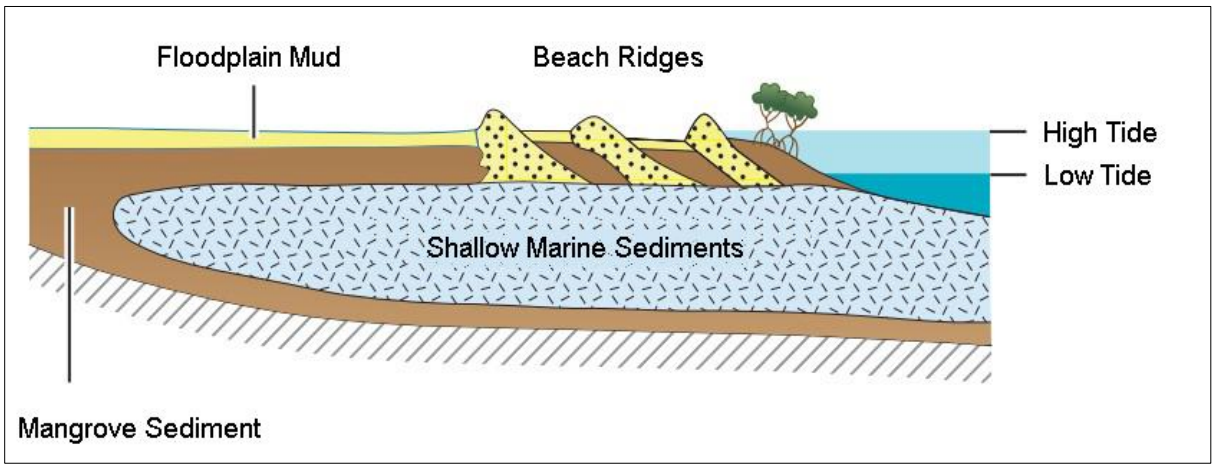

Figure 39: Mangrove sedimentation

Source: Woodroffe et al. (2016)

Despite some errors in UAV-CHM, the result shows that there is no significant difference between the tree height extracted from UAV-CHM and TLS point clouds which are consistent with some past studies. Among them, Wang et al. (2019) got a positive correlation with R^2= 0.96 between TLS and ALS measured height in a boreal forest. Similarly, Stovall et al. (2017) also found a positive correlation with a coefficient of determination (R^2) as 0.99 between TLS and field-measured height in a mixed land-use area while Mweresa et al. (2017) found R^2 as 0.75 between UAV and field-measured tree height in a tropical forest. The coefficient of determination is varied with those studies because the relationship between two tree height depends mostly on canopy and leaf structure which are dissimilar in mangrove compared to tropical or other forests (Larjavaara & Landau, 2013).

4.3. Image Segmentation and Accuracy Assessment

A total of three (03) different resolution (20cm, 25cm and 30cm) UAV-RGB filtered images were used to make an accurate assessment for both multi-resolution and SLIC segmentation. The high spatial resolution (6.2cm) UAV-RGB orthophoto was resampled to lower resolution. Because high-resolution image consists of minor cell size that makes the image comparatively sharper and lucent (Gao et al., 2017). Therefore, image segmentation in high-resolution images considers undesired objects which can affect segmentation accuracy (Clinton et al., 2010). Consequently, the high-resolution image (e.g., 5cm or 10cm) can segment objects well in an urban setting but not suitable for tree crown segmentation in forests (Tian et al., 2018). The UAV-RGB image was also filtered using a 3-by-3 low pass method for removing noises and small objects from the image (Kejriwal & Singh, 2016).

4.3.1. The accuracy of Multi-resolution Segmentation

Segmentation accuracy depends on some factors, i.e., image resolution, noise level and optimal parameters including scale, shape, compactness defined for the process of image segmentation (Möller et al., 2007). The scale parameter determines the homogeneity and size of resultant image objects (Drăgut et al., 2010). The ESP2 tool was used to identify the scale parameter for three different resolution UAV-RGB images. After that, shape and compactness was identified with the trial and error method by visual interpretation. In this study, the parameter 'shape' was defined as comparatively lower as 0.3 because defining lower value indicates higher influences of color on the process of image segmentation (Saba et al., 2013). The study area has a significant influence on image color due to it has mostly two species where *rhizophora* was found dark green while *avicennia* was whitish in UAV orthophoto. From visual interpretation, *avicennia* had found comparatively higher accuracy compared to other two species due to its different brightness. Also, the brightness value of the pixel helps to delineate trees from shadows in segmentation. Most of the trees are in similar age (12-15 year), and DBH and height of the trees lie in a range with 10-20cm and 12-18m respectively. The compactness was defined as comparatively higher as 0.7 due to dense canopies in the study area.

The result shows that multi-resolution segmentation has higher accuracy with 77.99% in 25cm resolution while 62.57% in 20cm and 60.44% in 30cm resolution respectively. Because, in a 25cm resolution image, the segmented polygons were fitted well with manually delineated polygons which make fewer under segmentation. The segmentation accuracy found in this study is consistent with some past studies. Among them, Pap & Kiraly (2018) obtained 74.85% with 25cm resolution UAV images. On the contrary, some researcher got comparatively higher segmentation accuracy in using resampled UAV images. Among them, Kavzoglu & Tonbul (2018) achieved 90.70% accuracy with 50cm resolution WorldView-2 images, and Sari & Kushardono (2015) achieved 90.47% accuracy with 16cm resolution UAV images. They got higher segmentation accuracy either in the tropical forest or in the boreal forest because the tree crowns are different in those forests compared to mangrove forests. In tropical or boreal forests, the canopies are multi-layered and sparse while the canopy of the mangrove forest was dense, flat, and intermingled. Therefore, it is comparatively easier to detect canopies in tropical or boreal forest but difficult in mangrove forest (Trettin et al., 2016). So, the accuracy achieved in this study was found lower compared to their research.

The image segmentation was also experimented with adding UAV-CHM layer in eCognition Developer for attaining better segmentation accuracy. Antolihao et al. (2015) were achieved higher accuracy (91.07%) for using CHM as an additional layer for image segmentation with a LiDAR image. But the result was not better compared to segmentation without UAV-CHM layer. The accuracy was found as 60.98%, 75.71% and 57.52% for 20cm, 25cm and 30cm resolution respectively (see Appendix 7).

4.3.2. The accuracy of SLIC Segmentation

The SLIC segmentation is created upon k-means clustering method which can generate similar size superpixels based on the proximity and color similarity. Generally, the SLIC algorithm follows 'k-parameter' which can control homogeneity of superpixel and 'm-parameter' that can maintain both homogeneity and boundary of superpixels. The parameters including iteration, minimum element size, region size, and ruler were defined with trial and error basis for achieving higher segmentation accuracy. The parameters (iterations=50, minimum element size=10, region size=30, and ruler=50) were found comparatively better for segmentation amongst other parameters from visual interpretation. In defined parameters, minimum element size, region size, and ruler values were set comparatively lower. Because the CPAs are found comparatively lower as a planted young forest. Also, the size of the canopies is not too dense and large compared to other forests. So these parameters were found comparatively better with the lower values for segmentation of tree crowns (Kavzoglu & Tonbul, 2018; Zimudzi et al., 2018).

The result shows that SLIC has higher segmentation accuracy of 51.18% in 20cm resolution while 25cm and 30cm resolution resampled UAV-RGB images have 48.85% and 47.22% respectively. The accuracy result of SLIC segmentation is consistent with some past studies. Among those, Crommelinck et al. (2017) achieved 64% accuracy with UAV-RGB images while Achanta et al. (2012) got 67.30% accuracy with a 20cm resolution UAV images. But those studies were conducted on a mixed land-use area where tree crowns were not mostly dense.

4.4. CPA Model Development and Validation

For the relation between CPA and DBH, the linear and quadratic model provides a higher coefficient of determination (R^2) with 0.87 and 0.89 while RMSE was 3.76cm and 3.50cm respectively. In general, there is a proportional relation between CPA and DBH for a fast-growing forest. But after a certain age, the growing rate of CPA is mostly affected by the competition of other trees. As a result, the rate of CPA growth becomes slow compared to the increase of DBH (Shimano, 1997). In this study, most of the trees are young fast-growing having DBH less than 25cm. Therefore, there has no competition amongst the trees in this forest. However, it is observed that 19 old trees have higher DBH ranging from 42.2cm to 108.9cm. The CPA of these old trees was not extended in proportion to its DBH. At this point, Hemery et al. (2005) showed that trees having more than 50cm DBH is fitted well with a non-linear regression model. Therefore, these old trees influence the CPA model fitness. Consequently, the model was fitted best in quadratic compared to linear or other regression models.

Another CPA model development and validation were also experimented for identifying its consistency with the adopted model. A total of 893 trees were considered where 600 trees from 20 plots were used for model development, and 393 trees from rest 10 plots were used for model validation. The experimented CPA model also find quadratic as the best-fitted model (see Appendix 8 & Appendix 9). In general, a model is developed with limited sample size for predicting it's in a broader context. So the adopted model was developed for identifying CPA-DBH relationship. But this model was experimented only for checking its accuracy and consistency considering all sample trees.

The model includes trees having biometric DBH ranging from 10.0cm to 58.8cm while most of the trees have DBH lies between 13.00cm to 25.00cm. That is why the trees were congested within this range while the higher range has only seven trees (>30cm DBH). As a comparison with some related studies, Zaki et al. (2016) and Oyebade and Anaba (2018) also found a quadratic model as best fit regression for modeling CPA with DBH and BA respectively in their studies.

4.5. The UAV Predicted DBH and Biometric DBH

The trees which have equal or more than 10cm DBH were considered in this study for aboveground biomass estimation. But after using the CPA model for predicting UAV predicted DBH, 16 trees were identified as less than 10cm DBH. This means that these trees were underestimated in UAV predicted DBH. It is observed that 523 trees are overestimated in UAV predicted DBH compared to biometric DBH. This could happen due to an error in the manual delineation of CPA and lack of model fitness. The DBH of the trees were measured at a 1.3m height from the ground. In some cases, the DBH of the species *rhizophora* were needed to estimate above the highest prop root that could be 2-2.5m height from the ground which was difficult to measure. Therefore, sometimes biometric DBH could not measure accurately at a 1.3m height from the ground. As a result, there is a deviation (average 0.61cm) in field-measured DBH compared to UAV predicted DBH for the species *rhizophora*. Moreover, 11 trees have more than 10cm deviation between UAV predicted DBH and biometric DBH. This case was happened with some old trees which have higher DBH but not having comparatively greater CPA. The mean deviation of these trees was found only 3.86cm between biometric and UAV predicted DBH. Because among 11 trees, 5 trees were overestimated and 6

were underestimated in UAV predicted DBH. Therefore, this minimal deviation does not affect in a larger extent to aboveground biomass estimation. Despite such deviation, these trees were considered for biomass estimation because these old trees have a significant influence on the estimation of total AGB per plot.

The relation between UAV-CPA predicted DBH and biometric DBH was found 0.8702 as a coefficient of determination (R^2) in this study. Iizuka et al. (2018) got 0.79 between UAV-CPA and biometric DBH in a cypress forest in Japan while Shimano (1997) achieved correlation coefficient (R) as 0.93 for deciduous forest and 0.87 for the coniferous forest. Those forests are dissimilar with a different type of climates, soils, tree species, and biodiversity's compared to the mangrove forest. The species of mangrove forests are salt tolerant and having aerial and prop roots and located in the intertidal zone while the plants of deciduous and coniferous forests are dependent on rainfall. The structure and density of tree crowns are also different in those forests (Taureau et al., 2019). Therefore, these different ecosystems make those forests dissimilar compared to mangrove which also has influences to tree crown segmentation.

4.6. The TLS 3D Point Clouds Extracted DBH and Biometric DBH

The TLS generated 3D point clouds can provide comparatively accurate data for measuring DBH and tree height. The DBH measured from TLS 3D point clouds were mostly close to the biometric measurement. In some cases, biometric DBH were not measured at the right point (1.3m height from the ground) due to inaccessibility while TLS measured DBH was more accurate than biometric measurement. But in TLS measurement 19 trees were excluded because those trees were not identified in 3D point clouds of TLS data due to occlusion.

The distance measurement tool was used to measure DBH from 3D point clouds of TLS data. The tree stem is not always in a circular shape especially for buttressed trees (Cushman et al., 2014). However, the circle fitting could not deliver accurate measurement of DBH due to fewer point generated because of occlusion. Also, Calders et al. (2015) showed that due to occlusion, circle fitting is not accurate for measuring DBH in 3D point clouds (see Figure 40). However, the distance measurement tool does not face such a problem. The distance measurement tool can estimate DBH comparatively with less error than the circle fitting method (Tan et al., 2018).

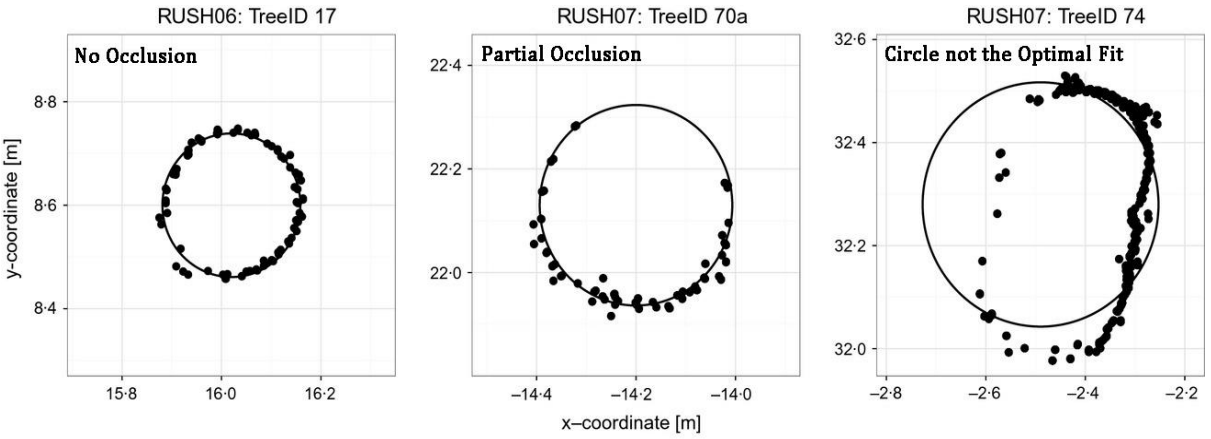

Figure 40: Measurement of DBH using circle fitting

Adapted from: Calders et al. (2015)

4.7. Aboveground Biomass and Carbon Stock

The aboveground biomass and carbon stock was estimated with biometric, TLS and UAV datasets. The maximum aboveground biomass was estimated as 303.10 ton/ha (in plot 5) and minimum as 33.25 ton/ha (in plot 12) by TLS. This is because aboveground biomass is dependent on DBH, tree height, wood density and number of trees inside the plot area. It is observed that higher aboveground biomass was estimated in the plots which are dominated by *rhizophora*. Also, the number of trees are found comparatively more in the plots having higher aboveground biomass. The DBH and tree height also has significant influences on estimating aboveground biomass in the plots.

In this study, average aboveground biomass was estimated as 112.38 ton/ha and 116.33 ton/ha from UAV and TLS respectively. The aboveground biomass estimation from UAV data was found consistent with related some past studies. Among them, Otero et al. (2018) estimated aboveground biomass from UAV as 143 Mg/ha (equivalent to 157.63 ton/ha) in Matang mangrove forest in Malaysia while Lucas et al. (2015) found 81 Mg/ha (equivalent to 89.29 ton/ha) AGB in Mozambique's mangrove forest using TLS. Apart from UAV and TLS, Ekhzarizal et al. (2018) estimated 133.97 Mg/ha (equivalent to 147.68 ton/ha) AGB using SPOT-5 image of Kuala Sepetang forest reserve in Malaysia. Also, Pham et al. (2019) got 150 Mg/Ha (equivalent to 165.35 ton/ha) AGB in Quang Ninh mangrove forest in Vietnam using ALOS PALSAR.

4.8. AGB Estimation by Tree Species

The mangrove trees are different from other forests for its aerial and long congested roots. The tree height and DBH need to be measured accurately for estimating AGB accurately. The average predicted DBH of UAV was found underestimated for *avicennia* while it was overestimated for *rhizophora* compared to TLS and biometric DBH. Because the *avicennia* has a sparse canopy which resultant less dense point clouds that may influence to underestimation in tree height. On the contrary, UAV-CHM derived tree height including all trees were found underestimated compared to height extracted from TLS point clouds. The percentage of deviation of tree height extracted from UAV-CHM compared to TLS measured height was found as -2.59 and -7.03 for *avicennia* and *rhizophora* respectively. The deviation of tree height of *rhizophora* was higher due to its congested root system. Also, there are some differences in the canopy and leave density among those species. The species *avicennia* has a spread canopy with leathery leaves while the *rhizophora* has a dense canopy with elliptic leaves (see Figure 41).

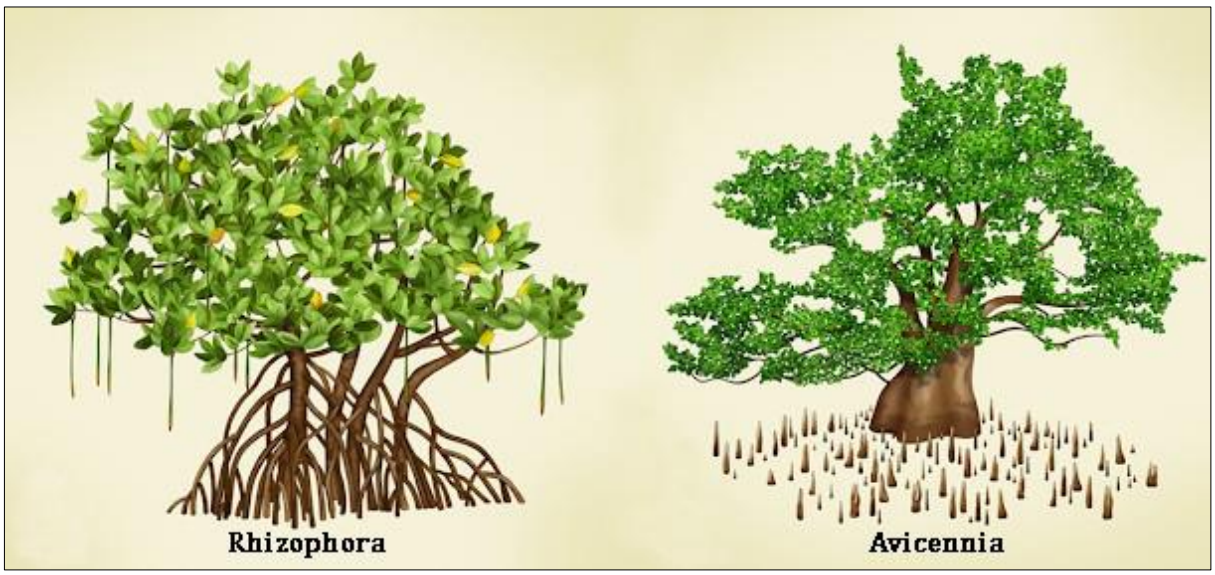

Figure 41: Physical structure of rhizophora and avicennia

Adapted from: http://graphiqueillustration.unblog.fr/category/dessin-scientifique/

The species *rhizophora* has long and congested aboveground roots up to 2.5-meter high from the ground. The DBH was measured at 1.3m from the ground or above the highest stilt root (Smith & Whelan, 2006; Kauffman & Donato, 2012). Because the allometric equation followed in this study was developed including aboveground roots for such type of tree species. But the other species, i.e., *avicennia* and *xylocarpus* have no congested aboveground roots like *rhizophora*. The measurement of DBH and tree height can be affected through the irregular structures as well as the quantity of leaves (Sumida et al., 2013). In this study, the deviation of tree height of *rhizophora* derived from UAV-CHM was found higher than *avicennia* and *xylocarpus* because the dense canopy structure of *rhizophora* is different from the other two species which may affect to height measurement (Taureau et al., 2019).

4.9. Limitations of the Research

There were some limitations faced in this study during data collection and processing stages. The major limitations are briefly highlighted below:

Measurement of Handheld GPS Coordinates

A handheld GPS (Garmin GPS) was used in the field to measure coordinates of the plot center and 4 (four) different trees in each sample plots. But the recorded coordinates of the GPS has not fitted accurately with the orthophoto image generated from UAV images. Because the handheld GPS did not provide an accurate measurement. So, it was challenging to identify the position of the plot center and the measured trees of each sample plot.

UAV Images

The quality of UAV images captured during the fieldwork was problematic for getting a good result. Therefore, new UAV images were re-captured after two months from the field in December 2018. So, time was very limited to process and analyze UAV data.

Sampling Design

The field study was not conducted according to a pre-identified sample plot. Because most of the pre-designed sample plot area was located in inaccessible place. Therefore, the location of sample plots was chosen purposively where the accessibility was convenient and safe.

Tree Crown Segmentation

The manual delineation of tree crown was challenging due to the intermingled situation in some sample plots. It was hard to found the crown area accurately while the crowns were intermingled.

Wet and Muddy Soil

As a mangrove forest, the study area is located in an intertidal zone having high and low tide situation. The field study was conducted during low tides. The ground was wet and muddy with up to 0.5m as well as congested root system. Besides, it was also challenging to move with a 25 kg TLS equipment from one plot to another.

5. CONCLUSION AND RECOMMENDATIONS

5.1. Conclusion

The overall objective of the study is aimed to make a comparative assessment on the applicability of UAV and TLS for estimating aboveground biomass and carbon stock in the mangrove forest. The study reveals that the applicability of UAV and TLS for estimating aboveground biomass in mangrove forest has no significant differences. The estimation of aboveground biomass from UAV and TLS found almost similar. The applicability of TLS in mangrove forest is difficult for its heavy-weight to move from one plot to another in the wet and muddy ground. Also, the use of TLS is not possible in inaccessible areas of mangrove forest. On the contrary, as a remote sensing technique, UAV can be used broadly in any inaccessible area of the mangrove forest. As a low-cost technology, UAV has great potentialities in mangrove forests for estimating aboveground biomass and carbon stock towards the implementation of MRV under REDD+ initiatives.

The following are the answers to the specified research questions under this study:

Research Question 1: How accurate is the tree height derived from CHM of UAV imagery compared to the tree height resultant from TLS?

The accuracy of tree height extracted from UAV-CHM compared to tree height measured from 3D point clouds of TLS is attained at $R^2 = 0.82$ and RMSE = 1.44m (%RMSE = 9.7%). Therefore, the accuracy of tree height extracted from UAV-CHM is 90.3% accurate compared to tree height resultant from 3D point clouds of TLS data. So, the null hypothesis is not rejected. Therefore, there is no significant difference between tree height estimated from CHM of UAV imagery and tree height resultant from TLS.

Research Question 2: Which algorithm provides higher segmentation accuracy of tree crowns on UAV imagery?

The multi-resolution and SLIC segmentation was used to check the accuracy of tree crown segmentation. Three different resolution resampled images (20cm, 25cm and 30cm) were considered for checking the level of accuracy. It is observed that multi-resolution segmentation has higher segmentation accuracy compared to SLIC. The result shows that multi-resolution segmentation has an accuracy of 62.57%, 77.99% and 60.44% for 20cm, 25cm and 30cm resolution images respectively. But, SLIC has lower accuracy of 51.18%, 48.85% and 47.22% for 20cm, 25cm and 30cm resolution images respectively. Therefore, the multi-resolution segmentation provides higher segmentation accuracy of tree crowns on UAV imagery.

Research Question 3: How accurate is the DBH derived from CPA segmentation of UAV imagery with the field-measured DBH?

The accuracy of DBH predicted from CPA segmentation of UAV imagery compared to field-measured DBH is achieved at $R^2 = 0.87$ and RMSE = 3.21cm (%RMSE = 19.97%). The DBH extracted from CPA segmentation of UAV imagery is 80.03% accurate compared to field-measured DBH. Consequently, the null hypothesis is not rejected. Therefore, there is no significant difference between DBH derived from CPA segmentation of UAV imagery and field-measured DBH.

Research Question 4: How accurate is the DBH derived from TLS with the field-measured DBH?

The accuracy of DBH measured in 3D point clouds of TLS compared to field-measured DBH is achieved at $R^2 = 0.99$ and RMSE of 0.30cm (%RMSE = 1.87%). So the DBH extracted from TLS 3D point clouds is 98.13% accurately measured in TLS point clouds compared to field-measured DBH. So, the null hypothesis is accepted. Therefore, there is no significant difference observed between the TLS measured DBH and field-measured biometric DBH.

Research Question 5: How accurate is the estimated amount of aboveground biomass from UAV imagery compared to aboveground biomass estimated from TLS?

The accuracy of aboveground biomass estimated from UAV imagery compared to aboveground biomass measured from TLS is attained at $R^2 = 0.93$ and RMSE of 3.78 ton/ha (%RMSE = 3.25%). Therefore, 96.75% of the aboveground biomass estimated from UAV imagery was accurate compared to aboveground biomass estimated from 3D point clouds of TLS data. Consequently, the null hypothesis is not rejected. Therefore, there is no significant difference between aboveground biomass estimated from UAV imagery and TLS point clouds.

5.2. Recommendations

The following recommendations are presented from the limitations faced under this study:

Differential GPS is essential for identifying the plot center and location of the field-measured trees from each sample plot. It was challenging and time-consuming to match exact trees between field-measured and UAV images. Differential GPS measurement can provide a more accurate measurement and can reduce the time for matching trees.

UAV acquired images need to be checked before leaving the study area. Because sometimes the acquired images are not well enough for getting good results. Besides, several alternative flights should be carried out as a safety in case of main flight is unable to work.

The GCP markers should be placed on the same day of UAV flight. Otherwise, the GCP markers could be floated away during high-tides in the mangrove area.

The scanners built-in GPS receiver in TLS should be activated before scanning of sample plots for getting coordinates of each scan position from TLS.

The congested roots and some branches of trees need to be cleaned before TLS scanning. It is better to prepare sample plots (plots that will be scanned on that day) first and then start TLS scanning. Because it can save time as well as reduce workload.

In mangrove forest, the tide is an important factor. So, the schedule of high-tide and low-tide should be considered in fieldwork plan.

LIST OF REFERENCES

Achanta, R., Shaji, A., Smith, K., Lucchi, A., Fua, P., & Süsstrunk, S. (2012). SLIC superpixels compared to state-of-the-art superpixel methods. *IEEE Transactions on Pattern Analysis and Machine Intelligence*, *34*(11), 2274–2281. https://doi.org/10.1109/TPAMI.2012.120

Aikawa, S., Akahori, S., Awaya, Y., Ehara, M., Hirata, Y., Furuya, N., … Yokota, Y. (2012). *REDD-plus cookbook: how to measure and monitor forest carbon*. *Forestry and Forest Products Research Institute (FFPRI)*. Retrieved from http://www.ffpri.affrc.go.jp/redd-rdc/en/reference/cookbook.html

Ali, I., Greifeneder, F., Stamenkovic, J., Neumann, M., & Notarnicola, C. (2015). Review of machine learning approaches for biomass and soil moisture retrievals from remote sensing data. *Remote Sensing*, *7*(12), 16398–16421. https://doi.org/10.3390/rs71215841

Alongi, D. M. (2012). Carbon sequestration in mangrove forests. *Carbon Management*, *3*(3), 313–322. https://doi.org/10.4155/cmt.12.20

Anderson, K., & Gaston, K. J. (2013). Lightweight unmanned aerial vehicles will revolutionize spatial ecology. *Frontiers in Ecology and the Environment*, *11*(3), 138–146. https://doi.org/10.1890/120150

Antolihao, J. A., Serna, A. M. de la, & Silapan, J. (2015). Remotely sensed data segmentation and classification in Bacolod city, Negros Occidental using DSM slope as an additional layer and kappa analysis of error matrix. In *2014 International Conference on Intelligent Agriculture* (Vol. 63, pp. 139–142). https://doi.org/10.7763/IPCBEE

Asner, G. P., Townsend, P. a, Martin, R. E., & Chadwick, K. D. (2015). Forest biophysical and biochemical properties from hyperspectral and LiDAR remote sensing. In *Land Resources Monitoring, Modeling, and Mapping with Remote Sensing* (pp. 429–448). https://doi.org/doi:10.1201/b19322-22

Baatz, M., Schäpe, a, & Schäpe, A. (2000). Multiresolution Segmentation - an optimization approach for high quality multi-scale image segmentation. *XII Angewandte Geographische Informationsverarbeitung* , 12–23. https://doi.org/Export Date 6 May 2013

Basuki, T. M., van Laake, P. E., Skidmore, A. K., & Hussin, Y. A. (2009). Allometric equations for estimating the aboveground biomass in tropical lowland Dipterocarp forests. *Forest Ecology and Management*, *257*(8), 1684–1694. https://doi.org/10.1016/j.foreco.2009.01.027

Blaschke, T. (2010). Object-based image analysis for remote sensing. *ISPRS Journal of Photogrammetry and Remote Sensing*, *65*(1), 2–16. https://doi.org/10.1016/j.isprsjprs.2009.06.004

BMKG. (2019). Meteorological, Climatological, and Geophysical Agency. Retrieved January 23, 2019, from https://www.bmkg.go.id/?lang=EN

Boone, J. K., & Bhomia, R. K. (2017). Ecosystem carbon stocks of mangroves across broad environmental gradients in West-Central Africa: Global and regional comparisons. *PLoS ONE*, *12*(11), 1–17. https://doi.org/10.1371/journal.pone.0187749

Brandeis, T. J., Delaney, M., Parresol, B. R., & Royer, L. (2006). Development of equations for predicting Puerto Rican subtropical dry forest biomass and volume. *Forest Ecology and Management*, *233*(1), 133–142. https://doi.org/10.1016/j.foreco.2006.06.012

Brown, S. (1997). *Estimating biomass and biomass change of tropical forest. A primer. A forest resources assessment publication. Food and Agriculture Organization, Roma. UN FAO Forestry Paper, No. 134*. Retrieved from http://www.fao.org/docrep/w4095e/w4095e00.HTM

Brown, S. (2002). Measuring carbon in forests: Current status and future challenges. *Environmental Pollution*, *116*(3), 363–372. https://doi.org/10.1016/S0269-7491(01)00212-3

Bu, L., & Zhang, Z. (2008). Application of point clouds from terrestrial 3D laser scanner for deformation measurements. *The International Archives of the Photogrammetry, Remote Sensing and Spatial Information Sciences*, *XXXVII*, 545–548. Retrieved from http://pdf.aminer.org/000/353/231/imaging_laser_scanners_for_d_modeling_and_surveying_applications.pdf

Calders, K., Newnham, G., Burt, A., Murphy, S., Raumonen, P., Herold, M., … Kaasalainen, M. (2015). Nondestructive estimates of above-ground biomass using terrestrial laser scanning. *Methods in Ecology and Evolution*, *6*(2), 198–208. https://doi.org/10.1111/2041-210X.12301

Chave, J., Andalo, C., Brown, S., Cairns, M. A., Chambers, J. Q., Eamus, D., … Yamakura, T. (2005). Tree allometry and improved estimation of carbon stocks and balance in tropical forests. *Oecologia*, *145*(1), 87–99. https://doi.org/10.1007/s00442-005-0100-x

Choong, E. T., Wirakusumah, R. S., & Achmadi, S. S. (1990). Mangrove forest resources in Indonesia. *Forest Ecology and Management Elsevier Science Publishers*, *3334*, 45–57.
Chubey, M. S., Franklin, S. E., & Wulder, M. a. (2006). Object-based analysis of Ikonos-2 imagery for extraction of forest inventory parameters. *Photogrammetric Engineering and Remote Sensing*, *72*(4), 383–394. https://doi.org/10.14358/PERS.72.4.383
Clinton, N., Holt, A., Scarborough, J., Yan, L., & Gong, P. (2010). Accuracy assessment measures for object-based image segmentation goodness. *Photogrammetric Engineering & Remote Sensing*, *76*(3), 289–299. https://doi.org/10.14358/PERS.76.3.289
Crommelinck, S., Bennett, R., Gerke, M., Koeva, M. N., Yang, M. Y., & Vosselman, G. (2017). SLIC superpixels for object delineation from UAV data. *ISPRS Annals of the Photogrammetry, Remote Sensing and Spatial Information Sciences*, *4*(2W3), 9–16. https://doi.org/10.5194/isprs-annals-IV-2-W3-9-2017
Cushman, K. C., Muller-Landau, H. C., Condit, R. S., & Hubbell, S. P. (2014). Improving estimates of biomass change in buttressed trees using tree taper models. *Methods in Ecology and Evolution*, *5*(6), 573–582. https://doi.org/10.1111/2041-210X.12187
Dandois, J. P., & Ellis, E. C. (2013). High spatial resolution three-dimensional mapping of vegetation spectral dynamics using computer vision. *Remote Sensing of Environment*, *136*, 259–276. https://doi.org/10.1016/j.rse.2013.04.005
Dhanachandra, N., Manglem, K., & Chanu, Y. J. (2015). Image Segmentation Using K-means Clustering Algorithm and Subtractive Clustering Algorithm. *Procedia Computer Science*, *54*, 764–771. https://doi.org/10.1016/j.procs.2015.06.090
Domingo, D., Lamelas-Gracia, M. T., Montealegre-Gracia, A. L., & de la Riva-Fernández, J. (2017). Comparison of regression models to estimate biomass losses and CO2emissions using low-density airborne laser scanning data in a burnt Aleppo pine forest. *European Journal of Remote Sensing*, *50*(1), 384–396. https://doi.org/10.1080/22797254.2017.1336067
Donato, D. C., Kauffman, J. B., Murdiyarso, D., Kurnianto, S., Stidham, M., & Kanninen, M. (2011). Mangroves among the most carbon-rich forests in the tropics. *Nature Geoscience*, *4*(5), 293–297. https://doi.org/10.1038/ngeo1123
Drăguţ, L., Tiede, D., & Levick, S. R. (2010). ESP: A tool to estimate scale parameter for multiresolution image segmentation of remotely sensed data. *International Journal of Geographical Information Science*, *24*(6), 859–871. https://doi.org/10.1080/13658810903174803
Duarte, C. M., Losada, I. J., Hendriks, I. E., Mazarrasa, I., & Marbà, N. (2013). The role of coastal plant communities for climate change mitigation and adaptation. *Nature Climate Change*, *3*(11), 961–968. https://doi.org/10.1038/nclimate1970
Food and Agriculture Organization. (2018). Mangrove management. Retrieved August 22, 2018, from http://www.fao.org/forestry/mangrove/vegetation/en/idn/
Gao, M., Klinger, Y., van der Woerd, J., Tapponnier, P., & Xu, X. (2017). High-resolution mapping based on an Unmanned Aerial Vehicle (UAV) to capture paleoseismic offsets along the Altyn-Tagh fault, China. *Scientific Reports*, *7*(1), 1–11. https://doi.org/10.1038/s41598-017-08119-2
Ghosh, S. M., & Behera, M. D. (2018). Aboveground biomass estimation using multi-sensor data synergy and machine learning algorithms in a dense tropical forest. *Applied Geography*, *96*(March), 29–40. https://doi.org/10.1016/j.apgeog.2018.05.011
Gibbs, H. K., Brown, S., Niles, J. O., & Foley, J. A. (2007). Monitoring and estimating tropical forest carbon stocks: Making REDD a reality. *Environmental Research Letters*, *2*(4). https://doi.org/10.1088/1748-9326/2/4/045023
Giri, C., Ochieng, E., Tieszen, L. L., Zhu, Z., Singh, A., Loveland, T., … Duke, N. (2011). Status and distribution of mangrove forests of the world using earth observation satellite data. *Global Ecology and Biogeography*, *20*(1), 154–159. https://doi.org/10.1111/j.1466-8238.2010.00584.x
Göltenboth, F., & Schoppe, S. (2006). Mangroves. In F. Göltenboth, K. H. Timotius, P. P. Milan, & J. Margraf (Eds.), *Ecology of Insular Southeast Asia* (pp. 187–214). Amsterdam: Elsevier. https://doi.org/https://doi.org/10.1016/B978-044452739-4/50011-5
Gómez-Candón, D., De Castro, A. I., & López-Granados, F. (2014). Assessing the accuracy of mosaics from unmanned aerial vehicle (UAV) imagery for precision agriculture purposes in wheat. *Precision Agriculture*, *15*(1), 44–56. https://doi.org/10.1007/s11119-013-9335-4

Griebel, A., Bennett, L. T., Culvenor, D. S., Newnham, G. J., & Arndt, S. K. (2015). Reliability and limitations of a novel terrestrial laser scanner for daily monitoring of forest canopy dynamics. *Remote Sensing of Environment*, *166*, 205–213. https://doi.org/10.1016/j.rse.2015.06.014

Gunawardena, A. R., Nissanka, S. P., Dayawansa, N. D. K., & Fernando, T. T. (2016). Above ground biomass estimation of mangroves located in Negombo - Muthurajawela wetland in Sri Lanka using ALOS PALSAR images. *Tropical Agricultural Research*, *27*(2), 137–146.

Hastie, T.; Tibshirani, R.; Friedman, J. (2009). Statistical applications of the multivariate skew normal distribution. *Journal of the Royal Statistical Society, Series B*, *61*(3), 579–602.

Hemery, G. E., Savill, P. S., & Pryor, S. N. (2005). Applications of the crown diameter-stem diameter relationship for different species of broadleaved trees. *Forest Ecology and Management*, *215*(1–3), 285–294. https://doi.org/10.1016/j.foreco.2005.05.016

Husson, E., Lindgren, F., & Ecke, F. (2014). Assessing biomass and metal contents in riparian vegetation along a pollution gradient using an unmanned aircraft system. *Water, Air, and Soil Pollution*, *225*(6). https://doi.org/10.1007/s11270-014-1957-2

Iizuka, K., Yonehara, T., Itoh, M., & Kosugi, Y. (2018). Estimating tree height and diameter at breast height (DBH) from digital surface models and orthophotos obtained with an unmanned aerial system for a Japanese Cypress (Chamaecyparis obtusa) forest. *Remote Sensing*, *10*(1). https://doi.org/10.3390/rs10010013

IPCC. (2006). 2006 IPCC guidelines for national greenhouse gas inventories. Retrieved from https://www.ipcc-nggip.iges.or.jp/public/2006gl/vol4.html

Irving, A. D., Connell, S. D., & Russell, B. D. (2011). Restoring coastal plants to improve global carbon storage: Reaping what we sow. *PLoS ONE*, *6*(3), 1–6. https://doi.org/10.1371/journal.pone.0018311

IUCN. (2017). Mangroves and REDD+: A new component of MFF. Retrieved August 1, 2018, from https://www.iucn.org/news/asia/201711/mangroves-and-redd-new-component-mff

Jiménez-Jiménez, S. I., Ojeda-Bustamante, W., Ontiveros-Capurata, R. E., Flores-Velázquez, J., Marcial-Pablo, M. de J., & Robles-Rubio, B. D. (2017). Quantification of the error of digital terrain models derived from images acquired with UAV. *Ingeniería Agrícola y Biosistemas*, *9*(2), 85–100. https://doi.org/10.5154/r.inagbi.2017.03.007

Kaku, K. (2011). An inconvenient truth-global warming on greenhouse gas (GHG) reduction under the Kyoto protocol regime to post Kyoto protocol in ASIA. *Procedia Engineering*, *8*, 515–519. https://doi.org/10.1016/j.proeng.2011.03.093

Karlson, M., Reese, H., & Ostwald, M. (2014). Tree crown mapping in managed woodlands (Parklands) of semi-arid West Africa using WorldView-2 imagery and geographic object-based image analysis. *Sensors*, *14*(12), 22643–22669. https://doi.org/10.3390/s141222643

Kauffman, J. B., & Donato, D. (2012). *Protocols for the measurement, monitoring, and reporting of structure, biomass and carbon stocks in mangrove forests* (86). https://doi.org/10.17528/cifor/003749

Kavzoglu, T., & Tonbul, H. (2017). A comparative study of segmentation quality for multi-resolution segmentation and watershed transform. In *Proceedings of 8th International Conference on Recent Advances in Space Technologies, RAST 2017* (pp. 113–117). https://doi.org/10.1109/RAST.2017.8002984

Kavzoglu, T., & Tonbul, H. (2018). An experimental comparison of multi-resolution segmentation, SLIC and K-means clustering for object-based classification of VHR imagery. *International Journal of Remote Sensing*, *39*(18), 6020–6036. https://doi.org/10.1080/01431161.2018.1506592

Ke, Y., & Quackenbush, L. J. (2011). A review of methods for automatic individual tree-crown detection and delineation from passive remote sensing. *International Journal of Remote Sensing*, *32*(17), 4725–4747. https://doi.org/10.1080/01431161.2010.494184

Kejriwal, L., & Singh, I. (2016). A hybrid filtering approach of digital video stabilization for UAV using kalman and low pass filter. *Procedia Computer Science*, *93*(September), 359–366. https://doi.org/10.1016/j.procs.2016.07.221

Kociuba, W., Kubisz, W., & Zagórski, P. (2014). Use of terrestrial laser scanning (TLS) for monitoring and modeling of geomorphic processes and phenomena at a small and medium spatial scale in the Polar environment (Scott River - Spitsbergen). *Geomorphology*, *212*, 84–96. https://doi.org/10.1016/j.geomorph.2013.02.003

Koji Shimano. (1997). Analysis of the Relationship between DBH and Crown Projection Area Using a New Model. *Journal of Forest Research*, *2*, 237–242.

Krauss, K. W., Cahoon, D. R., Allen, J. A., Ewel, K. C., Lynch, J. C., & Cormier, N. (2010). Surface elevation change and susceptibility of different mangrove zones to sea-level rise on Pacific high islands of Micronesia. *Ecosystems*, *13*(1), 129–143. https://doi.org/10.1007/s10021-009-9307-8

Larjavaara, M., & Muller-Landau, H. C. (2013). Measuring tree height: A quantitative comparison of two common field methods in moist tropical forest. *Methods in Ecology and Evolution*, *4*(9), 793–801. https://doi.org/10.1111/2041-210X.12071

Liu, J., Liang, X., Hyyppä, J., Yu, X., Lehtomäki, M., Pyörälä, J., … Chen, R. (2017). Automated matching of multiple terrestrial laser scans for stem mapping without the use of artificial references. *International Journal of Applied Earth Observation and Geoinformation*, *56*, 13–23. https://doi.org/10.1016/j.jag.2016.11.003

Lu, D. (2006). The potential and challenge of remote sensing-based biomass estimation. *International Journal of Remote Sensing*, *27*(7), 1297–1328. https://doi.org/10.1080/01431160500486732

Lu, S., Shi, R., & Zhu, G. (2008). Combinative representation of TLS point cloud and 3D virtual reality for cultural heritage preservation planning. *The International Archives of the Photogrammetry, Remote Sensing and Spatial Information Sciences*, (1), 1077–1080.

Lübker, T., & Schaab, G. (2009). Optimization of parameter settings for multilevel image segmentation in GEOBIA. *High-Resolution Earth Imaging*. Retrieved from http://www.ipi.uni-hannover.de/fileadmin/institut/pdf/isprs-Hannover2009/Luebker-142.pdf

Lucas, R. M., Mitchell, A. L., & Armston, J. (2015). Measurement of forest above-ground biomass using active and passive remote sensing at large (subnational to global) scales. *Current Forestry Reports*, *1*(3), 162–177. https://doi.org/10.1007/s40725-015-0021-9

Messinger, M., Asner, G. P., & Silman, M. (2016). Rapid assessments of Amazon forest structure and biomass using small unmanned aerial systems. *Remote Sensing*, *8*(8), 1–15. https://doi.org/10.3390/rs8080615

Mohan, M., Silva, C. A., Klauberg, C., Jat, P., Catts, G., Cardil, A., … Dia, M. (2017). Individual tree detection from the unmanned aerial vehicle (UAV) derived canopy height model in an open canopy mixed conifer forest. *Forests*, *8*(9), 1–17. https://doi.org/10.3390/f8090340

Mohd Zaki, N. A., Abd Latif, Z., Suratman, M. N., & Zainal, M. Z. (2016). Aboveground biomass and carbon stocks modeling using the non-linear regression model. *IOP Conference Series: Earth and Environmental Science*, *37*(1). https://doi.org/10.1088/1755-1315/37/1/012030

Möller, M., Lymburner, L., & Volk, M. (2007). The comparison index: A tool for assessing the accuracy of image segmentation. *International Journal of Applied Earth Observation and Geoinformation*, *9*(3), 311–321. https://doi.org/10.1016/j.jag.2006.10.002

Mustika Sari, N., & Kushardono, D. (2015). Object segmentation on UAV photo data to support the provision of rural area spatial information. *Forum Geografi*, *29*(1), 49–58. https://doi.org/10.23917/forgeo.v29i1.792

Mweresa, I. A., Odera, P. A., Kuria, D. N., & Kenduiywo, B. K. (2017). Estimation of tree distribution and canopy heights in Ifakara, Tanzania, using unmanned aerial system (UAS) stereo imagery. *American Journal of Geographic Information System*, *6*(5), 187–200. https://doi.org/10.5923/j.ajgis.20170605.03

Nam, V. T., Van Kuijk, M., & Anten, N. P. R. (2016). Allometric equations for aboveground and belowground biomass estimations in an evergreen forest in Vietnam. *PLoS ONE*, *11*(6), 6–9. https://doi.org/10.1371/journal.pone.0156827

NASA. (2018). Remote sensors. Retrieved August 21, 2018, from https://earthdata.nasa.gov/user-resources/remote-sensors

Newnham, G. J., Armston, J. D., Calders, K., Disney, M. I., Lovell, J. L., Schaaf, C. B., … Danson, F. M. (2015). Terrestrial laser scanning for plot-scale forest measurement. *Current Forestry Reports*, *2*(3), 214–214. https://doi.org/10.1007/s40725-016-0039-7

Nex, F., & Remondino, F. (2014). UAV for 3D mapping applications: A review. *Applied Geomatics*, *6*(1), 1–15. https://doi.org/10.1007/s12518-013-0120-x

Ni, W., Ranson, K. J., Zhang, Z., & Sun, G. (2014). Features of point clouds synthesized from multi-view ALOS/PRISM data and comparisons with LiDAR data in forested areas. *Remote Sensing of Environment*, *149*(2014), 47–57. https://doi.org/10.1016/j.rse.2014.04.001

Oyebade, B. A., & Anaba, J. C. (2018). Individual tree basal area equation for a young Tectona Grandis (Teak) plantation in Choba , Port Harcourt , Rivers State, Nigeria. *World News of Natural Sciences*, *16*(January), 144–154.

Pap, M., & Kiraly, S. (2018). Comparison of segmentation methods on images of energy plants obtained by UAVs. *2018 IEEE International Conference on Future IoT Technologies, Future IoT 2018*, *2018–Janua*, 1–8. https://doi.org/10.1109/FIOT.2018.8325601

Pham, L. T. H., & Brabyn, L. (2017). Monitoring mangrove biomass change in Vietnam using SPOT images and an object-based approach combined with machine learning algorithms. *ISPRS Journal of Photogrammetry and Remote Sensing*, *128*, 86–97. https://doi.org/10.1016/j.isprsjprs.2017.03.013

Priya, N., Ranjan, P., Sappal, S. M., & Ramanathan, A. L. (2017). Reactive Nitrogen Dynamics in the Mangroves of India. In *The Indian Nitrogen Assessment: Sources of Reactive Nitrogen, Environmental and Climate Effects, Management Options, and Policies* (pp. 335–359). Elsevier Inc. https://doi.org/10.1016/B978-0-12-811836-8.00022-7

Prosdocimi, M., Calligaro, S., Sofia, G., Dalla Fontana, G., Tarolli, P., Schenk, T., … Lane, S. N. (2015). Structure from motion (SfM) photogrammetry. *Department of Civil and Environmental Engineering and Geodetic Science, The Ohio State University*, *40*(14), 79–95. https://doi.org/10.1002/esp.3767

Qing Chen, Xiaoli Yang, & Petriu, E. M. (2004). Watershed segmentation for binary images with different distance transforms. In *Proceedings. Second International Conference on Creating, Connecting and Collaborating through Computing* (Vol. 2, pp. 111–116). https://doi.org/10.1109/HAVE.2004.1391891

Saba, F., Valadanzouj, M. J., & Mokhtarzade, M. (2013). The optimization of multi-resolution segmentation of remotely sensed data using genetic algorithm. *ISPRS - International Archives of the Photogrammetry, Remote Sensing and Spatial Information Sciences*, *XL-1/W3*(October), 345–349. https://doi.org/10.5194/isprsarchives-xl-1-w3-345-2013

Saha, R. R. S. K. (2008). Multi-resolution Segmentation for Object-based Classifi cation and assessment of accuracy for land cover _IRS.pdf, (June), 189–201.

Salunkhe, O., Khare, P. K., Sahu, T. R., & Singh, S. (2016). Estimation of tree biomass reserves in tropical deciduous forests of Central India by non- destructive approach. *Tropical Ecology*, *57*(2), 153–161.

Smith, T. J., & Whelan, K. R. T. (2006). Development of allometric relations for three mangrove species in South Florida for use in the Greater Everglades Ecosystem Restoration. *Wetlands Ecology and Management*, *14*(5), 409–419. https://doi.org/10.1007/s11273-005-6243-z

Stovall, A. E. L., Vorster, A. G., Anderson, R. S., Evangelista, P. H., & Shugart, H. H. (2017). Non-destructive aboveground biomass estimation of coniferous trees using terrestrial LiDAR. *Remote Sensing of Environment*, *200*(January), 31–42. https://doi.org/10.1016/j.rse.2017.08.013

Sumida, A., Miyaura, T., & Torii, H. (2013). Relationships of tree height and diameter at breast height revisited: Analyses of stem growth using 20-year data of an even-aged Chamaecyparis obtusa stand. *Tree Physiology*, *33*(1), 106–118. https://doi.org/10.1093/treephys/tps127

Tan, K., Zhang, W., Shen, F., & Cheng, X. (2018). Investigation of TLS intensity data and distance measurement errors from target specular reflections. *Remote Sensing*, *10*(7). https://doi.org/10.3390/rs10071077

Taureau, F., Robin, M., Proisy, C., Fromard, F., Imbert, D., Debaine, F., … Debaine, F. (2019). Mapping the mangrove forest canopy using spectral unmixing of very high spatial resolution satellite images. *Remote Sensing*, *11*(3), 367. https://doi.org/10.3390/RS11030367

Tian, T., Li, C., Xu, J., & Ma, J. (2018). Urban area detection in very high-resolution remote sensing images using deep convolutional neural networks. *Sensors*, *18*(3). https://doi.org/10.3390/s18030904

Tolpekin, V. A. (2012). *The core of GIScience : a systems-based approach. (ITC Educational Textbook Series; No. 2012). Enschede: the University of Twente, Faculty of Geo-Information Science and Earth Observation (ITC).* https://doi.org/10.1016/B978-0-12-385889-4.00013-2

Trettin, C., Lee, S., Simard, M., Lagomasino, D., Fatoyinbo, T., & Feliciano, E. (2016). A Comparison of mangrove canopy height using multiple independent measurements from land, air, and space. *Remote Sensing*, *8*(4), 327. https://doi.org/10.3390/rs8040327

USAID. (2013). REDD+ Measurement, Reporting, and Verification (MRV) Manual, 1–6. Retrieved from http://pfbc-cbfp.org/news_en/items/redd-measurement-USAID-EN.html

Wahyuni, S., Jaya, I. N. S., & Puspaningsih, N. (2016). Model for estimating above ground biomass of reclamation forest using unmanned aerial vehicles. *Indonesian Journal of Electrical Engineering and Computer Science*, *4*(3), 586–593. https://doi.org/10.11591/ijeecs.v4.i3.pp586-593

Wang, Y., Lehtomäki, M., Liang, X., Pyörälä, J., Kukko, A., Jaakkola, A., … Hyyppä, J. (2019). Is field-measured tree height as reliable as believed – A comparison study of tree height estimates from field measurement, airborne laser scanning and terrestrial laser scanning in a boreal forest. *ISPRS Journal of Photogrammetry and Remote Sensing*, *147*(May 2018), 132–145. https://doi.org/10.1016/j.isprsjprs.2018.11.008

Westoby, M. J., Brasington, J., Glasser, N. F., Hambrey, M. J., & Reynolds, J. M. (2012). "Structure-from-Motion" photogrammetry: A low-cost, effective tool for geoscience applications. *Geomorphology*, *179*(June 2018), 300–314. https://doi.org/10.1016/j.geomorph.2012.08.021

Wilson, J. P. (2016). Digital terrain modeling. *Regional Assessment of Global Change Impacts: The Project GLOWA-Danube*, *137*(1), 69–74. https://doi.org/10.1007/978-3-319-16751-0_7

Witharana, C., & Civco, D. L. (2014). Optimizing multi-resolution segmentation scale using empirical methods: Exploring the sensitivity of the supervised discrepancy measure Euclidean distance 2 (ED2). *ISPRS Journal of Photogrammetry and Remote Sensing*, *87*, 108–121. https://doi.org/10.1016/j.isprsjprs.2013.11.006

Woodroffe, C. D., Rogers, K., McKee, K. L., Lovelock, C. E., Mendelssohn, I. A., & Saintilan, N. (2016). Mangrove sedimentation and response to relative sea-level rise. *Annual Review of Marine Science*, *8*(1), 243–266. https://doi.org/10.1002/andp.18341081502

Wu, R., Chen, Y., Wang, C., & Li, J. (2018). Estimation of forest trees diameter from terrestrial laser scanning point clouds based on a circle fitting method. *IEEE International Geoscience and Remote Sensing Symposium*, 2821–2824. https://doi.org/http://doi.org/10.1109/IGARSS.2018.8517303

WWF. (2019). Deforestation. Retrieved February 19, 2019, from https://www.worldwildlife.org/threats/deforestation

Yuan, Y., & Hu, X. (2016). Random forest and objected-based classification for forest pest extraction from UAV aerial imagery. *International Archives of the Photogrammetry, Remote Sensing and Spatial Information Sciences - ISPRS Archives*, *2016–Janua*(July), 1093–1098. https://doi.org/10.5194/isprsarchives-XLI-B1-1093-2016

Yuheng, S., & Hao, Y. (2017). Image Segmentation Algorithms Overview, *1*. https://doi.org/http://dx.doi.org/10.1016/j.jpedsurg.2015.06.019

Zahawi, R. A., Reid, J. L., Dandois, J. P., Ellis, E. C., Holl, K. D., & Nadwodny, D. (2015). Using lightweight unmanned aerial vehicles to monitor tropical forest recovery. *Biological Conservation*, *186*, 287–295. https://doi.org/10.1016/j.biocon.2015.03.031

Zhang, H., Fritts, J. E., & Goldman, S. A. (2008). Image segmentation evaluation: A survey of unsupervised methods. *Computer Vision and Image Understanding*, *110*(2), 260–280. https://doi.org/10.1016/j.cviu.2007.08.003

Zhang, X., Feng, X., & Jiang, H. (2010). Object-oriented method for urban vegetation mapping using ikonos imagery. *International Journal of Remote Sensing*, *31*(1), 177–196. https://doi.org/10.1080/01431160902882603

Zimudzi, E., Sanders, I., Rollings, N., & Omlin, C. (2018). Segmenting mangrove ecosystems drone images using SLIC superpixels. *Geocarto International*, *0*(0), 1–15. https://doi.org/10.1080/10106049.2018.1497093

APPENDICES

Appendix 1: Flight plan for UAV image acquisition

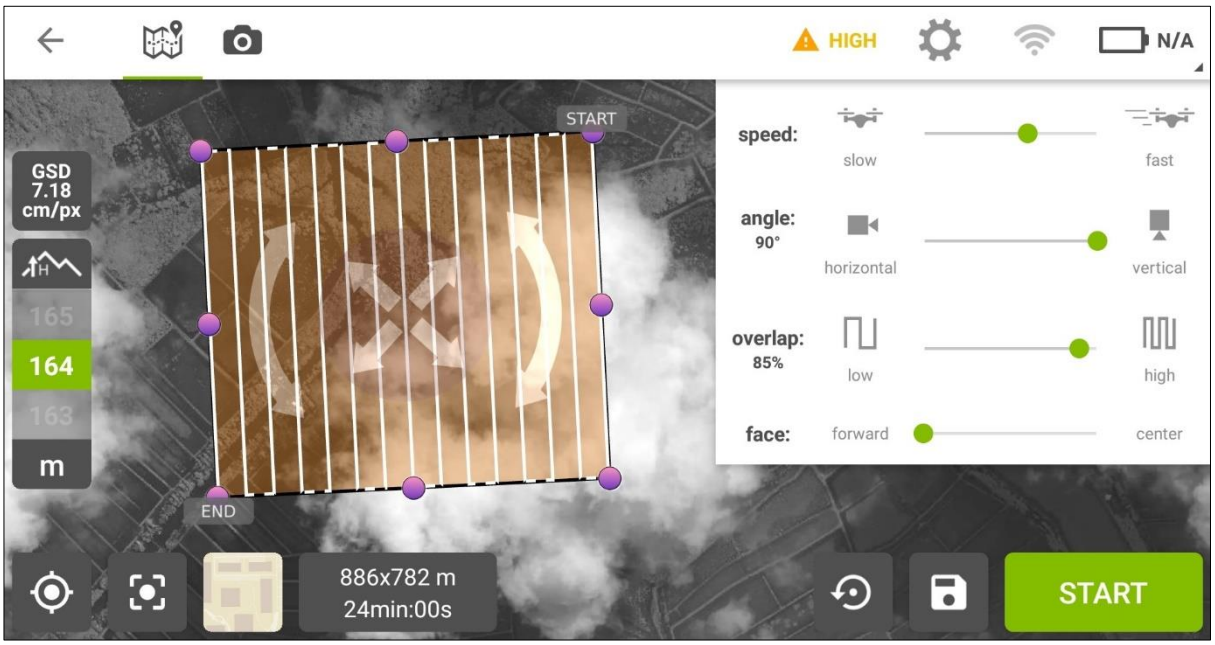

Appendix 2: Quality report of UAV image processing

Summary

Project	Experiment_2018_N_GCP
Processed	2018-12-22 04:12:35
Camera Model Name(s)	FC330_3.6_4000x3000 (RGB)
Average Ground Sampling Distance (GSD)	6.2 cm / 2.44 in
Area Covered	0.9786 km^2 / 97.8576 ha / 0.378 sq. mi. / 241.937 acres
Time for Initial Processing (without report)	16m:46s

Quality Check

Images	median of 41976 keypoints per image	✓
Dataset	369 out of 369 images calibrated (100%), all images enabled	✓
Camera Optimization	15.64% relative difference between initial and optimized internal camera parameters	⚠
Matching	median of 6556.47 matches per calibrated image	✓
Georeferencing	yes, 4 GCPs (4 3D), mean RMS error = 0.047 m	✓

Appendix 3: Parameters used for multi-resolution segmentation

Image	Scale	Shape	Compactness	Shadow Masking	Watershed Transformation	Remove Objects
Filtered UAV-RGB (20, 25, 30cm)	20	0.3	0.7	Trees: Brightness <= 170 Shadow: Brightness > 170	Length Factor: 40	Condition: Area <= 48 Pixel Roundness >= 1.1

Appendix 4: Parameters used for SLIC segmentation

Image	Iterations	Minimum Element Size	Region Size	Ruler	Shadow Masking	Watershed Transformation	Remove Objects
Filtered UAV-RGB (20, 25, 30cm)	50	10	30	50	Trees: Brightness <= 170 Shadow: Brightness > 170	Length Factor: 40	Condition: Area <= 48 Pixel Roundness >= 1.1

Appendix 5: Histogram of biometric, TLS and UAV estimated DBH

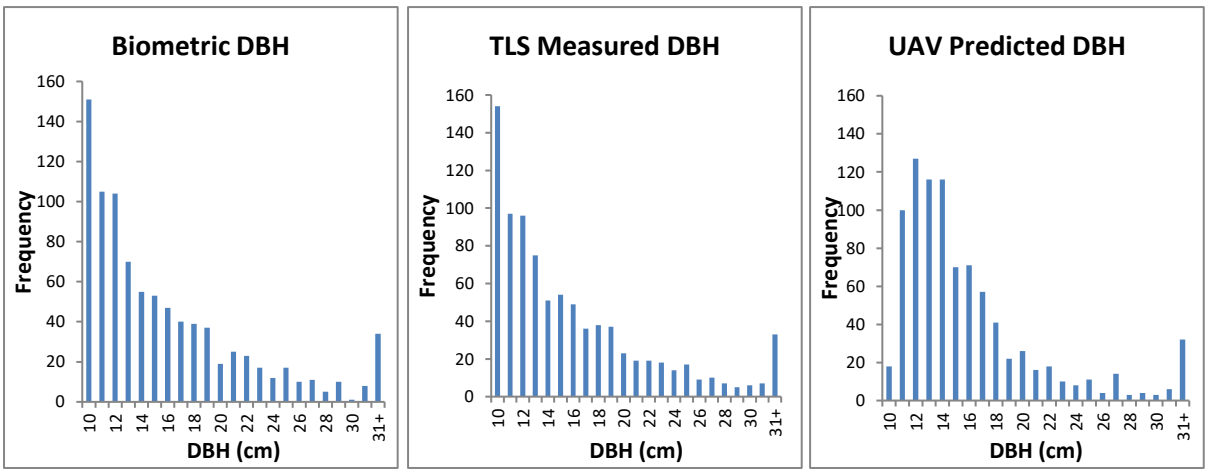

Appendix 6: Histogram of biometric, TLS and UAV estimated tree height

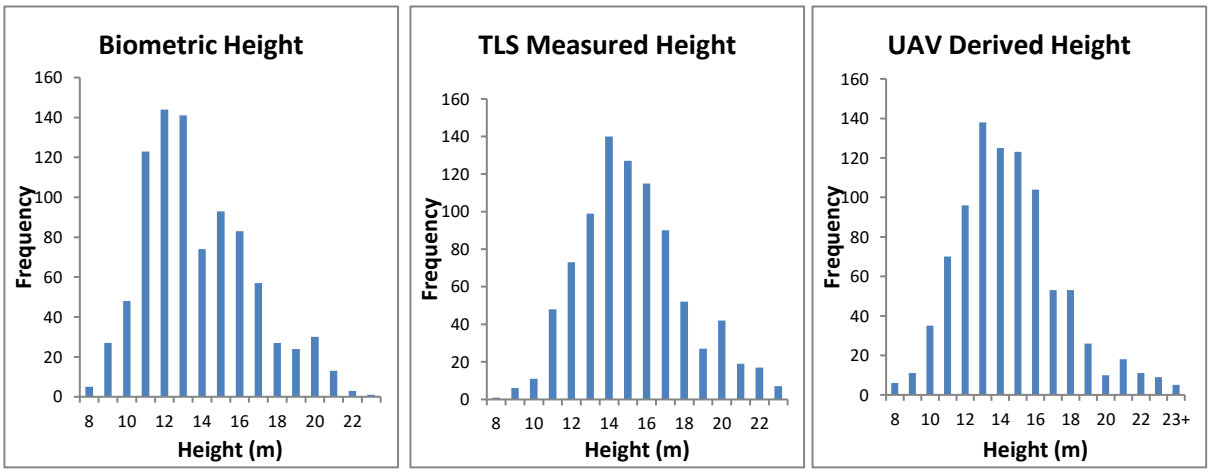

Appendix 7: Accuracy of multi-resolution segmentation including UAV-CHM layer

Reference Area (ARi)	**6768.33**	**6768.33**	**6768.33**
Segmented Area (ADi)	14941.32	10260.00	16903.00
Intersection (ADinARi	6697.78	6735.45	6749.06
Over Segmentation	0.55	0.34	0.60
Under Segmentation	1.0E-02	4.9E-03	2.8E-03
Error	0.39	0.24	0.42
Accuracy	60.98%	75.71%	57.52%

Appendix 8: Alternative CPA model developed using 600 trees from 20 sample plots

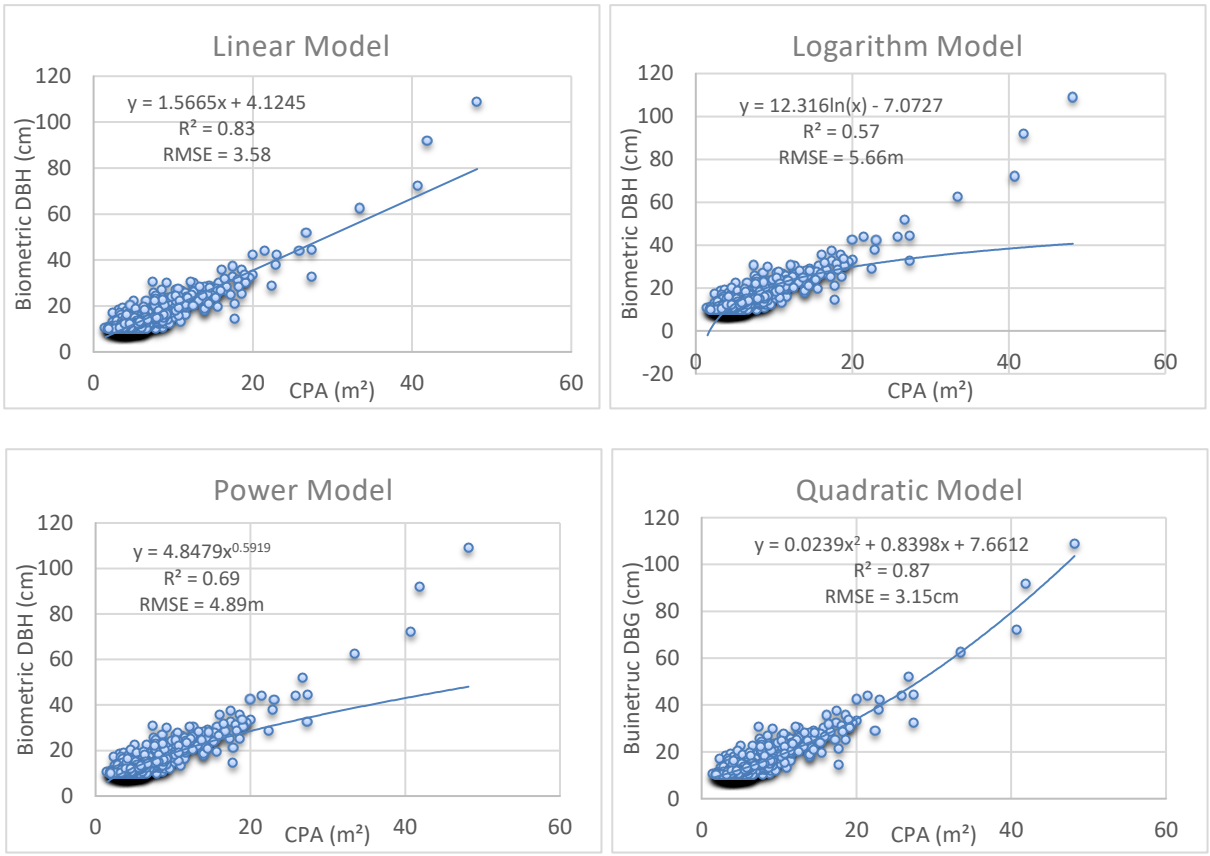

Appendix 9: Model validation for CPA model developed using 293 trees from 10 sample plots

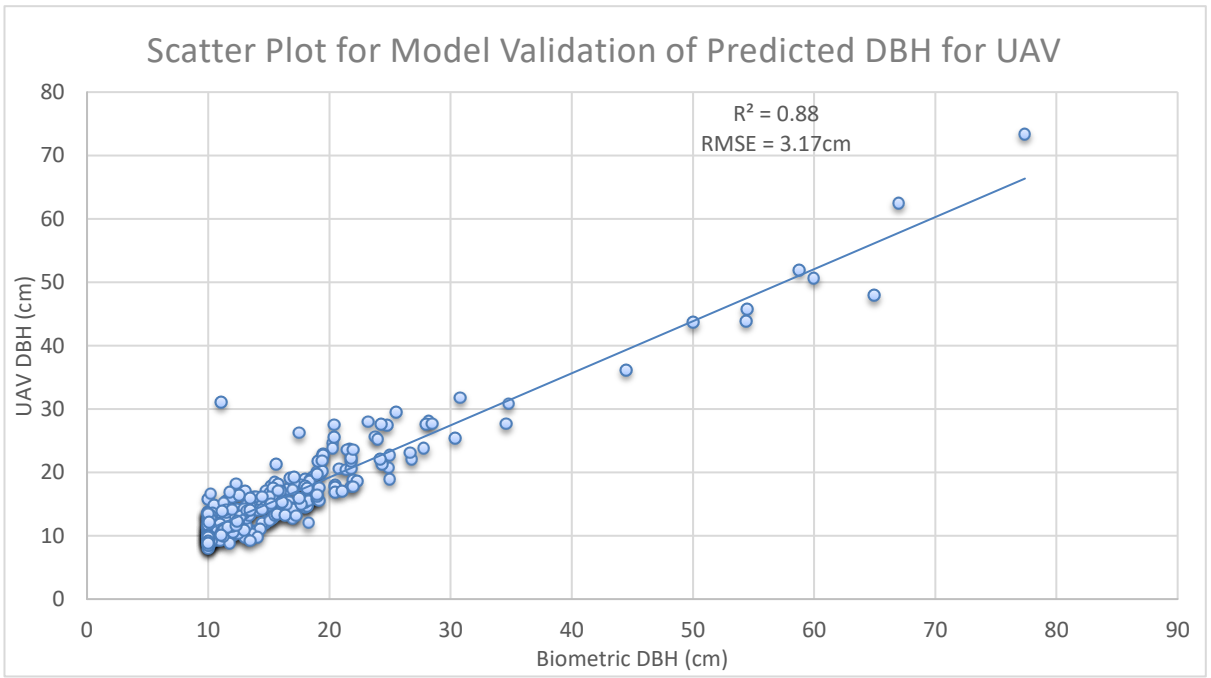

Appendix 10: Plot-wise summary of field-measured biometric data

Plot ID	No. of Trees	Field-measured Biometric Data				
		Mean DBH (cm)	Mean Height (m)	AGB (kg/plot)	AGB (Ton)	AGB (Ton/Ha)
1	25	15.70	10.48	105.03	2.63	52.52
2	30	18.51	14.17	215.31	6.46	129.19
3	38	15.58	10.38	97.38	3.70	74.01
4	24	18.80	16.09	321.49	7.72	154.31
5	44	18.42	15.41	304.94	13.11	262.25
6	18	20.12	13.58	269.52	4.85	97.03
7	44	13.62	13.33	122.32	5.38	107.64
8	40	12.05	13.24	90.36	3.61	72.29
9	41	12.43	13.35	88.20	3.62	72.32
10	36	13.91	12.98	96.79	3.48	69.69
11	27	14.60	12.78	111.23	3.00	60.07
12	26	11.91	10.46	56.84	1.48	29.56
13	40	14.05	12.66	106.34	4.25	85.08
14	31	16.20	12.36	161.21	5.00	99.95
15	26	15.76	11.71	155.07	4.03	80.64
16	32	14.07	13.09	140.69	4.50	90.04
17	21	22.51	12.04	469.56	9.86	197.22
18	17	14.78	10.99	121.39	2.06	41.27
19	32	15.06	12.49	147.09	4.71	94.14
20	24	17.16	12.94	212.29	5.09	101.90
21	22	19.35	15.40	237.72	5.23	104.60
22	28	17.54	19.60	255.19	7.15	142.91
23	25	21.21	18.65	396.24	9.91	198.12
24	23	18.00	16.90	238.71	5.49	109.81
25	21	16.72	14.31	258.86	5.44	108.72
26	20	23.79	12.36	408.46	8.17	163.38
27	28	22.04	12.97	419.47	11.75	234.90
28	41	12.90	11.43	89.45	3.67	73.35
29	36	12.86	11.33	83.55	3.01	60.15
30	33	16.26	13.23	200.63	6.62	132.42

Appendix 11: Plot-wise summary of TLS measured data

Plot ID	No. of Trees	Missing Trees	TLS Data				
			Mean DBH (cm)	Mean Height (m)	AGB (kg/plot)	AGB (Ton)	AGB (Ton/Ha)
1	25	1	15.62	11.77	117.38	2.82	56.34
2	30	0	18.43	15.78	233.50	7.00	140.10
3	38	2	15.41	11.60	104.57	3.76	75.29
4	24	1	18.85	17.36	342.86	7.89	157.71
5	44	4	18.69	18.69	378.87	15.15	303.10
6	18	0	20.05	15.16	295.87	5.33	106.51
7	44	2	13.68	14.74	136.52	5.73	114.67
8	40	0	11.98	15.08	100.78	4.03	80.62
9	41	1	12.42	14.81	96.59	3.86	77.27
10	36	2	13.55	14.32	100.51	3.42	68.35
11	27	0	14.50	14.21	123.48	3.33	66.68
12	26	0	11.84	11.66	63.93	1.66	33.25
13	40	2	14.06	13.70	112.92	4.29	85.82
14	31	0	16.10	14.22	187.11	5.80	116.01
15	26	0	15.83	13.36	163.50	4.25	85.02
16	32	0	14.11	14.75	154.93	4.96	99.15
17	21	0	22.39	12.99	483.84	10.16	203.21
18	17	0	14.68	11.01	120.08	2.04	40.83
19	32	1	15.28	13.59	157.23	4.87	97.48
20	24	0	17.15	13.69	214.04	5.14	102.74
21	22	1	19.23	16.51	250.54	5.26	105.23
22	28	0	17.43	19.98	255.69	7.16	143.19
23	25	0	21.11	20.54	432.23	10.81	216.11
24	23	0	17.88	17.43	250.59	5.76	115.27
25	21	0	16.61	15.43	264.59	5.56	111.13
26	20	0	23.63	14.08	476.47	9.53	190.59
27	28	0	21.95	13.28	387.43	10.85	216.96
28	41	1	12.88	13.14	94.77	3.79	75.81
29	36	1	12.78	15.13	108.31	3.79	75.82
30	33	0	16.12	14.15	196.41	6.48	129.63

Appendix 12: Plot-wise summary of UAV derived data

Plot ID	No. of Trees	UAV Derived Data				
		Mean DBH (cm)	Mean Height (m)	AGB (kg/plot)	AGB (Ton)	AGB (Ton/Ha)
1	25	17.43	10.10	126.53	3.16	63.26
2	30	15.79	14.81	157.01	4.71	94.21
3	38	11.54	11.58	58.59	2.23	44.53
4	24	19.36	15.88	327.48	7.86	157.19
5	44	17.29	16.68	358.67	15.78	315.63
6	18	20.45	14.50	296.89	5.34	106.88
7	44	14.61	13.22	146.80	6.46	129.18
8	40	12.79	13.91	107.02	4.28	85.61
9	41	14.71	13.63	130.51	5.35	107.02
10	36	14.87	13.42	112.49	4.05	80.99
11	27	16.49	13.38	143.58	3.88	77.53
12	26	13.67	11.44	81.98	2.13	42.63
13	40	13.50	13.60	100.31	4.01	80.25
14	31	15.96	14.73	169.63	5.26	105.17
15	26	16.25	12.46	151.41	3.94	78.73
16	32	15.35	13.85	155.48	4.98	99.51
17	21	21.23	11.51	437.58	9.19	183.79
18	17	15.65	10.32	116.95	1.99	39.76
19	32	14.95	12.99	138.59	4.43	88.70
20	24	18.62	13.28	254.64	6.11	122.23
21	22	18.57	15.91	217.88	4.79	95.87
22	28	17.65	20.05	255.67	7.16	143.18
23	25	20.37	20.26	414.99	10.37	207.49
24	23	15.62	17.49	187.92	4.32	86.44
25	21	16.90	14.44	224.16	4.71	94.15
26	20	24.02	13.43	447.94	8.96	179.18
27	28	20.37	12.38	358.76	10.05	200.90
28	41	13.33	12.08	89.29	3.66	73.22
29	36	13.27	15.12	115.06	4.14	82.84
30	33	15.07	14.46	159.53	5.26	105.29

Appendix 13: Field data collection sheet

Name of Recorder ..... **Date**..... **Plot Radius Size** .....

Sample Plot No.	Map Scale	Sample Plot Center X	Y	Dist. to Center of the plot (m)	Elevation	Slope (%)	Aspect

Land cover				Forest use type							Crown cover (%)	Undergrowth		
F	D	A	AF	M	P	N	T	A	R	E		H	M	L

Tree No.	Species	Coordinate		DBH	Height	Crown	Tree class				
		X	Y	(cm)	(m)	Diameter (m)	1	2	3	4	d
1											
2											
3											
4											
5											
6											
7											
8											
9											
10											
11											
12											
13											
14											
15											
16											
17											
18											
19											
20											
21											
22											
23											

Legend/Guide for Field Work Inventory form

Land cover:	**Forest use type:**	**Undergrowth:**	**Tree class:**
F = Forest D = Deforestation A= Agriculture AF= Agroforestry	M = Management forest P = Protection forest N = Nature Reserve T = Tourism forest A = Arboretum R = Research forest E = Education forest	H = High M = Medium L = Low/Nil	1 = Dominant 2 = Co-dominant 3 = Dominated 4 = Suppressed D = Dead/dying